

Charge Storage in Electret Polymers: Mechanisms, Characterization and Applications

Habilitationsschrift zur Erlangung des akademischen Grades

doctor rerum naturalium habilitatus

(Dr. rer. nat. habil.)

der Mathematisch-Naturwissenschaftlichen Fakultät
der Universität Potsdam

vorgelegt von

DR. AXEL MELLINGER

geb. am 25. August 1967 in München

Potsdam, 06. Dezember 2004

Abstract

Electrets are materials capable of storing oriented dipoles or an electric surplus charge for long periods of time. The term “electret” was coined by OLIVER HEAVISIDE in analogy to the well-known word “magnet”. Initially regarded as a mere scientific curiosity, electrets became increasingly important for applications during the second half of the 20th century. The most famous example is the electret condenser microphone, developed in 1962 by SESSLER and WEST. Today, these devices are produced in annual quantities of more than 1 billion, and have become indispensable in modern communications technology.

Even though space-charge electrets are widely used in transducer applications, relatively little was known about the microscopic mechanisms of charge storage. It was generally accepted that the surplus charges are stored in some form of physical or chemical traps. However, trap depths of less than 2 eV, obtained via thermally stimulated discharge experiments, conflicted with the observed lifetimes (extrapolations of experimental data yielded more than 100 000 years). Using a combination of photostimulated discharge spectroscopy and simultaneous depth-profiling of the space-charge density, the present work shows for the first time that at least part of the space charge in, e. g., polytetrafluoroethylene, polypropylene and polyethylene terephthalate is stored in traps with depths of up to 6 eV, indicating major local structural changes. Based on this information, more efficient charge-storing materials could be developed in the future.

The new experimental results could only be obtained after several techniques for characterizing the electrical, electromechanical and electrical properties of electrets had been enhanced with *in situ* capability. For instance, real-time information on space-charge depth-profiles were obtained by subjecting a polymer film to short laser-induced heat pulses. The high data acquisition speed of this technique also allowed the three-dimensional mapping of polarization and space-charge distributions.

A highly active field of research is the development of piezoelectric sensor films from electret polymer foams. These materials store charges on the inner surfaces of the voids after having been subjected to a corona discharge, and exhibit piezoelectric properties far superior to those of traditional ferroelectric polymers. By means of dielectric resonance spectroscopy, polypropylene foams (presently the most widely used ferroelectret) were studied with respect to their thermal and UV stability. Their limited thermal stability renders them unsuitable for applications above 50 °C. Using a solvent-based foaming technique, we found an alternative material based on amorphous Teflon[®] AF, which exhibits a stable piezoelectric coefficient of 600 pC/N at temperatures up to 120 °C.

Zusammenfassung

Elektrete sind Materialien, welche orientierte elektrische Dipole oder eine elektrische Überschussladung über längere Zeit speichern können. Der Begriff wurde 1885 von OLIVER HEAVISIDE in Anlehnung an das Wort „Magnet“ eingeführt. Zunächst nur als wissenschaftliche Kuriosität betrachtet, wurden sie seit Mitte des 20. Jahrhunderts in zunehmendem Maße für technische Anwendungen interessant. Als bekanntestes Beispiel sei hier das 1962 von SESSLER und WEST entwickelte Elektret-Kondensator-Mikrofon erwähnt, welches in jährlichen Stückzahlen von mehr als 1 Milliarde hergestellt wird und aus der modernen Kommunikationstechnik nicht mehr wegzudenken ist.

Trotz der weit verbreiteten Anwendungen in der Sensorik war bisher nur wenig über die mikroskopischen Mechanismen der Ladungsspeicherung bekannt. Allgemein wird davon ausgegangen, dass die Überschussladungen in physikalischen oder chemischen Haftstellen gespeichert sind. Bisherige Experimente zur thermisch stimulierten Entladung ergaben Bindungsenergien unterhalb von 2 eV, was im Widerspruch zu den beobachteten Lebensdauern (extrapoliert wur-

den Werte von mehr als 100000 Jahren) steht. Mittels photostimulierter Entladung sowie simultaner Messung des Ladungsprofils konnte nun für eine Reihe wichtiger Elektret-Polymere (darunter das unter dem Handelsnamen Teflon[®] bekannte Polytetrafluorethylen, Polypropylen und Polyethylenterephthalat) erstmals gezeigt werden, dass zumindest ein Teil der Ladungen in tiefen Haftstellen von bis zu 6 eV gespeichert wird, was auf eine tiefgreifende lokale Strukturänderung hinweist. Ausgehend von dieser Information könnten in Zukunft Materialien mit verbesserter Ladungsspeicherung gezielt entwickelt werden.

Die neuen Messungen waren erst möglich, nachdem mehrere Verfahren zur Bestimmung elektrischer, elektromechanischer und mechanischer Eigenschaften von Elektreten für einen *In Situ*-Einsatz weiterentwickelt wurden. So konnten z. B. durch Anregung von kurzen Wärmepulsen in der Polymerfolie Informationen über das Tiefenprofil der Raumladung in Echtzeit gewonnen werden. Die schnelle Abtastung ermöglichte darüber hinaus die dreidimensionale Kartierung von Polarisationsprofilen und Raumladungen.

Ein zur Zeit sehr aktives Forschungsgebiet ist die Entwicklung piezoelektrischer Sensorfolien aus geschäumten Elektret-Polymeren. Nach elektrischer Aufladung in einer Korona-Entladung werden Ladungen an der Innenseite der Gasbläschen gespeichert, wodurch das Material piezoelektrische Eigenschaften erhält, welche deutlich besser sind als die der herkömmlichen ferroelektrischen Polymere. Für die bisher gebräuchlichen Polypropylenschäume wurde neben der Temperaturstabilität mittels dielektrischer Resonanzspektroskopie auch das Verhalten unter UV-Bestrahlung untersucht. Aufgrund ihrer beschränkten thermischen Stabilität sind diese Schäume nicht für Anwendungen oberhalb von 50 °C geeignet. Mittels eines Lösungsmittelbasierten Schäumungsverfahrens wurde ein alternativer Werkstoff auf der Basis von amorphem Teflon[®] entwickelt, welcher einen stabilen piezoelektrischen Koeffizienten von 600 pC/N bei Temperaturen von bis zu 120 °C aufweist.

Contents

1	Introduction	1
2	A Brief History of Space Charge Electrets	2
3	Charge Storage Mechanisms	4
4	Characterization	8
4.1	Polarization and Space Charge Profiling	9
4.1.1	Acoustic Methods	9
4.1.2	Thermal Methods	10
4.2	Piezoelectric Resonances	12
5	Applications	14
6	Conclusions and Outlook	18
	References	20
	Appendix	32
A	Journal and Review Articles	32
	Thermally stable dynamic piezoelectricity... (Appl. Phys. Lett. 79 , 1852 (2001))	33
	Ultraviolet-induced discharge currents... (Appl. Phys. Lett. 82 , 254 (2003)) . .	36
	Dielectric Resonance Spectroscopy... (IEEE TDEI 10 , 842 (2003))	39
	Photostimulated discharge in electret polymers... (IEEE TDEI 11 , 218 (2004))	59
	Unbiased iterative reconstruction... (Meas. Sci. Technol. 15 , 1347 (2004))	69
	Fast thermal pulse measurements... (Rev. Sci. Instr. 76 , <i>in press</i> (2005))	77
	Three-dim. mapping of polarization... (Appl. Phys. Lett., <i>submitted</i> (2004)) . .	83
B	ITG Award Certificate	86
C	Curriculum Vitae	88
	Acknowledgments	89

1 Introduction

In today's world of sophisticated mechanical, electromechanical and electronic applications, polymers are playing an increasingly important part. Their most significant advantage over other materials is their complex structure, which can be physically or chemically tailored for specific applications. For electrical applications, they can be divided into two categories: (semi-)conducting and insulating polymers. The former have only recently started to enter the market on a large scale, but show great promise in applications ranging from antistatic coatings to optoelectronics and all-polymer integrated circuits. In 2000, the pioneering work by HEEGER, MACDIARMID and SHIRAKAWA was awarded with the Nobel Prize in Chemistry [1].

In contrast, highly insulating polymers have been used extensively for, e. g., electrical cable insulation since their invention in the first half of the 20th century. Some of these materials, such as various fluoropolymers, were shown to store injected electrical charges for long periods of time [2], even at elevated temperatures. The invention of the electret condenser microphone [3] and the discovery of piezo- and pyroelectricity in polyvinylidene fluoride [4] opened up a wide market for electromechanical transducer applications. Additionally, electrets are used in radiation dosimeters and gas filters [5]. In recent years, non-polar *ferroelectrets* [6] with high piezoelectric coefficients have received considerable attention. On the other hand, injected space charge may also have detrimental effects on the host polymer [7]. For example, oxidation of cross-linked polyethylene is known to enhance the accumulation of space charge near the electrodes, and in turn lead to electric breakdown [8], thus causing premature failure of high-voltage cable insulations. DISSADO *et al.* developed a model based on the reduction of the free-energy barrier to degradation which is in good agreement with thermo-electrical degradation measurements [9], although it should be mentioned that there is still some controversy as to whether space charge is a precursor to aging or merely its consequence [10]. Nevertheless, being able to characterize, control and limit charge injection appears to be an important factor in the prevention of high-voltage accidents which pose a severe risk of property damage and injury.

While applications of space-charge electrets are well established, understanding the unusually high stability of space charges in some materials is still an evolving topic. Traditionally, charge transport phenomena in organic semiconductors have been described using the same continuum descriptions and models originally developed for inorganic semiconductors [11], such as band theory, space-charge limited currents, etc., although there now appears to be a consensus that effects of discrete charged particles and their interactions with their local environments need to be taken into account [12]. Possible charge trapping mechanisms and experimental evidence will be covered in section 3.

In view of the importance of space-charge electrets for commercial applications, it is evident that accurate techniques of characterizing space charge with respect to their concentration, distribution and stability are needed. Even more important, future electret research will increasingly depend on a multi-technique approach, combining electrical with thermal, optical and mechanical methods. It is therefore essential that space-charge characterization techniques be made compatible with each other. Section 4 summarizes some recent developments in this area.

A deeper understanding of the mechanisms of charge storage will ultimately lead to improved materials for applications, particularly in the area of electromechanical transducers. Already, the new class of non-polar *ferroelectrets* based on charge-storing polymers has become available on the market [13]. Recent developments in this area are discussed in section 5.

2 A Brief History of Space Charge Electrets

Charge storage in dielectric materials can be traced back at least to ancient Greece. At that time, it was well-known that by rubbing amber against a fur cloth it would attract other things (such as straw) in its vicinity. In fact, the Greek word for amber, *ηλεκτρον* (*electron*), was later used to name not only a fundamental elementary particle carrying negative charge, but – in various derivatives, such as electricity, electrodynamics or electronics – entire branches of modern physics and engineering. For more than two millennia, this effect was regarded as a mere scientific curiosity. However, this did not prevent people from studying the phenomenon in greater detail. In the 18th century, GRAY [14] investigated the electrostatic attraction of a number of charged materials, such as resins and waxes. A century later, FARADAY [15] gave a definition of electret materials that still in use today, by describing them as dielectrics “which retain an electric moment after the externally-applied field has been reduced to zero”. The term *electret* was coined by HEAVISIDE in 1885¹ [16] in analogy to the already established *magnet*. The first systematic investigation of electrets was performed by EGUCHI in 1919 [18], who introduced the important technique of *thermal charging*, where the material is exposed to a high electric field while being cooled down from an elevated temperature (cf. Fig. 1). He also discovered that the charge adjacent to the electrode may have either the same sign as than on the electrode (subsequently named *homocharge* by GEMANT [19]) or the opposite sign (*heterocharge*). The latter was later shown by Gross [20, 21] to be due to oriented molecular dipoles while the former results from injected interfacial charges. In the following years, other charging methods, such as high-energy electrons [22], corona discharge [23] and liquid contacts [24, 25] were introduced.

¹The commonly quoted year of 1892 is that of a reprint of the original work [17].

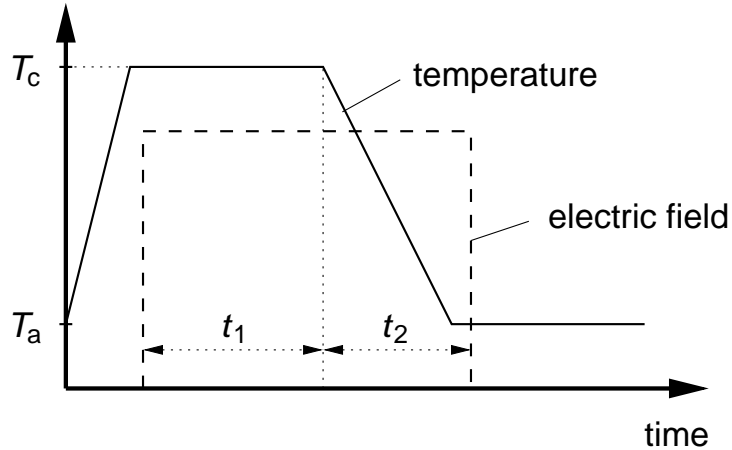


Figure 1: Thermal charging of electrets: the material is heated from ambient temperature T_a to an elevated charging temperature T_c , where an electric field is applied for a time of t_1 . The electric field is maintained for a time t_2 during and after the cool-down phase.

Table 1: Selected insulating polymers. Years indicate the beginning of commercialization. (From [27, 28, 29].)

Polymer	Producer	Year	conductivity $[(\Omega \text{ cm})^{-1}]$
Poly(vinyl chloride) (PVC)	B. F. Goodrich	1927	10^{-16}
Polystyrene (PS)	I. G. Farben/Dow	1930	$< 10^{-16}$
Polyethylene (PE)	ICI	1939	$10^{-15} \dots 10^{-18}$
Polyethylene terephthalate (PETP)	ICI	1941	$< 10^{-14}$
Polytetrafluoroethylene (PTFE)	Dupont	1945	10^{-18}
Poly(vinylidene fluoride) (PVDF)	Dupont		10^{-14}

Until the 1940s electret research focused on naturally available materials, such as Carnauba wax (which, ironically, is still quoted by some physics textbooks as one of the few existing electret materials [26]). An important breakthrough came with the industrial synthesis of insulating polymers, such as polyethylene (PE), polypropylene (PP) and polytetrafluoroethylene (PTFE) (Tab. 1). Their high specific resistance made them natural candidates for electret materials. Their electret properties were studied extensively by FUKADA [30]. A turning point in the quest for applications of charge-storing materials was the invention of the electret condenser microphone by SESSLER and WEST in 1962 [3], where sound causes a charged fluoropolymer membrane to vibrate in front of a static metal back electrode (Fig. 2). Unlike earlier condenser microphones, this design needs no external bias voltage. Together with its high-quality, linear performance, this property soon turned it into the microphone of choice in numerous applications; the present annual production is estimated to be around 2×10^9 units. Another important finding was the discovery of piezoelectricity in poly(vinylidene fluoride) (PVDF) by KAWAI in 1969 [4].

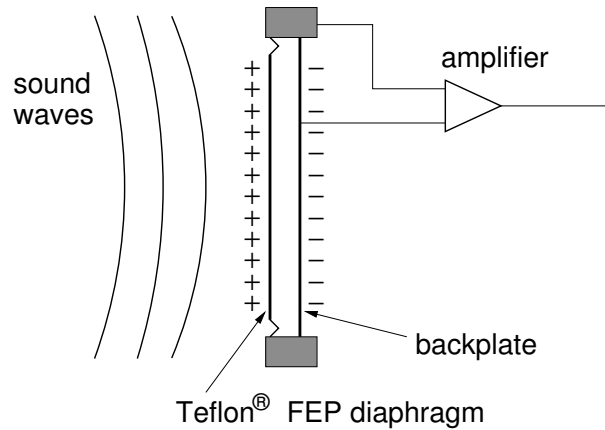


Figure 2: Cross section of an electret condenser microphone.

Since then, this material and its copolymers has found many uses in ultrasound transducers [31]. In recent years, new materials, such as amorphous Teflon[®] AF [32, 33] or Cyclic Olefin Copolymers (COCs) [34] have been found to have useful charge-storing properties. Research into electrets received a further boost when a new class of non-polar porous or cellular space charge electrets were found to have useful quasi-piezoelectric and ferroelectric properties [35]. These materials have received much attention in basic research as well as for transducer applications [36]. For a more detailed account of the history of electret research, see Refs. [5] and [28].

3 Charge Storage Mechanisms

Even though the phenomenon of charge storage in dielectric materials has been known to mankind for more than two millennia, and widespread industrial use started more than 40 years ago, surprisingly little is known about the microscopic mechanisms of charge storage. One may ask why no better understanding has been achieved in this field, when investigations of processes at a molecular level are commonplace [37]. Part of the reason is that the electrical charge is highly diluted even in the best charge-storing polymers. For example, peak surface charge densities of 2500 C/m^3 have been reported in corona-charged PTFE [38]. This is equivalent to $16\,000 \text{ traps } \mu\text{m}^{-3}$ or 1 charge in a cube with 40 nm edges. In contrast, bulk charge densities are 1...2 orders of magnitude smaller. With typical interatomic distances in the 0.1...0.2 nm range, the charge “concentration” relative to the host material is of the order of 0.5 parts per million (ppm), even in the most optimistic case. In addition, the presence of impurities (traces of polymerization catalysts, additives, radicals) in the bulk and the effects of the electrode-polymer interface [39] provides an often ill-defined environment. It is not surprising, therefore, that charging behavior was found to depend on the specific details of sample preparation, surface condition and

residual stresses [40]. In spite of these problems, a number of important observations and theoretical calculations have recently shed some light onto the problem of charge storage.

Despite its high dilution in the polymer host, space charge is easily detected at the macroscopic level using sensitive electrometers. For example, in a polymer film of 25 μm thickness and an area of 1 cm^2 , the above mentioned charge densities amount to a space charge in the nC... μC range. Many early measurements of charge-storing polymers were therefore carried out by observing conduction and discharge currents. Thermally stimulated discharge (TSD) and thermally stimulated currents (TSC) have provided a large amount of information on the thermal stability of space charges in electrets [2, 41]. By far the most stable space charge was observed in negatively charged Teflon[®] PTFE and FEP. From open-circuit TSC data, VON SEGGERN and REMKE deduced that the charges must be located in traps with energies around 0.7-1.25 eV near the surface and up to 1.7 eV in the bulk [42, 43]. Charging at temperatures between 200 and 250 °C resulted in a nearly homogeneous volume charge [38]. The nature of these traps, however, remained unknown. Any trap site must stabilize the charge via interactions with its molecular environment. Therefore, trap depths may be expected to cover a wide energy range, from less than 0.1 eV for dipolar and van der Waals interactions, as well as conformational disorders (sometimes named “physical traps”), up to 8 eV if the trapped charge modifies the covalent bonding of the polymer (chemical traps). Assuming an Arrhenius behavior, the charge life-time in the trap is given by

$$\tau = \tau_0 e^{E_{\text{trap}}/(kT)}, \quad (1)$$

where E_{trap} is the trap depth, T is the temperature, k is Boltzmann’s constant and τ_0^{-1} is the “attempt-to-escape” frequency, which is of the order of typical molecular vibration frequencies (10^{13} Hz). Extrapolated from measurements at elevated temperature [44, 45], room temperature lifetimes in the range of $10^3 \dots 2.6 \times 10^5$ years have been found. According to Eq. (1), these values require trap-depths of at least 1.5 eV, which is near the top end of the observed TSD lifetimes and suggests that chemical bond modification plays an important part. This was further supported by a recent molecular modeling approach: MEUNIER *et al.* calculated trap energies in the presence of impurities commonly found in the type of polyethylene used for cable insulation [46] and found charge carrier densities of up to 10^{17} cm^{-3} with lifetimes of 30 000 years. In addition, some of the impurities have been identified through their luminescence spectra [47]. A direct observation of trapped space charges at a molecular level was reported by LEGRAND *et al.* who used electron spin resonance (ESR) on electron-beam irradiated isotactic polypropylene films [48]. Besides the formation of radicals, they also observed an extra line in the ESR spectrum which they attributed to trapped electrons.

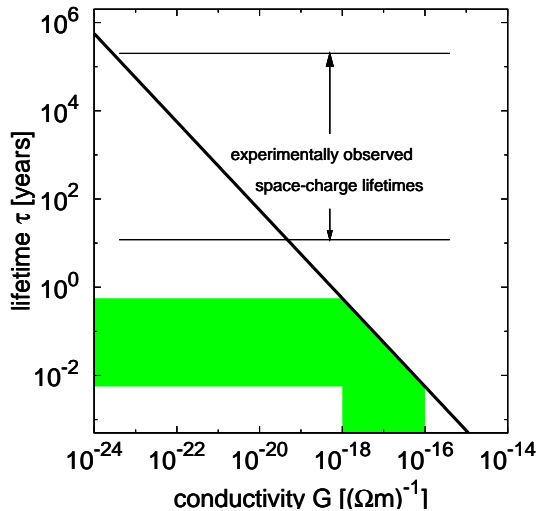


Figure 3: Space-charge lifetime τ versus electrical conductivity G , as given by Eq. (5). With experimental conductivities between 10^{-16} and $10^{-18} (\Omega\text{m})^{-1}$ (shaded area), space charge should decay on a timescale of days or months, rather than millennia. (Adapted from [49].)

Another puzzle is the apparent conflict of these lifetimes with the published conductivities of PTFE in the range of $10^{-16} \dots 10^{-18} (\Omega\text{m})^{-1}$. For the case of ohmic conductivity, the current density j is given by [28]

$$j = -\frac{d\sigma}{dt} = GE, \quad (2)$$

where σ is the surface charge density, G is the conductivity and E is the internal electric field. Assuming a thin space-charge layer near one of the electrodes, the electric field in the sample is nearly homogeneous and given by

$$E = \frac{\sigma}{\epsilon_0\epsilon}, \quad (3)$$

where ϵ_0 is the permittivity of free space and ϵ is the dielectric constant of the polymer. Typical values for PTFE and its copolymers are $\epsilon \approx 2$. Solving the differential equation obtained by inserting Eq. (3) into (2) yields

$$\sigma = \sigma_0 \exp(-t/\tau) \quad (4)$$

with the charge lifetime

$$\tau = \frac{\epsilon_0\epsilon}{G}. \quad (5)$$

For the conductivities given above, this results in lifetimes of the order of days, weeks or months (cf. Fig. 3), but fails to explain the extrapolated lifetimes of up to 2.6×10^5

years. MAŁECKI suggested an elegant rate equation model [49], where carrier annihilation at the electrode and by free, implanted charges causes a transition from a short-term, exponential decay – resulting from ohmic conductivity – to a long-term linear decay over thousands of years. Again, this model requires the presence of deep traps to minimize thermal activation of charge carriers.

Due to thermal decomposition of polymers at higher temperatures, trap energies above 1.5 eV are inaccessible by thermal methods. Photostimulated discharge (PSD) spectroscopy [50], a technique where charge carriers are excited out of their traps by absorption of monochromatic visible or UV radiation, can fill in the missing information. PSD was initially used in the near-infrared and visible spectral range to analyze trap parameters in crystalline organic materials, such as anthracene [51]. Its advantages over TSD are a superior energy resolution (limited, in most cases, by homogeneous line broadening) and access to energy levels in the range up to 8 eV, similar to those of chemical bonds in the polymer chain. For example, ODA *et al.* found evidence for a single trapping level in Teflon[®] FEP at 4.9 eV [52]. Special care must be taken, though, to separate the various sources of photocurrents [53], such as the external photoeffect and photoconductivity. It is therefore essential that PSD be combined with other techniques to monitor changes in the space charge density. This was demonstrated on PTFE, PETP and PP, as presented on p. 59 ff. [54]. The PSD spectrum of PTFE shows an onset of the photocurrent at $\lambda = 250$ nm. Irradiation at 240 nm for 50 min caused a reduction of charge in the bulk, as measured with the acoustic PPS method (see section 4.1.1). Due to the limited spatial resolution, it was not possible, though, to distinguish between near-surface charges in the polymer and compensation charges on the metal electrode. The PSD spectrum and the observed change in space charge density are consistent with the release of trapped charges from traps with a depth of 4.6 eV, in fair agreement with ODA's results [52].

Due to its large band gap of 8.4 eV [55], PTFE is transparent down to the vacuum ultraviolet (VUV) region. In PETP, on the other hand, the presence of the phenyl ring gives rise to a strong optical absorption edge near 310 nm, resulting from a transition derived from the benzene $^1A_{1g} \rightarrow ^1B_{2u}$ (1L_b) absorption band [56]. In the same region, a pronounced peak appears in the PSD spectrum [54]. Successive irradiation of PETP at 303 and 310 nm results in a red-shifted current maximum, which can be explained by preferential de-trapping of charge carriers from traps with energies between 4.0 and 4.2 eV. The observed state-selective detrapping also gives support to the hypothesis of direct photo-induced detrapping over any indirect process.

The most pronounced case of state-selective detrapping was found in cellular polypropylene [54, 57]. The material exhibits three PSD current maxima at 276, 223 and 198 nm, which can be (at least partially) selectively bleached by irradiation at the respective wavelengths. Due to the attenuation of pressure-pulses in this soft material, no space-charge measurements were performed. Instead, its piezoelectric activity (cf. section 5)

was monitored *in situ* with the piezoelectric resonance technique described in section 4.2. No change in its d_{33} coefficient was found during irradiation at 276 and 223 nm, whereas irradiation below 210 nm resulted in a gradual reduction of d_{33} . As the piezoelectric properties are caused by charges trapped on the inner surfaces of the voids, this observation directly links these charges to the 6.2 eV traps corresponding to the 198 nm maximum in the PSD spectrum. Recently, UV-induced charge depletion has also been observed in cyclic olefin copolymer (COC) films [58,59]. Here, the acoustic space-charge profiling was replaced by the thermal pulse method (cf. section 4.1.2), which can be used while the sample is being irradiated.

With the increasing evidence for deep-level charge traps, how can this picture be reconciled with the lower activation energies obtained from thermal methods? One possibility is a distribution of traps over a broad range of energies, from less than 1 eV up to at least 6 eV. This is supported by the fact that photoinduced removal of space charge from 4...6 eV traps has only led to a partial reduction of the space charge density in PTFE, PETP and PP [54]. On the other hand, thermally stimulated discharge experiments are known to quantitatively discharge the polymer, which manifests itself as the so-called ρ peak in the TSD thermogram [41]. The ρ peak generally appears at a higher temperature than the α relaxation associated with the glass transition temperature, indicating the importance of polymer chain mobility in the discharge process [60]. With increasing chain mobility, charges located in deep traps could be transported through the polymer matrix and may eventually reach the surface region where detrapping or charge compensation will take place. This “charge transport” mechanism is similar to the “wet dog” effect described by KRYSZEWSKI *et al.* [61]. A third possible discharge mechanism is compensation by movable ions.

4 Characterization

Characterization of fundamental material parameters, as well as measurement of specific sample or device properties, are key elements in the quest for understanding the microscopic mechanisms of charge storage. The progress in electret research would not have been possible without a wide range of methods to characterize electrets with respect to their electrical, thermal, mechanical and chemical properties. Ultimately, the improved understanding of material properties will lead to improved materials and devices, such as electromechanical transducers or high-voltage cable insulation. In the history of electret research, numerous characterization techniques have been developed, some of which are still in active use today. In many cases, the precision and sensitivity can be improved substantially by implementing them with modern laboratory and computer equipment. Moreover, progress in this field increasingly depends on combining several methods in order to gain a complete picture of the chemical, physical and electrical properties of the

material under investigation. In this section, we shall focus on non-destructive, *in situ* techniques to map out space charge densities in one and three dimensions, as well as to obtain electrical, electromechanical and mechanical parameters and monitor their changes under, e. g., ultraviolet irradiation.

4.1 Polarization and Space Charge Profiling

During the past three decades, numerous techniques for obtaining space charge and polarization depth profiles in insulating materials have been developed [62] and applied to a wide range of topics, such as the accumulation of space charge in high-voltage cable insulations [63], the development and optimization of pyroelectric and piezoelectric sensors [64, 65], and basic research into the mechanisms of charge storage [54] in electret polymers. All depth-profiling methods use an external stimulus (usually thermal, mechanical, or electrical) to generate a response (electrical or mechanical) which carries information on the spatial distribution of embedded electric dipoles or space charges.

4.1.1 Acoustic Methods

Acoustic techniques rely on a pressure step or wave, generated via the absorption of an ultrashort laser pulse (Laser Induced Pressure Pulse, LIPP) [66, 67] or a fast piezoelectric transducer (Pressure Wave Propagation (PWP) method [68, 69], also known as Piezoelectrically generated Pressure Pulse (PPS) method [70]) to obtain a short-circuit current which is recorded with a fast oscilloscope. Alternatively, a short electrical pulse applied to a piezoelectric material or space-charge electret generates a traveling pressure front which can be picked up with a microphone (Pulsed Electro-Acoustic technique, PEA) [71]. Using modern laboratory equipment, a time resolution of 1 ns can be achieved for both PPS [38] and PEA. With a speed of sound of approx. 2 $\mu\text{m}/\text{ns}$ (a typical value for many polymers [72]), this translates into a the spatial resolution of 2 μm , which remains approximately constant throughout the sample. A potential advantage of PEA is the fact that the detection circuit is electrically decoupled from the sample, so that investigations under high electric fields can be performed without the risk of damaging expensive and sensitive amplifier equipment [73]. Very recently, IMAI *et al.* demonstrated an open-electrode PEA system where the specimen surface is accessible so that surface and internal charge distributions can be measured simultaneously [74]. For all acoustic techniques, extracting polarization and space charge profiles from the measured current response is straightforward. LEAL FERREIRA and GERHARD-MULTHAUPT derived first-order response equations [75] applicable to both acoustic and thermal methods (cf. Section 4.1.2).

Several research groups have combined acoustic depth-profiling with in-plane scanning to obtain two- or three-dimensional polarization or space charge maps. ALQUIÉ *et al.* used LIPP to map out the surface distribution of space charges on Teflon[®] FEP [67] with a

lateral resolution of 0.2 mm, while IMAIZUMI reported three-dimensional images of the space-charge distribution in polymethyl methacrylate (PMMA) with a 1 mm resolution using a PEA setup with spatially confined electrodes [76, 77]. Data acquisition for each point took about 1 min. A much faster system (3 s acquisition time per point) was built by QIN *et al.* who used an acoustic lens to focus a pressure wave on a small region of approx. 1 mm² [78, 79]. Acoustic focusing was later applied to PEA by MAENO, enabling him to probe only a small region (approx. 0.5 mm in diameter) of the sample [80]. HOLÉ and LEWINER compared two approaches, one using LIPP with wedge-shaped target electrodes at different angles of incidence, the other using PEA with a transducer array, and visualized the space charge distributions with anaglyph images [81].

Both PWP and PEA usually require an acoustic coupling between generator and sample on the one hand, and sample and detector on the other hand. This can be a severe constraint if the charge profile investigation is to be performed in real time and *in situ*, especially when at least one of the electrodes must be accessible by, e. g., visible or UV radiation. Nevertheless, changes in the space charge depth profile of polyethylene terephthalate have been detected using the PPS technique [54]. No such constraint exists for LIPP; the only requirement here is that the front electrode be opaque to the laser light and capable of withstanding the light pulses for at least one shot. Recently, LIPP has been used to detect surface charges in inhomogeneous dielectrics [82, 83]. Standard mode-locked Nd:YAG lasers deliver pulse lengths of approx. 5 ns, equivalent to a spatial resolution of 10 μm . Thus, achieving a resolution on a μm scale already requires the use of expensive lasers capable of delivering picosecond pulses [66]. In combination with a new generation of ultra-fast digital storage oscilloscopes achieving bandwidths of up to 10 GHz, a sub- μm resolution appears feasible, albeit at substantial cost.

4.1.2 Thermal Methods

Thermal techniques use the absorption of a short light pulse or a periodically modulated laser beam by an opaque surface layer to create a time-dependent, spatially varying temperature distribution. In samples that are either pyroelectric or contain an electric space charge, this gives rise to a short-circuit current, which again carries information on the polarization or space-charge depth profile. Although initial insights into the potential of these techniques were obtained by PHELAN and PETERSON in their investigation of the frequency response of pyroelectric detectors [84, 85], the first dedicated study of space charge profiles by means of thermal pulses was reported by COLLINS [86, 87]. A key difference to acoustic methods is the fact that the propagation of the thermal pulse or wave is a diffusion phenomenon rather than a linear propagation, which greatly complicates signal analysis. Initially, it was assumed that thermal pulses are only suitable for obtaining charge centroids [88], since extracting a charge or polarization profile from the measured current involves solving a Fredholm integral equation of the first kind, which

is an ill-conditioned problem [89]. Later, however, several deconvolution methods were shown to yield polarization depth-profiles [90,91,92,93], albeit with decreasing resolution at larger depths. While the first thermal pulse experiments were carried out with Xenon flashlamps delivering pulse durations in the $\mu\text{s} \dots \text{ms}$ range (which is not short compared to the diffusion time for distances in the μm range) [87], later implementations used mode-locked pulsed laser sources with pulse durations in the ns range (and corresponding diffusion lengths well below $0.1 \mu\text{m}$), which simplifies data analysis.

A frequency-domain counterpart to the thermal pulse technique was introduced by LANG and DAS-GUPTA [94], now commonly referred to as thermal wave technique or Laser Intensity Modulation Method (LIMM). Here, the top electrode is irradiated with an intensity-modulated continuous-wave (cw) laser beam while the short-circuit current is recorded with a phase-sensitive lock-in amplifier. With relatively modest laboratory equipment, this technique is capable of achieving a near-surface depth resolution of less than $0.1 \mu\text{m}$ [95]. The deconvolution process of the signal is similar to that used for thermal pulses. The LIMM equation [96] which relates the polarization or space-charge depth profile to the measured current was solved using, e. g., Tikhonov regularization [97,98], polynomial expansion [99], neural networks [100] and a *Monte Carlo*-based technique [101]. A particularly simple and straightforward scale transformation technique was introduced by PLOSS *et al.* who demonstrated that the difference between the real and imaginary part of the pyroelectric current is proportional to the pyroelectric coefficient [102]. However, this method is limited to regions near the heated surface. For depths larger than one quarter of the sample thickness, the accuracy decreases significantly.

Modern computational power permitted a new promising approach using an iterative method [103] (cf. p. 69), previously known from digital image processing and signal reconstruction. Simulations showed slightly smaller residuals than those obtained using Tikhonov regularization. In addition, this technique also appeals from an educational point of view, since it visualizes how the “true” depth profile gradually emerges from a starting solution as the iteration progresses. One suitable initial distribution is the scale transformation solution. With increasing number of iterations, its deficiencies at larger depths are gradually corrected.

A direct comparison between the time- and frequency-domain approaches [59] (cf. p. 77) showed excellent agreement for a space-charge profile in corona-charged PTFE. However, the thermal-pulse data was acquired up to 50 times faster than the LIMM measurement. This allows the real-time monitoring of thermally or optically induced charge decay on a timescale of minutes, rather than hours, as demonstrated on a pyrene-doped COC (TOPAS[®] 8007, Ticona) film, where irradiation at 300 nm significantly accelerated the space-charge decay [59,58]. The frequency-domain data analysis, well established for LIMM, was shown to be also applicable to thermal data which had been transformed to the frequency domain via a Fast Fourier Transform (FFT). This approach

has the advantage that it easily accommodates the correction of amplifier-induced phase shifts.

The fast data acquisition of the thermal pulse technique was used for obtaining a three-dimensional polarization profile of a corona-poled PVDF film [104] (cf. p. 83) by means of a tightly focused laser beam. The lateral resolution of 40 μm (combined with a depth resolution of better than 0.5 μm) represents a significant advance over previous attempts of multi-dimensional polarization or space-charge mapping. Acoustic techniques have not yet resolved features less than 0.5 mm wide [80]. With focused LIMM (FLIMM) [105], a resolution in the 10 μm range has been reported, but the long measurement times in the frequency domain either severely limited the number of beam pointings [105] or constrained the number of frequencies to a few selected values [106]. However, the modelling of the focused thermal pulse propagation through the two-layer system consisting of the metal electrode and the polymer film (and its influence on the pyroelectric current) is a non-trivial problem and currently under investigation [107]. There is evidence, however, that metal electrodes with their high thermal diffusivity² will limit the lateral resolution to approx. 1/30th of the sample thickness [104].

A review of thermal depth-profiling techniques was published in Ref. [108]. Their strengths, but also their limitations are highlighted by a recent discussion of the spatial resolution [109]. Comparisons between thermal and acoustic techniques [110, 111] have shown good agreement. All-optical techniques, such as thermal pulses and LIMM, are the method of choice for investigating soft, piezoelectric polymer foams [112], which are easily deformed upon applying a mechanical stress. They can be applied *in situ* [58], even when the sample is stored in vacuum. In addition, they have been successfully applied to study heat diffusion processes in solids. Even in the absence of polarization or space charge, information on the thermal diffusivity of polymers has been obtained by applying a bias voltage and detecting the electric-field-induced pyroelectricity [113]. Alternatively, diffusivity values have been calculated by recording the phase-shift of the transient temperature at the front and back electrode as a function of the modulation frequency [58, 114].

4.2 Piezoelectric Resonances

Since the discovery of the piezoelectric properties of poly(vinylidene fluoride) (PVDF) by KAWAI in 1969 [4], piezoelectric polymers have been used in a wide range of sensor and actuator applications. [115]. Compared to their inorganic counterparts they have the advantage of mechanical flexibility, good acoustic coupling to aqueous media, and relatively low cost per unit area, which opens up the possibility of large-area transducers. For most applications, the material of choice is PVDF or one of its copolymers with, e. g., trifluoroethy-

²Typical thermal diffusivity values are $\approx 10^{-4} \text{ cm}^2 \text{ s}^{-1}$ for metals and $\approx 10^{-7} \text{ cm}^2 \text{ s}^{-1}$ for polymers.

lene (TrFE) or hexafluoropropylene (HFP) [116]. Several other polymers have been shown to have potentially useful piezoelectric properties, such as odd-numbered polyamides [117], copolymers of vinylidene cyanide (VDCN) [118], polyureas [119], polyurethane [120], and polythioureas [121]. In all these materials, the basis of their piezoelectric behavior is the orientation of molecular dipoles, either in the form of a remanent polarization in ferroelectric domains or a frozen-in polarization in the amorphous phase. Typical room-temperature piezoelectric coefficients are of the order of 20...40 pC/N. Recently, however, several materials and systems have been described in the literature [36] that contain macroscopic rather than molecular dipoles and exhibit an electrical response under mechanical stress (and, conversely, a mechanical response upon an electrical stimulus) which matches or exceeds that of traditional piezoelectric polymers³.

The very active research in the field of piezoelectric polymers necessitates efficient methods for measuring their electrical, electromechanical and mechanical properties. One technique that has proven to be extremely useful and versatile is the analysis of resonances in the dielectric spectrum [122]. Just as in traditional dielectric or impedance spectroscopy [123], the electroded sample is subjected to an AC voltage while the current response is monitored with a phase-sensitive detector. In piezoelectric materials, this electrically induced stress will excite mechanical resonances at specific frequencies that depend on the elastic and piezoelectric properties as well as the geometry and density. Analysis of these resonances and comparison with a theoretical model thus yields a range of material parameters from a single dielectric spectrum. By using samples with suitable geometric shapes (such as thin plates, long strips or thin cylinders), individual components of the elastic and piezoelectric tensors can be probed. In contrast to traditional dielectric spectroscopy, where the covered frequency range extends over many orders of magnitude [124], resonance scans cover only a relatively narrow range (often substantially less than one decade), but with a much higher frequency resolution.

Piezoelectric resonances have been known since at least 1919 [125], and the first theoretical descriptions were given by CADY [126] and VON LAUE [127]. Soon, this technique found numerous applications in the study of, e. g., quartz resonators and piezo ceramics [128]. A systematic collection of equations applicable to simple geometries was compiled by BERLINCOURT *et al.* [129] and later incorporated into the *IEEE Standard on Piezoelectricity* [130]. However, its relevance to piezoelectric polymers was not recognized until 1976 when OHIGASHI recorded resonance spectra of PVDF [131] at temperatures between -170 and 100°C , and was thus able to obtain the temperature dependence of several piezoelectric coefficients. A similar study was conducted by SCHEWE [132], while PVDF copolymers were investigated by FURUKAWA [133] and OMOTE *et al.* [134]. The relatively few number of publications making use of the resonance technique on piezoelec-

³Some authors use the term *quasi-piezoelectricity* materials (cf. section 5) to distinguish this property from that of materials based on molecular dipoles.

tric polymers may be partly due to the fact that the signal amplitude (i. e., the modulation of the dielectric frequency spectrum by the resonance) is approximately proportional to the *square* of the piezoelectric coefficient. For materials with small coefficients the measurement accuracy may therefore be inferior to that achieved with, e. g., interferometric or quasistatic techniques. With the advent of electroactive polymer foams with large d_{33} coefficients, however, the lower sensitivity is no longer a limiting factor. On the other hand, dielectric measurements yield more parameters than interferometric methods. They also can be performed *in situ*, without applying a mechanical stress, so that small changes ($< 0.5\%$) in the piezoelectric coefficients and elastic moduli can be observed. This has been used advantageously to characterize very soft porous Teflon[®] AF films [135], and to monitor the decay of the piezoelectric activity in cellular polypropylene (PP) under UV irradiation [57] (cf. p. 36). The latter in particular has led to a new appreciation of the role of deep trap levels in the microscopic mechanisms of charge storage [54]. In addition, using modern dielectric spectrometers capable of measuring sample with loss factors as low as 10^{-5} , d_{33} coefficients of less than 10 pC/N in odd-numbered polyamides have been successfully measured via the resonance method [136]. While these values are not as high as those found in PVDF (let alone the d_{33} coefficients in cellular materials), they were shown to be stable up to 200 °C and are thus of interest for high-temperature applications.

The current state of dielectric resonance spectroscopy on piezoelectric polymers has been summarized in a recent review article [122] (cf. p. 39). Apart from an overview of recent work in this area, the paper also serves as a tutorial for acquiring and analyzing resonance data.

5 Applications

As described in section 2, electret condenser microphones are still the most widely used application of charge-storing polymers, although several recent publications (see, e. g., [137, 138]) have demonstrated the feasibility of using inorganic SiO₂ layers or SiO₂/Si₃N₄ double layers as charge-storing membranes, which are more compatible with silicon-based semiconductor devices than polymer electret films and can be manufactured in very small sizes using well-known micro-machining techniques. On the other hand, polymers are the material of choice for large-scale pyroelectric and piezoelectric transducers. Their properties most often used are piezoelectricity and pyroelectricity. The former requires a non-centrosymmetric material, while the presence of oriented dipoles is a prerequisite for the latter. Traditionally, polymer transducers have been based on ferroelectric polymers, such as PVDF or odd-numbered polyamides (see section 4.2). The good acoustic impedance match to aqueous environments is widely used in underwater hydrophone probes [139, 140] and in ultrasound transducers for medical imaging [141]. As thin films

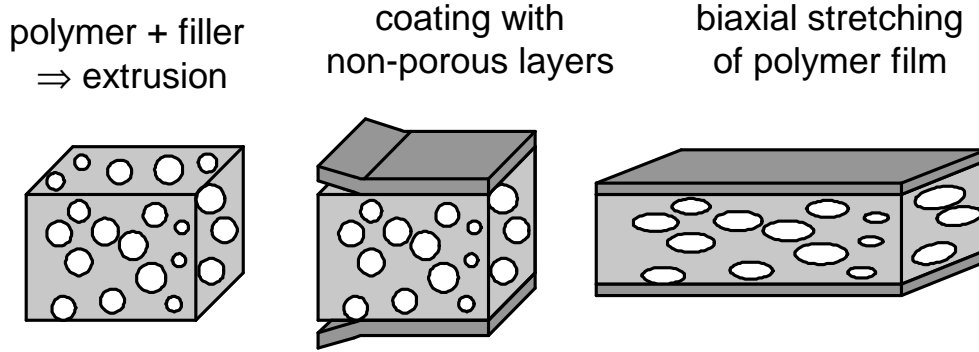


Figure 4: Preparation of cellular polypropylene films. (From [146].)

exhibit a high thickness extension resonance frequency [122], device bandwidths of up to 24 GHz have been reported [142]. The main drawback of ferroelectric polymers as compared to ceramic materials are their relatively low piezo- and pyroelectric coefficients.

A major break-through in the quest for polymer films with high piezoelectric coefficients came when it was realized that a piezoelectricity-like effect can also result from electric dipoles at a macroscopic, rather than a molecular level. For instance, KACPRZYK described a two-layer system of corona-charged PP and elastic polyurethane (PU) films [143], while GERHARD-MULTHAUPT *et al.* investigated stacks of corona-charged porous and non-porous polytetrafluoroethylene (PTFE) [144] and reported piezoelectric d_{33} coefficients of up to 35 pC/N. Even higher values of up to 150 pC/N were obtained by KÜNSTLER *et al.* with single layers of porous PTFE carrying a bipolar space charge [145]. Perhaps most significant is a new class of cellular space charge electrets [36] based on a concept by KIRJAVAINEN [35]. As shown in Fig. 4, flat voids are created by means of biaxially stretching a composite film consisting of a polypropylene polymer host and an inorganic filler, such as CaCO_3 . After inflation, typical void dimensions are 30...100 μm in diameter and 1...5 μm in height (Fig. 5(a)). Very similar films are also used in the packaging industry, where the microvoids serve both as thermal insulation and to give the polymer film an attractive glossy look [148]. Subjecting these films to a high electric field is thought to initiate Paschen breakdown in the cavities, with subsequent charge separation and charge trapping on the inner surfaces (Fig. 5(b)). This model is supported by several recent experimental observations. Microdischarges have been observed through their luminescence [149, 150], and the bipolar charge distribution was visualized via the secondary emission yield in a scanning electron microscope (SEM) [151]. The induced macroscopic polarization can be reversed by applying a sufficiently high electric field in the opposite direction [150] (a characteristic of *ferroelectric* materials). Even electrical and electromechanical hysteresis was observed [6], although this behavior was recently shown not to be related to the polarization, but rather results from interfacial charge injection and/or charge generation by external gas-discharges at the electrode edges [152]. Due

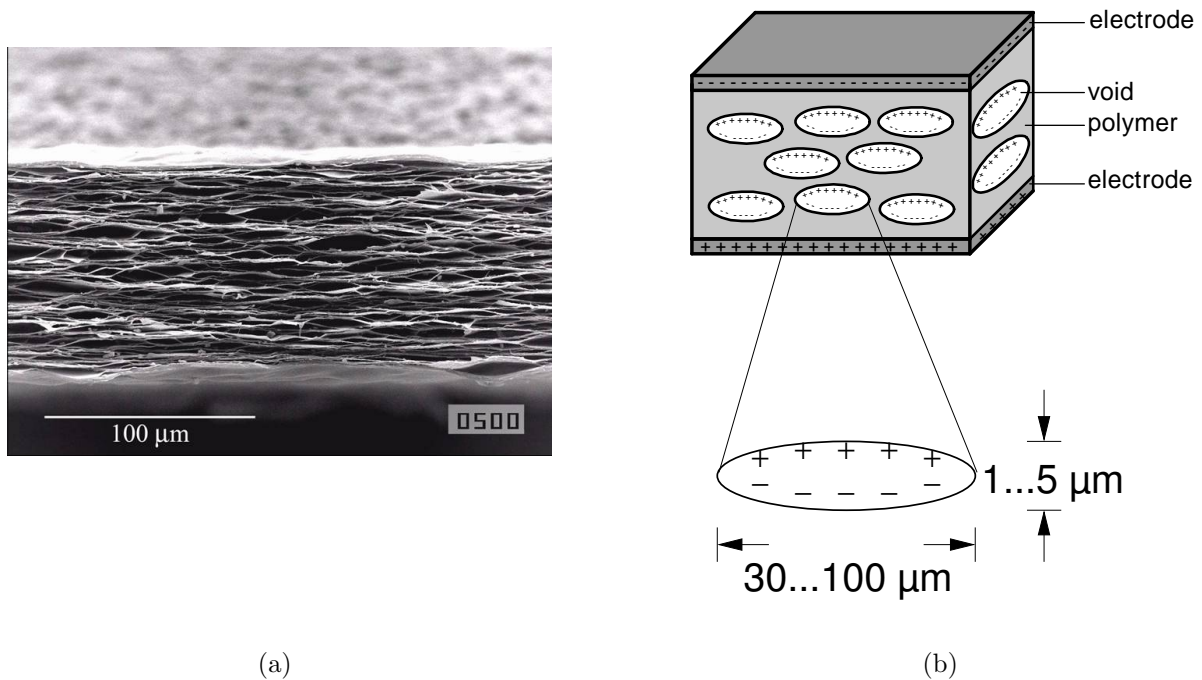


Figure 5: Cross-sectional view of a cellular polypropylene film. (a) Scanning electron micrograph (from [147]). (b) Schematic view of the void sizes and charge distribution.

to their piezoelectric properties (see below) and switchable polarization (both of which are characteristic properties of ferroelectric materials), the term *ferroelectrets* has been introduced in the literature [6].

Applying a mechanical stress to these materials changes the vertical dimensions of the voids and therefore the dipole moment of the separated $+/-$ charges trapped on the internal surfaces. Consequently, the macroscopic polarization changes, giving rise to a quasi-piezoelectric response. As these polymer foams are relatively soft perpendicular to their film plane (typical c_{33} elastic moduli are between 1 and 10 MPa [153]), the resulting piezoelectric d_{33} coefficients are at least 1 order of magnitude larger than those found in conventional ferroelectric polymers, such as PVDF [154]. Through charging in a suitable dielectric gas atmosphere at elevated pressure [147], these coefficients were increased up to 790 pC/N. The shape of the cavities can be optimized by means of a gas inflation treatment [155], resulting in even higher coefficients of up to 1500 pC/N [156,157]. Biaxially stretched polymer foams are highly anisotropic media, and therefore exhibit large d_{33} coefficients but relatively small d_{31} values and little pyroelectricity [158]. This may be advantageous for certain applications to minimize cross-sensitivities.

Based on these ferroelectrets, numerous applications for large-area transducers have been suggested or are already commercially available. For instance, using large mats of these films it is possible to monitor the motion of people and even identify individuals [159]

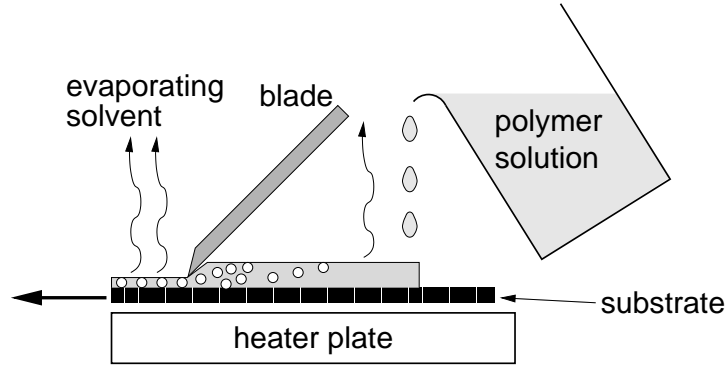


Figure 6: “Doctor blade” technique for producing a porous Teflon[®] AF film (an amorphous copolymer of the PTFE family with excellent optical transmission [166] and good solubility in several perfluorinated organic solvents) from a polymer solution in Fluorinert[®] FC-77. The pores are created through fast evaporation of the solvent on the hot substrate.

based on single footsteps. Cellular PP films have further been used for monitoring physiological processes in humans and animals [160] and as audio pickups in musical instruments and in loudspeakers [161, 162]. Another promising area of applications is active vibration and noise control [163]. With large-area transducers, this would be easier to achieve than with an array of relatively few loudspeakers.

A severe drawback for applications in, e. g., the automotive sector, is the relatively low thermal stability of cellular PP films. At temperatures above 50 °C the increased conductivity leads to a gradual charge neutralization [164] and thus a loss of their piezoelectric properties, although short-term heating up to 60 °C actually increases the d_{33} coefficient as the material becomes softer [165]. On the other hand, fluoropolymers have long been known to have excellent charge storage properties up to 150-250 °C [38]. The difficulty lies in finding a suitable processing technique to produce fluoropolymer foams with the required mechanical and electromechanical properties. Using a “doctor-blade” technique (Fig. 6), porous Teflon[®] AF films were drop-cast from a solution in Fluorinert[®] FC-77. After sealing the open pores with a layer of non-porous Teflon[®] AF and subsequent corona-charging, the samples exhibited a piezoelectric coefficient of 600 pC/N at temperatures of up to 120 °C [57] (cf. p. 33). The large d_{33} coefficient is caused by the low elastic modulus of only $c_{33} \approx 150$ kPa. Although this is very close to the bulk modulus of air, experiments at reduced pressure have demonstrated that this low value is due to the porous morphology of the polymer rather than the trapped gas. Similar piezoelectric coefficients have also been found in porous PTFE [167]. However, production of transducer devices on an industrial scale is currently hampered by the complex manufacturing process or the high cost of the polymer resin. The quest for a thermally stable ferroelectret with

high piezoelectric activity is a very active field of research, as, e. g., in the DURASMART cooperation [168].

Apart from terrestrial applications, piezoelectric polymers are also being used in a variety of space missions. For example, the Dust Flux Monitor Instrument (DFMI), which is part of the Stardust mission instrument payload [169], uses a PVDF film to monitor impacting dust particles with a mass of $< 10^{-7}$ kg. Active vibration damping with piezoelectric actuators has been considered as an alternative to heavy electromagnetic systems [170]. Evidently, these systems would benefit from the higher piezoelectric coefficients of the new ferroelectrets. However, as the material may be exposed to the extraterrestrial solar radiation field, the stability against ultraviolet (UV) radiation is of prime concern. Using dielectric resonance spectroscopy as a sensitive probe to monitor small changes in the electromechanical properties (cf. p. 36 and 59) it was shown [57] that prolonged irradiation at wavelengths below 210 nm leads to a gradual reduction of the d_{33} coefficient in cellular PP. For a UV flux similar to that of the standard “air mass zero” (AM0) solar spectrum [171], a 3.5 h irradiation at 200 nm decreased the piezoelectric activity by as much as 4% [54]. Adequate shielding from solar UV radiation is therefore essential for space-based applications.

6 Conclusions and Outlook

Space-charge electrets have been playing an important part in electromechanical transducer applications for more than 40 years. Recent developments in cellular space-charge electrets (the so-called *ferroelectrets*) will undoubtedly enhance their role and spawn new applications. On the other hand, much has yet to be learned about the microscopic mechanisms of charge storage. Recently, evidence has been found for deep-level trapping of charge carriers in polypropylene, polytetrafluoroethylene, polyethylene terephthalate and cyclic olefin copolymers. In particular, state-selective bleaching of current peaks in the photostimulated discharge spectra of PETP and PP indicates a distribution of trap levels at energies above 4 eV. A picture is now emerging where the long-term lifetime of surplus charge carriers is governed by their strong binding to the molecular chains, whereas the lower trap depths measured in thermally stimulated discharge experiments may result from shallower physical traps, charge compensation by movable ions, or from the transport of trapped charges along with the moving polymer chains.

Refined space-charge detection techniques allow the *in situ* monitoring of space charge distributions, thus permitting a multi-disciplinary approach to study charges as they are injected, trapped and de-trapped. However, they are limited to measuring the net charge density, and therefore cannot detect charges that are locally compensated by carriers of the opposite sign. Despite the recent advances in single-molecule detection, it remains to be seen whether the study of single charges can be achieved in the near to medium-term

future. Once this important goal has been achieved, specially engineered space-charge electrets with optimized charge storage properties could become reality.

While research into the fundamentals of charge storage is still underway, new piezoelectric materials based on voided space-charge electrets are already entering the market. It is very likely that films with a thermal stability up to 100°C will be available within the next few years, thus opening up a wide range of applications. From active noise control in cars and airplanes to flat-panel loudspeakers at home, use of cellular electrets may become as ubiquitous as the electret microphone invented more than 40 years ago.

References

- [1] B. Goss Levi, *Nobel prize in chemistry salutes the discovery of conducting polymers*. *Physics Today* **53**, 19 (2000).
- [2] J. van Turnhout, *Thermally Stimulated Discharge of Polymer Electrets*. Elsevier, Amsterdam (1975).
- [3] G. M. Sessler and J. E. West, *Self-biased condenser microphone with high capacitance*. *J. Acoust. Soc. Am* **34**, 1787 (1962).
- [4] H. Kawai, *The piezoelectricity of poly(vinylidene fluoride)*. *Jpn. J. Appl. Phys.* **8**, 975–977 (1969).
- [5] R. Gerhard-Multhaupt (ed.), *Electrets*, vol. 2. 3rd ed., Laplacian Press, Morgan Hill, CA (1999).
- [6] S. Bauer, R. Gerhard-Multhaupt and G. M. Sessler, *Ferroelectrets: Soft electroactive foams for transducers*. *Physics Today* **57**, 37–43 (2004).
- [7] L. A. Dissado and J. C. Fothergill, *Electrical Degradation and Breakdown in Polymers*. Peter Peregrinus Ltd., London (1992).
- [8] T. Mizutani, *Space charge measurement techniques and space charge in polyethylene*. *IEEE Trans. Diel. Electr. Insul.* **1**, 923–933 (1994).
- [9] L. A. Dissado, G. Mazzanti and G. C. Montanari, *The role of trapped space charges in the electrical aging of insulating materials*. *IEEE Trans. Diel. Electr. Insul.* **4**, 496–506 (1997).
- [10] J.-P. Crine, *On the interpretation of some electrical aging and relaxation phenomena in solid dielectrics*. In: *Annual Report, Conference on Electrical Insulation and Dielectric Phenomena*, pp. 1–16, IEEE Service Center, Piscataway, NJ (2004).
- [11] M. Pope and C. E. Swenberg, *Electronic processes in organic crystals and polymers*. Oxford Univ. Press, New York (1999).
- [12] J. C. Fothergill and L. A. Dissado, *Fere libenter homines id quod volunt credunt – so what have [we] learnt about space charge?*. In: J. C. Fothergill and L. A. Dissado (eds.), *Space Charge in Solid Dielectrics*, pp. 327–333, Dielectrics Society, Leicester, England (1998).
- [13] EMFIT Ltd., Vaajakoski, Finland. <http://www.emfit.com/>.
- [14] S. Gray, *A letter from Mr. Stephen to Dr. Mortimer, Secr. R. S., containing a farther account of his experiments concerning electricity*. *Phil. Trans. R. Soc. London, Ser. A* **37**, 285–291 (1732).
- [15] M. Faraday, *Experimental Researches in Electricity*. Richard and John Edward Taylor, London (1839).
- [16] O. Heaviside, *Electromagnetic induction and its propagation. Electrization and Electrification. Natural Electrets*. *The Electrician* pp. 230–231 (7 Aug. 1885).

- [17] —, *Electromagnetic induction and its propagation. Electrization and Electrification. Natural Electrets*. In: O. Heaviside (ed.), *Electrical Papers*, vol. 1, pp. 488–493, Chelsea, New York (1892).
- [18] M. Eguchi, *On dielectric polarisation*. Proc. Phys. Math. Soc. Jpn., Series 3 **1**, 326–331 (1919).
- [19] A. Gemant, *Electrets*. Philos. Mag. **20**, 929 (1935).
- [20] B. Gross, *Experiments on electrets*. Phys. Rev. **66**, 26–28 (1944).
- [21] —, *On permanent charges in solid dielectrics. II. Surface charges and transient currents in carnauba wax*. J. Chem. Phys. **17**, 866–872 (1949).
- [22] —, *Irradiation effects in plexiglass*. J. Polym. Sci. **27**, 135–143 (1958).
- [23] J. A. Giacometti, S. Fedosov and M. M. Costa, *Corona charging of polymers: Recent advances on constant current charging*. Braz. J. Phys. **29**, 269–279 (1999).
- [24] P. W. Chudleigh, *Charging of polymer foils using liquid contacts*. Appl. Phys. Lett. **21**, 547 (1972).
- [25] —, *Mechanism of charge transfer to a polymer surface by a conducting liquid contact*. J. Appl. Phys. **47**, 4475 (1976).
- [26] W. Raith, L. Bergmann, C. Schäfer and H. Gobrecht, *Lehrbuch der Experimentalphysik*, vol. 2: *Elektromagnetismus*. De Gruyter, Berlin (1999).
- [27] L. H. Sperling, *Introduction to physical polymer science*. 3rd ed., Wiley, New York (2001).
- [28] G. M. Sessler and R. Gerhard-Multhaupt (eds.), *Electrets*, vol. 1. 3rd ed., Laplacian Press, Morgan Hill, CA (1999).
- [29] Goodfellow Corp. <http://www.goodfellow.com>.
- [30] E. Fukada, *Piezoelectricity in polymers and biological materials*. Ultrasonics **6**, 229 (1968).
- [31] G. Eberle, H. Schmidt, B. Dehlen and W. Eisenmenger, *Piezoelectric polymer electrets*. In: R. Gerhard-Multhaupt (ed.), *Electrets*, vol. 2, 3 ed., chap. 11, pp. 81–128, Laplacian Press, Morgan Hill, CA (1999).
- [32] P. Günther and R. Gerhard-Multhaupt, *Electret properties of spin-coated Teflon-AF films*. In: *Annual Report, Conference on Electrical Insulation and Dielectric Phenomena*, pp. 197–202, IEEE Service Center, Piscataway, NJ (1993).
- [33] H. Ding, *Charge decay and transportation in Teflon AF films*. Proceedings, 8th International Symposium on Electrets pp. 89–94 (1994).
- [34] G. M. Sessler, G. M. Yang and W. Hatke, *Electret properties of cycloolefin copolymers*. In: *Annual Report, Conference on Electrical Insulation and Dielectric Phenomena*, pp. 467–470, IEEE Service Center, Piscataway, NJ (1997).

- [35] K. Kirjavainen, *Electromechanical film and procedure for manufacturing same*. US Patent No. 4,654,546 (1987).
- [36] R. Gerhard-Multhaupt, *Less can be more: Holes in polymers lead to a new paradigm of piezoelectric materials for electret transducers*. IEEE Trans. Diel. Electr. Insul. **9**, 850–859 (2002).
- [37] T. Basché, W. E. Moerner and M. Orrit, *Single-Molecule Optical Detection, Imaging and Spectroscopy*. Wiley-VCH, Weinheim (1996).
- [38] R. Gerhard-Multhaupt, W. Künstler, G. Eberle, W. Eisenmenger and G. Yang, *High space-charge densities in the bulk of fluoropolymer electrets detected with piezoelectrically generated pressure steps*. In: J. C. Fothergill and L. A. Dissado (eds.), *Space Charge in Solid Dielectrics*, pp. 123–132, Dielectrics Society, Leicester, England (1998).
- [39] H. Wintle, *Charge motion in technical insulators: Facts, fancies and simulations*. IEEE Trans. Diel. Electr. Insul. **10**, 826–841 (2003).
- [40] G. Damamme, C. L. Gressus and A. S. DeReggi, *Space charge characterization for the 21st century*. IEEE Trans. Diel. Electr. Insul. **4**, 558–584 (1997).
- [41] J. van Turnhout, *Thermally stimulated discharge of electrets*. In: *Electrets*, vol. 1, 3 ed., chap. 3, pp. 81–215, Laplacian Press, Morgan Hill, CA (1999).
- [42] H. von Seggern, *Isothermal and thermally stimulated current studies of positively corona charged (Teflon FEP) polyfluoroethylenepropylene*. J. Appl. Phys. **52**, 4081–4085 (1981).
- [43] R. L. Remke and H. von Seggern, *Modelling of thermally stimulated currents in polytetrafluoroethylene*. J. Appl. Phys. **54**, 5262–5266 (1983).
- [44] Z. Xia, R. Gerhard-Multhaupt, W. Künstler, A. Wedel and R. Danz, *High surface charge stability of porous polytetrafluoroethylene electret film at room and elevated temperatures*. J. Phys. D Appl. Phys. **32**, L83–L85 (1999).
- [45] Z. Xia, A. Wedel and R. Danz, *Charge storage and its dynamics in porous polytetrafluoroethylene (PTFE) film electrets*. IEEE Trans. Diel. Electr. Insul. **10**, 102–108 (2003).
- [46] M. Meunier, N. Quirke and A. Aslanides, *Molecular modeling of electron traps in polymer insulators: Chemical defects and impurities*. J. Chem. Phys. **115**, 2876–2881 (2001).
- [47] G. Teyssedre, C. Laurent, A. Aslanides, N. Quirke, L. A. Dissado, G. C. Montanari, A. Campus and L. Martinotto, *Deep trapping centers in crosslinked polyethylene investigated by molecular modeling and luminescence techniques*. IEEE Trans. Diel. Electr. Insul. **8**, 744–752 (2001).
- [48] M. Legrand, G. Dreyfus and J. Lewiner, *First E.S.R. observation of injected electrons trapped in electrets*. J. Physique Lett. **38**, L439–L440 (1977).

- [49] J. A. Małecki, *Linear decay of charge in electrets*. Phys. Rev. B **59**, 9954–9960 (1999).
- [50] J. D. Brodribb, D. O’Colmain and D. M. Hughes, *The theory of photon-stimulated current spectroscopy*. J. Phys. D **8**, 856–862 (1975).
- [51] —, *Photon-stimulated current analysis of trap parameters in anthracene*. J. Phys. D **9**, 256–263 (1976).
- [52] T. Oda, T. Utsumi, T. Kumano and M. Itami, *Observation of photo-stimulated detrapping currents of FEP Teflon electrets*. In: G. M. Sessler and R. Gerhard-Multhaupt (eds.), *Proceedings, 5th International Conference on Electrets*, pp. 288–293, IEEE Service Center, Piscataway, NJ (1985).
- [53] J. P. Crine and A. Yelon, *Photogeneration and transport of carriers in atactic polystyrene*. J. Appl. Phys. **51**, 2106–2114 (1980).
- [54] A. Mellinger, F. Camacho González and R. Gerhard-Multhaupt, *Photostimulated discharge in electret polymers: an alternative approach for investigating deep traps*. IEEE Trans. Diel. Electr. Insul. **11**, 218–226 (2004).
- [55] M. Yun, K. Yoshino, Y. Inuishi and M. Kawatsu, *Photoconduction in polytetrafluoroethylene induced by vacuum-ultraviolet light*. Jpn. J. Appl. Phys. **21**, 1592–1595 (1982).
- [56] J. P. LaFemina and G. Arjavalingam, *Photophysics of poly(ethylene terephthalate): Ultraviolet absorption and emission*. J. Phys. Chem. **95**, 984–988 (1991).
- [57] A. Mellinger, F. Camacho González and R. Gerhard-Multhaupt, *Ultraviolet-induced discharge currents and reduction of the piezoelectric coefficient in cellular polypropylene films*. Appl. Phys. Lett. **82**, 254–256 (2003).
- [58] A. Mellinger, R. Singh, F. Camacho González, Z. Szamel and I. Głowacki, *In situ observation of optically and thermally induced charge depletion in chromophore-doped cyclic olefin copolymers*. In: *Annual Report, Conference on Electrical Insulation and Dielectric Phenomena*, pp. 498–501, IEEE Service Center, Piscataway, NJ (2004).
- [59] A. Mellinger, R. Singh and R. Gerhard-Multhaupt, *Fast thermal-pulse measurements of space charge distributions in electret polymers*. Rev. Sci. Instr. **76** (2005, *in press*).
- [60] D. K. Das-Gupta, *Molecular processes in polymer electrets*. J. Electrostatics **51-52**, 159–166 (2001).
- [61] M. Kryszewski, J. Ulański, J. K. Jezka and M. Zielinski, *Chain and carrier mobility in polymer systems as investigated by thermally stimulated current techniques*. Polymer Bull. **8**, 187–192 (1982).
- [62] S. Bauer and S. Bauer-Gogonea, *Current practice in space charge and polarization profile measurements using thermal techniques*. IEEE Trans. Diel. Electr. Insul. **10**, 883–902 (2003).

- [63] K. R. Bambery and R. J. Fleming, *Space charge accumulation in two power cable grades of XLPE*. IEEE Trans. Dielect. Electr. Insul. **5**, 103–109 (1998).
- [64] S. Bauer, *Poled polymers for sensors and photonic applications*. J. Appl. Phys. **80**, 5531–5558 (1996).
- [65] M. Wegener and R. Gerhard-Multhaupt, *Electric poling and electromechanical characterization of 0.1-mm-thick sensor films and 0.2-mm-thick cable layers from piezoelectric poly(vinylidene fluoride-trifluoroethylene)*. IEEE Trans. Ultrason., Ferroelectr., Freq. Contr. **50**, 921–931 (2004).
- [66] G. M. Sessler, J. E. West, R. Gerhard-Multhaupt and H. von Seggern, *Nondestructive laser method for measuring charge profiles in irradiated polymer films*. IEEE Trans. Nucl. Sci. **29**, 1644–1648 (1982).
- [67] C. Alquié, G. Charpak and J. Lewiner, *Pulsed laser determination of surface electric charge distributions*. J. Physique Lett. **43**, L687–L693 (1982).
- [68] P. Laurenceau, G. Dreyfus and J. Lewiner, *New principle for the determination of potential distributions in dielectrics*. Phys. Rev. Lett. **38**, 46–49 (1977).
- [69] C. Alquié and J. Lewiner, *A new method for studying piezoelectric materials*. Revue Phys. Appl. **20**, 395–402 (1985).
- [70] W. Eisenmenger and M. Haardt, *Observation of charge compensated polarization zones in polyvinylidene fluoride (PVDF) films by piezoelectric acoustic step-wave response*. Solid State Communications **41**, 917–920 (1982).
- [71] T. Takada, T. Maeno and H. Kushibe, *An electric stress pulse technique for the measurement of charges in a plastic plate irradiated by an electron beam*. In: *Proceedings, 5th International Symposium on Electrets*, pp. 450–455, IEEE Service Center, Piscataway, NJ (1985).
- [72] D. R. Lide and H. P. R. Frederikse (eds.), *CRC Handbook of Chemistry and Physics*. 75th ed., CRC Press (1995).
- [73] T. Takada, *Acoustic and optical methods for measuring electric charge distributions in dielectrics*. IEEE Trans. Dielect. Electr. Insul. **6**, 519–547 (1999).
- [74] S. Imai, Y. Tanaka, T. Fukao, T. Takada and T. Maeno, *Development of new PEA system using open upper electrode*. In: *Annual Report, Conference on Electrical Insulation and Dielectric Phenomena*, IEEE Service Center, Piscataway, NJ (2004).
- [75] G. F. Leal Ferreira and R. Gerhard-Multhaupt, *Derivation of response equations for the nondestructive probing of charge and polarization profiles*. Phys. Rev. B **42**, 7317–7321 (1990).
- [76] Y. Imaizumi, K. Suzuki, Y. Tanakoa and T. Takada, *Three-dimensional space charge distribution measurement in solid dielectrics using pulsed electroacoustic method*. In: *Proceedings, International Symposium on Electrical Insulating Materials, Tokyo*, pp. 315–318, IEEE Service Center, Piscataway, NJ (1995).

- [77] Y. Imaizumi, K. Suzuki, Y. Tanaka and T. Takada, *Three-dimensional space charge distribution measurement in electron beam irradiated PMMA*. Trans. IEEJ **116-A**, 684–689 (1996).
- [78] X. Qin, K. Suzuki, M. Sasaki, Y. Tanaka and T. Takada, *Electric charge 3-dimensional profile measurement in dielectrics using acoustic microscope probe head*. In: *Proceedings, IEEE International Conference on Conduction and Breakdown in Solid Dielectrics*, pp. 13–16, IEEE Service Center, Piscataway, NJ (1998).
- [79] X. Qin, K. Suzuki, Y. Tanaka and T. Takada, *Three-dimensional space-charge measurement in a dielectric using the acoustic lens and PWP method*. J. Phys. D: Appl. Phys. **32**, 157–160 (1999).
- [80] T. Maeno, *Three-dimensional PEA charge measurement system*. IEEE Trans. Diel. Electr. Insul. **8**, 845–848 (2001).
- [81] S. Holé and J. Lewiner, *High-resolution multidimensional space charge measurement using elastic wave methods*. Phys. Rev. B **64**, 104106 (2001).
- [82] D. Malec and T. Lebey, *Laser-induced pressure pulse as a tool to determine surface charges in inhomogeneous (solid/gas) dielectric*. Appl. Phys. Lett. **80**, 1421–1423 (2002).
- [83] D. Malec, *Study of static electricity using the laser-induced pressure pulse method*. Meas. Sci. Technol. **15**, N1–N5 (2004).
- [84] R. J. Phelan Jr., R. L. Peterson, C. A. Hamilton and G. W. Day, *The polarization of PVF and PVF₂ pyroelectrics*. Ferroelectrics **7**, 375–377 (1974).
- [85] R. L. Peterson, G. W. Day, P. M. Gruzensky and R. J. Phelan Jr., *Analysis of response of pyroelectrical optical detectors*. J. Appl. Phys. **45**, 3296–3303 (1974).
- [86] R. E. Collins, *Distribution of charge in electrets*. Appl. Phys. Lett. **26**, 675–677 (1975).
- [87] —, *Analysis of spatial distribution of charges and dipoles in electrets by a transient heating technique*. J. Appl. Phys. **47**, 4804–4808 (1976).
- [88] H. von Seggern, *Thermal-pulse technique for determining charge distributions: Effect of measurement accuracy*. Appl. Phys. Lett. **33**, 134–137 (1978).
- [89] E. W. Weisstein, *Fredholm integral equation of the first kind*. From MathWorld – A Wolfram Web Resource, <http://mathworld.wolfram.com/FredholmIntegralEquationoftheFirstKind.html>.
- [90] F. I. Mopsik and A. S. DeReggi, *Numerical evaluation of the dielectric polarization distribution from thermal-pulse data*. J. Appl. Phys. **53**, 4333–4339 (1982).
- [91] S. Bauer, *Method for the analysis of thermal-pulse data*. Phys. Rev. B **47**, 11049–11055 (1993).
- [92] B. Ploss, *Probing of pyroelectric distributions from thermal wave and thermal pulse measurements*. Ferroelectrics **156**, 345–350 (1994).

- [93] P. Bloß, A. S. DeReggi and H. Schäfer, *Electric-field profile and thermal properties in substrate-supported dielectric films*. Phys. Rev. B. **62**, 8517–8530 (2000).
- [94] S. B. Lang and D. K. Das-Gupta, *A technique for determining the polarization distribution in thin polymer electrets using periodic heating*. Ferroelectrics **39**, 1249–1252 (1981).
- [95] T. Sandner, G. Suchaneck, R. Koehler, A. Suchaneck and G. Gerlach, *High frequency LIMM – a powerful tool for ferroelectric thin film characterization*. Integr. Ferroelectr. **46**, 243–257 (2002).
- [96] S. B. Lang and D. K. Das-Gupta, *Laser-intensity-modulation method: A technique for determination of spatial distributions of polarization and space charge in polymer electrets*. J. Appl. Phys. **59**, 2151–2160 (1986).
- [97] A. N. Tikhonov, A. V. Goncharskii, V. V. Stepanov and I. V. Kochikov, *Ill-posed image processing problems*. Sov. Phys.-Doklady **32**, 456–458 (1987).
- [98] J. Weese, *A reliable and fast method for the solution of Fredholm integral equations of the first kind based on Tikhonov regularization*. Computer Phys. Commun. **69**, 99–111 (1992).
- [99] S. B. Lang, *Polynomial solution of the Fredholm integral equation in the laser intensity modulation method (LIMM)*. Integr. Ferroelectr. **38**, 111–118 (2001).
- [100] —, *Use of neural networks to solve the integral equation of the laser intensity modulation method (LIMM)*. Ferroelectrics **238**, 281–289 (2000).
- [101] E. Tuncer and S. B. Lang, *Numerical extraction of distributions of space-charge and polarization from laser intensity modulation method* (2004), <http://arxiv.org/abs/cond-mat/0409316>.
- [102] B. Ploss, R. Emmerich and S. Bauer, *Thermal wave probing of pyroelectric distributions in the surface region of ferroelectric materials: A new method for the analysis*. J. Appl. Phys. **72**, 5363–5370 (1992).
- [103] A. Mellinger, *Unbiased iterative reconstruction of polarization and space-charge profiles from thermal-wave experiments*. Meas. Sci. Technol. **15**, 1347–1353 (2004).
- [104] A. Mellinger, R. Singh, M. Wegener, W. Wirges, R. Gerhard-Multhaupt and S. B. Lang, *Three-dimensional mapping of polarization profiles with thermal pulses*. Appl. Phys. Lett. (2004, *submitted*).
- [105] D. Marty-Dessus, L. Berquez, A. Petre and J. L. Franceschi, *Space charge cartography by FLIMM: a three-dimensional approach*. J. Phys. D: Appl. Phys. **35**, 3249–3256 (2002).
- [106] A. Quintel, J. Hulliger and M. Wübbenhorst, *Analysis of the polarization distribution in a polar perhydrotriphenylene inclusion compound by scanning pyroelectric microscopy*. J. Phys. Chem. B **102**, 4277–4283 (1998).
- [107] A. Mellinger, R. Singh, M. Wegener, W. Wirges, R. Gerhard-Multhaupt and S. B. Lang. J. Appl. Phys. (*in preparation*).

- [108] S. B. Lang, *Laser intensity modulation method (LIMM): Review of the fundamentals and a new method for data analysis*. IEEE Trans. Diel. Electr. Insul. **11**, 3–12 (2004).
- [109] B. Ploss, *The resolution of thermal profiling techniques*. In: *Proceedings, 11th International Symposium on Electrets*, pp. 177–180, IEEE Service Center, Piscataway, NJ (2002).
- [110] D. K. Das-Gupta, J. S. Hornsby, G. M. Yang and G. M. Sessler, *Comparison of charge distributions in FEP measured with thermal wave and pressure pulse techniques*. J. Phys. D: Appl. Phys. **29**, 3113–3116 (1996).
- [111] P. Bloß, M. Steffen, H. Schäfer, G.-M. Yang and G. M. Sessler, *Determination of the polarization distribution in electron-beam-poled PVDF using heat wave and pressure pulse techniques*. IEEE Trans. Diel. Electr. Insul. **3**, 182–190 (1996).
- [112] J. van Turnhout, R. E. Staal, M. Wübbenhorst and P. H. de Haan, *Distribution and stability of charges in porous polypropylene films*. In: *Proceedings, 10th International Symposium on Electrets*, pp. 785–788, IEEE Service Center, Piscataway, NJ (1999).
- [113] S. Bauer and A. S. DeReggi, *Pulsed electrothermal technique for measuring the thermal diffusivity of dielectric films on conducting substrates*. J. Appl. Phys. **80**, 6124–6128 (1996).
- [114] S. Bauer and B. Ploss, *A method for the measurement of the thermal, dielectric, and pyroelectric properties of thin pyroelectric films and their applications for integrated heat sensors*. J. Appl. Phys. **68**, 6361–6367 (1990).
- [115] E. Fukada, *History and recent progress in piezoelectric polymers*. IEEE Trans. Ultrason., Ferroelectr., Freq. Contr. **47**, 1277–1290 (2000).
- [116] H. Nalwa (ed.), *Ferroelectric Polymers*. Marcel Dekker Inc., New York (1995).
- [117] B. Newman, J. Scheinbeim, J. Lee and Y. Takase, *A new class of ferroelectric polymers, the odd-numbered nylons*. Ferroelectrics **127**, 229–234 (1992).
- [118] S. Miyata, M. Yoshikawa, S. Tasaka and M. Ko, *Piezoelectricity revealed in the copolymer of vinylidene cyanide and vinyl acetate*. Polym. J. **12**, 857–860 (1980).
- [119] S. Tasaka, T. Shouko and N. Inagaki, *Ferroelectric polarization reversal in polyureas with odd number of CH₂ groups*. Jpn. J. Appl. Phys. **31**, L1086–L1088 (1992).
- [120] S. Tasaka, T. Shouko, K. Asami and N. Inagaki, *Ferroelectric behavior in aliphatic polyurethanes*. Jpn. J. Appl. Phys. **33**, 1376–1379 (1994).
- [121] S. Tasaka, K. Ohishi and N. Inagaki, *Ferroelectric behavior in aliphatic polythioureas*. Ferroelectrics pp. 203–210 (1995).
- [122] A. Mellinger, *Dielectric resonance spectroscopy: a versatile tool in the quest for better piezoelectric polymers*. IEEE Trans. Diel. Electr. Insul. **10**, 842–861 (2003).
- [123] A. K. Jonscher, *Dielectric Relaxation in Solids*. Chelsea Dielectrics Press, London (1983).

- [124] F. Kremer and A. Schönhalz (eds.), *Broadband Dielectric Spectroscopy*. Springer, Heidelberg (2003).
- [125] A. M. Nicolson, *The piezo electric effect in the composite rochelle salt crystal*. AIEE Transactions **38**, 1467–1485 (1919).
- [126] W. G. Cady, *Theory of longitudinal vibrations of viscous rods*. Phys. Rev. Lett. **19**, 1–6 (1922).
- [127] M. v. Laue, *Piezoelektrisch erzwungene Schwingungen von Quarzstäben*. Z. für Physik **34**, 347–361 (1925).
- [128] W. G. Cady, *Piezoelectricity*. Dover Publications (1962).
- [129] D. A. Berlincourt, D. R. Currand and H. Jaffe, *Piezoelectric and piezomagnetic materials*. In: W. P. Mason (ed.), *Physical Acoustics*, vol. I, Pt. A, Academic, New York (1967).
- [130] *IEEE standard on piezoelectricity*. ANSI/IEEE Std. 176-1987 (1987).
- [131] H. Ohigashi, *Electromechanical properties of polarized polyvinylidene fluoride films as studied by the piezoelectric resonance method*. J. Appl. Phys. **47**, 949–955 (1976).
- [132] H. Schewe, *Piezoelectricity of uniaxially oriented polyvinylidene fluoride*. In: *IEEE International Ultrasonics Symposium*, pp. 519–524, IEEE Service Center, Piscataway, NJ (1982).
- [133] T. Furukawa, *Structure and functional properties of ferroelectric polymers*. Adv. Coll. Interf. Sci. **71-72**, 183–208 (1997).
- [134] K. Omote, H. Ohigashi and K. Koga, *Temperature dependence of elastic, dielectric, and piezoelectric properties of “single crystalline” films of vinylidene fluoride trifluoroethylene copolymer*. J. Appl. Phys. **81**, 2760–2768 (1997).
- [135] A. Mellinger, M. Wegener, W. Wirges and R. Gerhard-Multhaupt, *Thermally stable dynamic piezoelectricity in sandwich films of porous and nonporous amorphous fluoropolymer*. Appl. Phys. Lett. **79**, 1852–1854 (2001).
- [136] P. Frübing, A. Kremmer, W. Neumann, R. Gerhard-Multhaupt and I. L. Guy, *Dielectric relaxation of polyamide 11 in relation to piezo- and pyroelectricity*. IEEE Trans. Diel. Electr. Insul. **11**, 271–279 (2004).
- [137] H. Amjadi and G. M. Sessler, *Inorganic electret layers for miniaturized devices*. In: *Annual Report, Conference on Electrical Insulation and Dielectric Phenomena*, pp. 668–671, IEEE Service Center, Piscataway, NJ (1995).
- [138] H. Amjadi, *Electret membranes and backelectrodes for application in micromechanical transducers*. J. Electrostatics **48**, 179–191 (2000).
- [139] P. A. Howie and H. R. Gallantree, *Transducer applications of PVDF*. In: *Proceedings, IEEE International Ultrasonics Symposium*, pp. 566–569, IEEE Service Center, Piscataway, NJ (1983).

- [140] R. H. Tancrrell, D. T. Wilson and D. Ricketts, *Properties of PVDF for sonar*. In: *IEEE International Ultrasonics Symposium*, pp. 624–629, IEEE Service Center, Piscataway, NJ (1985).
- [141] F. S. Foster, K. A. Harasiewicz and M. D. Sherar, *A history of medical and biological imaging with polyvinylidene fluoride (PVDF) transducers*. *IEEE Trans. Ultrason., Ferroelectr., Freq. Contr.* **47**, 1363–1371 (2000).
- [142] A. Ambrosy and K. Holdik, *Piezoelectric PVDF films as ultrasonic transducers*. *J. Phys. E - Sci. Instr.* **17**, 856–859 (1984).
- [143] R. Kacprzyk, *Piezoelectric properties of nonuniform electrets*. *J. Electrostatics* **35**, 161–166 (1995).
- [144] R. Gerhard-Multhaupt, Z. Xia, W. Künstler and A. Pucher, *Preliminary study of multi-layer space-charge electrets with piezoelectric properties from porous and non-porous Teflon films*. In: *Proceedings, 10th International Symposium on Electrets*, IEEE Service Center, Piscataway, NJ (1999).
- [145] W. Künstler, Z. Xia, T. Weinhold, A. Pucher and R. Gerhard-Multhaupt, *Piezoelectricity of porous polytetrafluoroethylene single- and multiple-film electrets containing high charge densities of both polarities*. *App. Phys. A* **70**, 5–8 (2000).
- [146] M. Wegener and W. Wirges, *Optimized electromechanical properties and applications of cellular polypropylene, a new voided space-charge electret material*. In: H.-J. Fecht and M. Werner (eds.), *The Nano Micro Interface: Bringing the Nano and Micro Worlds Together*, pp. 303–317, Wiley-VCH (2004).
- [147] M. Paaajanen, M. Wegener and R. Gerhard-Multhaupt, *Charging of cellular space-charge electret films in various gas atmospheres*. In: *Annual Report, Conference on Electrical Insulation and Dielectric Phenomena*, pp. 24–27, IEEE Service Center, Piscataway, NJ (2001).
- [148] Treofan, Raunheim, Germany. <http://www.treofan.com>.
- [149] M. Wegener, M. Paaajanen, W. Wirges and R. Gerhard-Multhaupt, *Corona-induced partial discharges, internal charge separation and electromechanical transducer properties in cellular polymer films*. In: *Proceedings, 11th International Symposium on Electrets*, pp. 54–57, IEEE Service Center, Piscataway, NJ (2002).
- [150] M. Lindner, S. Bauer-Gogonea, S. Bauer, M. Paaajanen and J. Raukola, *Dielectric barrier microdischarges: Mechanism for the charging of cellular piezoelectric polymers*. *J. Appl. Phys.* **91**, 5283–5287 (2002).
- [151] J. Hillenbrand and G. M. Sessler, *Piezoelectric properties of polypropylene/air and poly(vinylidene fluoride)/air composites*. In: *Annual Report, Conference on Electrical Insulation and Dielectric Phenomena*, pp. 161–165, IEEE Service Center, Piscataway, NJ (2000).
- [152] S. Bauer, S. Bauer-Gogonea, M. Dansachmüller, I. Graz, G. Leonhartsberger and R. Schwödianer, *Do ferroelectrets always behave like ferroelectrics?*. In: *Annual Report, Conference on Electrical Insulation and Dielectric Phenomena*, IEEE Service Center, Piscataway, NJ (2004).

- [153] M. Wegener, W. Wirges, R. Gerhard-Multhaupt, M. Dansachmüller, R. Schwödiauer, S. Bauer-Gogonea, S. Bauer, M. Paaajanen, H. Minkkinen and J. Raukola, *Controlled inflation of voids in cellular polymer ferroelectrets: Optimizing electromechanical transducer properties*. Appl. Phys. Lett. **84**, 392–394 (2004).
- [154] R. Kressmann, *Linear and nonlinear piezoelectric response of charged cellular polypropylene*. J. Appl. Phys. **90**, 3489–3496 (2001).
- [155] M. Wegener, W. Wirges, J. Fohlmeister, B. Tiersch and R. Gerhard-Multhaupt, *Two-step inflation of cellular polypropylene films: void-thickness increase and enhanced electromechanical properties*. J. Phys. D: Appl. Phys. **37**, 623–627 (2004).
- [156] X. Zhang, J. Hillenbrand and G. M. Sessler, *Piezoelectric d_{33} coefficient of cellular polypropylene subjected to expansion by pressure treatment*. Appl. Phys. Lett. **85**, 1226–1228 (2004).
- [157] —, *Improvement of piezoelectric activity of cellular polymers using a double-expansion process*. J. Phys. D: Appl. Phys. **37**, 2146–2150 (2004).
- [158] G. S. Neugschwandtner, R. Schwödiauer, S. Bauer-Gogonea, S. Bauer, M. Paaajanen and J. Lekkala, *Piezo- and pyroelectricity of a smart polymer-foam space-charge electret*. J. Appl. Phys. **89**, 4503–4511 (2001).
- [159] J. Suutala and J. Röning, *Towards the adaptive identification of walkers: Automated feature selection of footsteps using distinction-sensitive lq*. In: *Int'l. Workshop on Processing Sensory Information for Proactive Systems (PSIPS 2004)*, Oulu, Finland (June 14-15, 2004).
- [160] J. Lekkala, R. Poramo, K. Nyholm and T. Kaikkonen, *EMF-force sensor – a flexible and sensitive electret film for physiological applications*. Medical & Biological Engineering & Computing **34**, Supplement 1, Part 1 (1996).
- [161] J. Backman, *Audio applications of electrothermomechanical film (ETMF)*. J. Audio Eng. Soc. **38**, 364–371 (1990).
- [162] J. Backman and M. Karjalainen, *Audio and ultrasonic transducers based on electrothermomechanical film ETMF*. In: *Proceedings, IEEE International Conference on Acoustics, Speech, and Signal Processing*, vol. 2, pp. 1173–1176, IEEE Service Center, Piscataway, NJ (1990).
- [163] H. Nykänen, M. Antila, J. Kataja, J. Lekkala and S. Uosukainen, *Active control of sound based on utilizing EMFi-technology*. In: *Proceedings, ACTIVE 99*, pp. 1159–1170, Ft. Lauderdale (Dec. 4-6, 1999).
- [164] J. Lekkala and M. Paaajanen, *EMFi – new electret material for sensors and actuators*. In: A. A. Konsta, A. Vassilikou-Dova and K. Vartzeli-Nikaki (eds.), *Proceedings, 10th International Symposium on Electrets*, pp. 743–746, IEEE Service Center, Piscataway, NJ (1999).
- [165] A. Mellinger and F. Camacho González, *Verhalten von quasi-piezoelektrischen Sensorfolien aus geschäumtem Polypropylen unter Wärme- und Lichteinwirkung*. In: *Sensoren und Messsysteme 2004. 12. GMA/ITG-Fachtagung*, Ludwigsburg (2004).

- [166] J. H. Lowry, J. S. Mendlowitz and N. S. Subramanian, *Optical characteristics of Teflon AF fluoroplastic materials*. *Optical Engineering* **31**, 1982–1985 (1992).
- [167] R. Gerhard-Multhaupt, W. Künstler, T. Görne, A. Pucher, T. Weinhold, M. Seiß, Z. Xia, A. Wedel and R. Danz, *Porous PTFE space-charge electrets for piezoelectric applications*. *IEEE Trans. Dielectr. Electr. Insul.* **7**, 480–488 (2000).
- [168] *DURASMART: Durable cellular polymer films with giant electromechanical response for smart transducer applications*. <http://www.vtt.fi/virtual/durasmart/>.
- [169] A. J. Tuzzolino, T. E. Economou, R. B. McKibben, J. A. Simpson, J. A. M. McDonnell, M. J. Burchell, B. A. M. Vaughan, P. Tsou, M. S. Hanner, B. C. Clark and D. E. Brownlee, *Dust flux monitor instrument for the Stardust mission to comet Wild 2*. *J. Geophys. Res. - Planets* **108 (E10)**, 8115 (2003).
- [170] G. Bohannan, H. Schmidt, D. Brandt and M. Mooibroek, *Piezoelectric polymer actuators for active vibration isolation in space applications*. *Ferroelectrics* **224**, 639–645 (1999).
- [171] C. Wehrli, *Extraterrestrial solar spectrum*. Publication 615, Physikalisch-Meteorologisches Observatorium and World Radiation Center, Davos Dorf, Switzerland (1985).

Appendix

A Journal and Review Articles

The following articles represent relevant contributions to the field of charge-storing electret polymers:

1. A. Mellinger, M. Wegener, W. Wirges and R. Gerhard-Multhaupt, "Thermally stable dynamic piezoelectricity in sandwich films of porous and nonporous amorphous fluoropolymer", *Appl. Phys. Lett.* **79**, 1852-1854 (2001).
2. A. Mellinger, F. Camacho González and R. Gerhard-Multhaupt, "Ultraviolet-induced discharge currents and reduction of piezoelectric coefficient in cellular polypropylene films", *Appl. Phys. Lett.* **82**, 254-256 (2003).
3. A. Mellinger, "Dielectric resonance spectroscopy: a versatile tool in the quest for better piezoelectric polymers", *IEEE Trans. Diel. Electr. Insul.* **10**, 842-861 (2003).
This review article won the 2004 award of the *Informationstechnische Gesellschaft* in the German Association of Electrical Engineers (VDE).
4. A. Mellinger, F. Camacho González, and R. Gerhard-Multhaupt, "Photostimulated discharge in electret polymers: an alternative approach for investigating deep traps," *IEEE Trans. Diel. Electr. Insul.*, **11**, 218- 226 (2004).
5. A. Mellinger, "Unbiased iterative reconstruction of polarization and space-charge profiles from thermal-wave experiments", *Meas. Sci. Technology* **15**, 1347-1353 (2004).
6. A. Mellinger, R. Singh and R. Gerhard-Multhaupt, "Fast thermal-pulse measurements of space charge distributions in electret polymers", *Rev. Sci. Instr.* **76**, *in press* (2005).
7. A. Mellinger, R. Singh, M. Wegener, W. Wirges, R. Gerhard-Multhaupt and S. B. Lang, "Three-dimensional mapping of polarization profiles with thermal pulses", *Appl. Phys. Lett.*, *submitted* (2004).

Thermally stable dynamic piezoelectricity in sandwich films of porous and nonporous amorphous fluoropolymer

Axel Mellinger,^{a)} Michael Wegener, Werner Wirges, and Reimund Gerhard-Multhaupt
Department of Physics, University of Potsdam, Am Neuen Palais 10, 14469 Potsdam, Germany

(Received 11 May 2001; accepted for publication 18 July 2001)

Porous amorphous fluoropolymer films of very low stiffness were produced by a solvent evaporation technique. Corona-charged sandwich films consisting of a porous and a nonporous layer exhibit piezoelectric thickness-extension resonances in their dielectric spectrum, through which the temperature dependence of their dynamic stiffness, coupling factor, and piezoelectric coefficient could be determined. Their strong piezoelectricity with coefficients of up to 600 pC/N at temperatures of at least 120 °C could make these polymer electret films interesting candidates for sensor and actuator applications in elevated temperature environments. © 2001 American Institute of Physics. [DOI: 10.1063/1.1404405]

Piezoelectric sensors and actuators are used in a wide range of applications. Until recently, the favored materials were crystalline and inorganic, such as lead zirconate titanate. In the early 1970s, ferroelectric polymers (such as polyvinylidene fluoride) were shown to have piezoelectric properties,¹ but the piezoelectric coefficients are usually at least one order of magnitude smaller than those of their inorganic counterparts. A major improvement came with the invention of cellular polypropylene (PP) films.² After corona or electrode charging, these heterogeneous space-charge electrets exhibit piezoelectric coefficients of more than 200 pC/N,^{3,4} but their relatively low thermal stability is a major drawback for many applications. Recently, large quasistatic d_{33} coefficients were reported in fluoroethylene-propylene copolymer⁵ and porous polytetrafluoroethylene films.^{6,7} In this letter, a strong piezoelectric effect has been observed in corona-charged sandwich films of amorphous Teflon[®] AF fluoropolymer. Piezoelectric resonances⁸ in their dielectric spectra were used to determine their mechanical and electrical properties.

Films of porous Teflon[®] AF were prepared by drop casting a solution (2%–10%) of Teflon[®] AF (Dupont) resin in Fluorinert[®] FC-77 (3M). Boiling of the solvent produces a film with open pores and approximate thicknesses of 3–10 μm . Between 3 and 8 layers were drop cast on top of each other in order to achieve a thickness of between 9 and 60 μm . Typical densities of the porous films were around 500 kg/m^3 . The open pores were then sealed at 180 °C with a 12 μm Teflon[®] AF 1600 film which had been previously prepared by drop casting at room temperature, followed by annealing at 150 °C for 24 h. After one side had been metalized with 60 nm of aluminum in high vacuum, the sandwich films were charged in a point-to-plane corona discharge at –15 kV with an air gap of 4 cm. Charging time was 15–30 s at room temperature, after which the surface potential reached values between –1.0 and –1.5 kV. Another circular aluminum electrode was subsequently evaporated onto the previously unmetalized side of the sample.

The dielectric spectrum shown in Fig. 1 was measured in the temperature range between –100 and +170 °C, and the frequency range between 100 Hz and 10 MHz with a Novocontrol ALPHA high-resolution dielectric analyzer and a Novocontrol QUATRO cryosystem. The data were acquired as a function of frequency under nearly isothermal conditions ($\Delta T_{\text{max}}=0.25$ K) in 10 K intervals. The samples were mounted in such a way that they could freely vibrate with minimal disturbance by the spring-loaded electrode contacts.

The dielectric resonance spectrum of a piezoelectric film near the thickness-extension (TE) mode anti-resonance frequency is given by^{9,10}

$$C(\omega) = \frac{\epsilon_r \epsilon_0 A}{h} \frac{1}{1 - k_{33}^2 \frac{\tan(\omega/4f_p)}{(\omega/4f_p)}} - iC_{\text{loss}}, \quad (1)$$

where ϵ_r is the relative permittivity of the sample, A and h are the electroded sample area and thickness, respectively, k_{33} is the complex electromechanical coupling factor, and f_p is the complex anti-resonance frequency of the TE mode. Between 10^3 and 10^6 Hz, Teflon[®] AF shows a nearly constant dielectric loss¹¹ which is represented by the $-iC_{\text{loss}}$ term in Eq. (1). For a free-standing film, f_p is related to the complex elastic stiffness c_{33} and the sample density ρ via

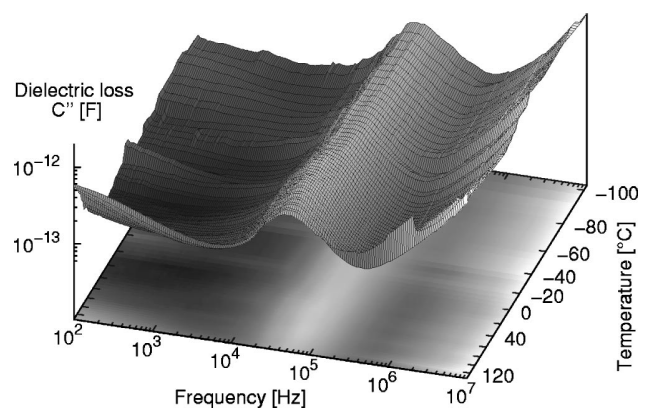


FIG. 1. Frequency-temperature map of the dielectric loss (C'') of a 55 μm porous Teflon[®] AF 2400/nonporous Teflon AF 1600 sandwich film.

^{a)}Electronic mail: axm@rz.uni-potsdam.de

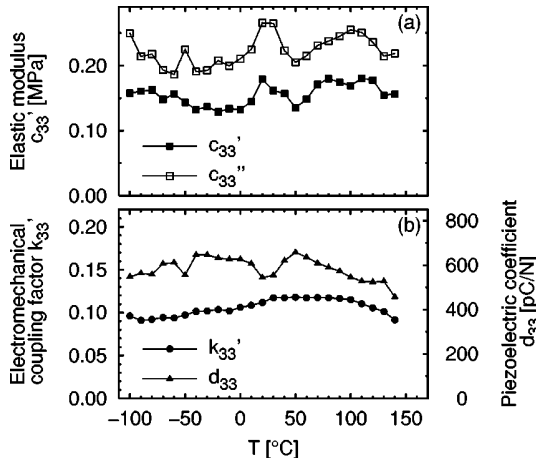


FIG. 2. Temperature dependence of the real and imaginary elastic modulus c'_{33} and c''_{33} , the real part of the electromechanical coupling factor k'_{33} , and the piezoelectric coefficient d_{33} for the porous/nonporous Teflon[®] AF sandwich film of Fig. 1.

$$f_p = \frac{1}{2h} \sqrt{\frac{c_{33}}{\rho}} \quad (2)$$

and the coupling factor k_{33} is given by

$$k_{33}^2 = d_{33}^2 c_{33} / (\epsilon_r \epsilon_0). \quad (3)$$

For each temperature, the quantities f_p , k_{33} , and C_{loss} were determined via a least squares fit; c_{33} and d_{33} were then calculated using Eqs. (2) and (3), respectively. The temperature dependence of the real parts of these quantities is shown in Fig. 2. The Teflon[®] AF sandwich films show a very low nearly constant elastic modulus c_{33} in the temperature range between -100 and $+130$ °C [Fig. 2(a)]. The low real part of the elastic modulus is accompanied by an imaginary (loss) part equal to or even exceeding the real part. The electromechanical coupling factor k_{33} at room temperature is near 0.1, and the piezoelectric coefficient d_{33} reaches values of about 600 pC/N, owing to the low stiffness of the porous layer. The Teflon[®] AF samples showed very little sensitivity loss up to

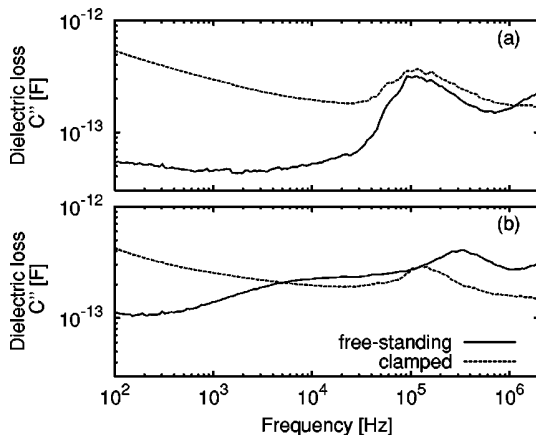


FIG. 3. Dielectric loss C'' of a free-standing 45 μm (solid line) or clamped 19 μm (dashed line) porous/nonporous Teflon[®] AF sandwich film. The films were glued to a glass substrate either with the sealed (a) or the porous side (b) facing the substrate.

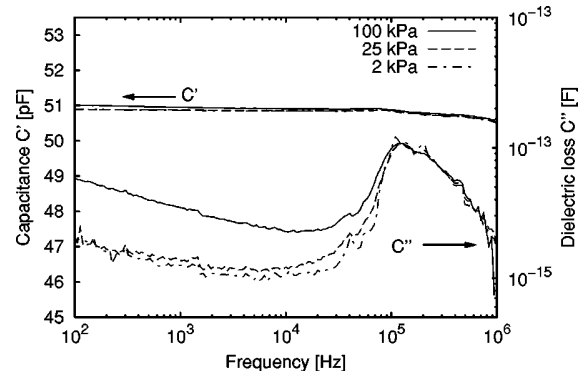


FIG. 4. Capacitance C' and dielectric loss C'' of a porous/nonporous Teflon[®] sandwich film at various pressures.

120 °C; this is a clear improvement over the cellular PP material where prolonged storage at 50 °C or higher is known to decrease its sensitivity.³

A different boundary condition can be imposed on the piezoelectric resonator by gluing the film onto a glass substrate with a thin layer of epoxy. In this case, the factor 2 in the denominator of Eq. (2) must be replaced by 4, thus lowering the anti-resonance frequency by a factor of 2.^{4,12} However, the dielectric loss spectrum in Fig. 3(a) shows no such decrease when the sealed (nonporous) side of the film is glued onto the substrate. This effect can be explained if we assume that the porous layer alone is oscillating under the influence of the ac electric field, with the nonporous layer acting as a clamping substrate. On the other hand, when the porous side faces the substrate, a substantial decrease of the anti-resonance frequency is observed [cf. Fig. 3(b)] due to the additional mass of the nonporous layer which is now forced to oscillate.

Dielectric spectra recorded at different pressures are shown in Fig. 4. No change in capacitance is observed in the range between 2 and 100 kPa. Therefore, the sample thickness must remain constant, indicating that the air can freely escape through the voids. Also, the resonance frequency and hence the elastic modulus is constant in this pressure range, showing that the observed elastic modulus is that of the porous polymer film itself, rather than that of air trapped inside the voids.

The frequency dependence of the inverse piezoelectric effect (Fig. 5) was measured with an acoustical

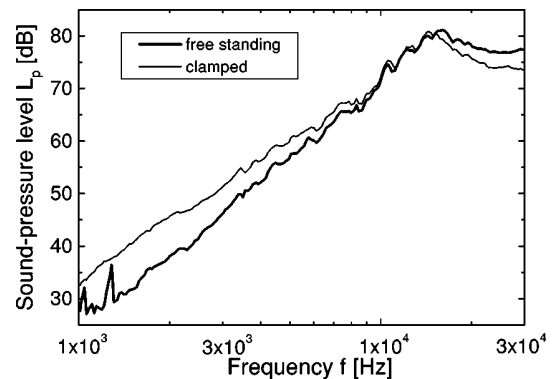


FIG. 5. Frequency-dependent sound pressure level generated by a 19 μm porous/nonporous Teflon[®] AF sandwich film.

technique.^{6,13,14} The sound pressure level L_p was recorded with a 1/2 in. electret microphone (Brüel & Kjær) in the near field (distance <1 mm) of the sample in a noise-reducing box. A sine generator in the measuring system (Audio Teknology LMS) and an amplifier (Metra LV 102) were used to apply a voltage of 10 V in the frequency range between 1 and 30 kHz to the film. At a frequency of about 16 kHz, we determined a sound pressure level of 81 dB for both the free-standing and the clamped films. From these values, we calculated an absolute sound pressure amplitude of 0.23 Pa, and therefore a transducer sensitivity of 23 mPa/V. From the effective displacement amplitude of 5.5 nm at a frequency of 16 kHz, an inverse piezoelectric coefficient of 550 pC/N was derived, which is in good agreement with the result obtained from the dielectric spectra.

In conclusion, we have demonstrated that corona-charged sandwich films of porous and nonporous Teflon® AF can be produced with a simple solvent evaporation technique and show a large piezoelectric response at temperatures up to 120 °C.

The authors are indebted to A. Pucher for his experimental support.

- ¹ *Electrets*, 3rd ed., edited by G. M. Sessler and R. Gerhard-Multhaupt (Laplacian, Morgan Hill, CA, 1999).
- ² K. Kirjavainen, US Patent No. 4,654,546 (31 March 1987).
- ³ J. Lekkala and M. Paajanen, in *Proceedings, 10th International Symposium on Electrets*, edited by A. A. Konsta, A. Vassilikou-Dova, and K. Vartzeli-Nikaki (IEEE Service Center, Piscataway, NJ, 1999), pp. 743–746.
- ⁴ G. S. Neugschwandtner, R. Schwödiauer, M. Vieytes, S. Bauer-Gogonea, S. Bauer, J. Hillenbrand, R. Kressmann, G. M. Sessler, M. Paajanen, and J. Lekkala, *Appl. Phys. Lett.* **77**, 3827 (2000).
- ⁵ R. M. Faria, *Appl. Phys. Lett.* **69**, 1972 (1996).
- ⁶ R. Gerhard-Multhaupt, W. Künstler, T. Görne, A. Pucher, T. Weinhold, M. Seiß, Z. Xia, A. Wedel, and R. Danz, *IEEE Trans. Dielectr. Electr. Insul.* **7**, 480 (2000).
- ⁷ W. Künstler, Z. Xia, T. Weinhold, A. Pucher, and R. Gerhard-Multhaupt, *Appl. Phys. A: Mater. Sci. Process.* **70**, 5 (2000).
- ⁸ K. Omote, H. Ohigashi, and K. Koga, *J. Appl. Phys.* **81**, 2760 (1997).
- ⁹ IEEE Standard on Piezoelectricity, ANSI/IEEE Std. 176-1987 (1987).
- ¹⁰ W. P. Mason, *Physical Acoustics* (Academic, New York, 1967), Vol. I, Part A.
- ¹¹ P. Avakian, J. H. W. Starkweather, J. J. Fontanella, and M. C. Wintersgill, in *Dielectric Spectroscopy of Polymeric Materials*, edited by J. P. Runt and J. J. Fitzgerald (American Chemical Society, Washington, DC, 1997).
- ¹² G. S. Neugschwandtner, R. Schwödiauer, S. Bauer-Gogonea, S. Bauer, M. Paajanen, and J. Lekkala, *J. Appl. Phys.* **89**, 4503 (2001).
- ¹³ J. Backman, *J. Audio Eng. Soc.* **38**, 364 (1990).
- ¹⁴ J. Backman and M. Karjalainen, in *Proceedings, IEEE International Conference on Acoustics, Speech, and Signal Processing* (IEEE Service Center, Piscataway, NJ, 1990), Vol. 2, pp. 1173–1176.

Ultraviolet-induced discharge currents and reduction of the piezoelectric coefficient in cellular polypropylene films

Axel Mellinger,^{a)} Francisco Camacho González,^{b)} and Reimund Gerhard-Multhaupt^{c)}
Department of Physics, University of Potsdam, Am Neuen Palais 10, D-14469 Potsdam, Germany

(Received 27 September 2002; accepted 21 November 2002)

Photostimulated discharge spectroscopy of cellular polypropylene films between 200 and 400 nm showed the existence of at least three distinct trapping levels at 4.6, 5.6, and 6.3 eV. The effects of UV irradiation on the piezoelectric d_{33} coefficient was studied by monitoring thickness-extension resonances in the dielectric spectrum. Prolonged irradiation at wavelengths below 210 nm led to a reduction of the piezoelectric coefficient, caused by partial discharge of the polymer foam. © 2003 American Institute of Physics. [DOI: 10.1063/1.1537051]

In recent years, cellular polypropylene (PP) films with high piezoelectric coefficients have become commercially available.^{1,2} Unlike conventional materials, such as polyvinylidene fluoride (PVDF), their piezoelectric activity is not based on the presence of molecular dipoles. Instead, symmetry breaking occurs on a macroscopic scale, when the polymer foam is exposed to a high electric field in, e.g., a corona discharge, resulting in Paschen breakdown inside the voids, followed by charge separation and trapping at the internal surfaces of the cellular structure. At room temperature, piezoelectric coefficients of up to 230 pC/N have been reported for the high-sensitivity 70 μm films.³ This value is around ten times higher than the piezoelectric activity found in PVDF, and can be enhanced up to 790 pC/N if the samples are treated in dielectric gases during or before corona charging.⁴ A drawback of cellular PP is its low thermal stability,² which restricts its use to temperatures below 60 °C.

While the thermal stability has been addressed in several articles, little is known about the short-term effects of UV radiation on the piezoelectric properties of cellular PP, although the long-term UV degradation of PP is well understood.⁵ In addition, the mechanism of charge trapping in highly insulating electret polymers is still subject to debate.⁶ Very recently, research on polyethylene has demonstrated the coexistence of physical (conformational) traps (trap depths ≤ 0.3 eV) and deep chemical traps (trap depths ≥ 1 eV).^{7,8} In the present work, the photostimulated discharge (PSD) current of cellular PP was studied under irradiation with monochromatic UV light in order to obtain information on the trap energies. Unlike the frequently used technique of thermally stimulated discharge, PSD spectroscopy yields direct information on the depth and population of trapping levels.⁹ For example, Oda *et al.* inferred the presence of a single trapping level at 4.9 eV in Teflon® FEP from photostimulated detrapping currents¹⁰ and concluded that an indirect process (charge injection from the electrodes) rather than direct detrapping is the principal mechanism through which the photocurrent is generated in this material.¹¹

Samples of cellular PP (nominal thickness 70 μm) were coated with a 40 nm gold back electrode in high vacuum and charged in a point-to-plane corona discharge at a needle voltage of -28 kV. Subsequently, a semitransparent 16 nm gold electrode was deposited on the front side. The films were irradiated with monochromatic light (Fig. 1) generated by a 450 W Xe arc lamp (Oriel) and a monochromator (Photon Technology International, bandwidth between 2 and 20 nm) equipped with an UV-enhanced grating (blaze angle for 250 nm). The UV flux was monitored with an UV-sensitive photodiode (Hamamatsu S1336-BQ). At the sample position, the photon irradiance at 400 nm was about $3 \times 10^{14} \text{ cm}^{-2} \text{ s}^{-1} \text{ nm}^{-1}$. The short-circuit discharge current was measured with a Keithley 6517A electrometer. Dielectric spectra were recorded using a Novocontrol ALPHA high-resolution dielectric analyzer with a modified open sample holder, where the samples were mounted so that they could freely vibrate in the thickness direction. Unlike Debye relaxations, where the full width at half maximum is 1.14 decades, resonance peaks are much narrower, requiring a frequency resolution of $\Delta f/f \leq 0.02$.

Figure 2(a) shows the photostimulated discharge current of cellular polypropylene. The initial scan shows three distinct current peaks at 276, 223, and 198 nm, corresponding to energies of 4.6, 5.6, and 6.3 eV, respectively. For all three wavelengths, a decaying discharge current was observed [Fig. 2(b)], ruling out photoconductivity as the major source of the photocurrent. Instead, the discharge peaks can be attributed to charge traps being emptied upon irradiation. Irradiation at a fixed wavelength leads to preferential bleaching.

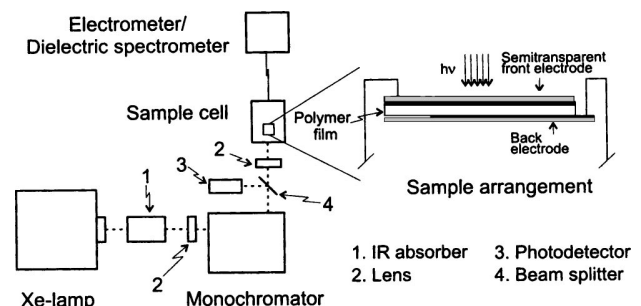


FIG. 1. Experimental setup for photostimulated discharge spectroscopy.

^{a)}Electronic mail: axm@rz.uni-potsdam.de

^{b)}Electronic mail: fcamacho@canopus.physik.uni-potsdam.de

^{c)}Electronic mail: rgm@rz.uni-potsdam.de

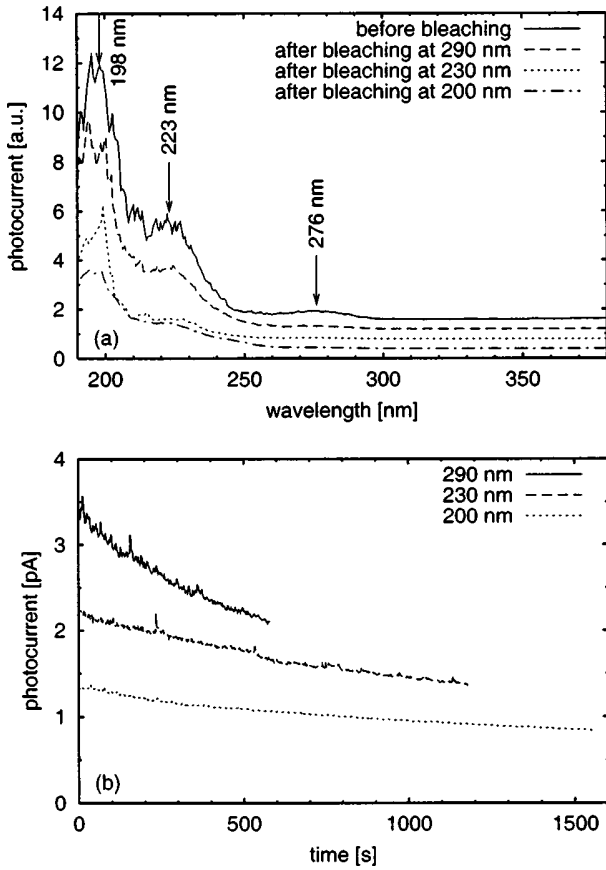


FIG. 2. Photostimulated discharge of a cellular PP film (nominal thickness 70 μm). (a) irradiance-normalized discharge current as a function of wavelength and (b) time-dependence of discharge current at selected wavelengths.

For example, Fig. 2 shows that the 198 and 223 peaks are only weakly affected by a 550 s exposure at 290 nm, which completely bleaches the 276 nm peak. Also, irradiation at 200 nm did not substantially bleach the 223 nm peak.

To study the effects of charge detrapping on the piezoelectric properties, the d_{33} coefficient was measured via the dielectric resonance technique. This method, which was first applied to piezoelectric polymer foams by Neugschwandtner *et al.*,¹² allows the *in situ* measurement of mechanical, electromechanical, and electrical properties, thus avoiding errors introduced by mechanically stressing the sample during transfer between different analytical equipment. The room temperature dielectric spectrum was measured between 200 and 1000 kHz with a Novocontrol ALPHA high-resolution dielectric analyzer and a modified sample holder where the samples could freely vibrate with minimal disturbance by the spring-loaded electrode contacts. Data analysis was performed by fitting the real part of the measured permittivity (cf. the inset of Fig. 3) to the expression^{13,14}

$$C'(\omega) = \frac{\epsilon_r \epsilon_0 A}{h} \Re \left\{ \left[1 - k_x^2 \frac{\tan(\omega/4f_p)}{(\omega/4f_p)} \right]^{-1} \right\}, \quad (1)$$

where \Re denotes the real part, ϵ_r is the relative permittivity of the sample, A and h are the electroded sample area and thickness, respectively, k_x is the electromechanical coupling factor, and f_p is the antiresonance frequency of the thickness-extension mode. Both k_x and f_p are taken as com-

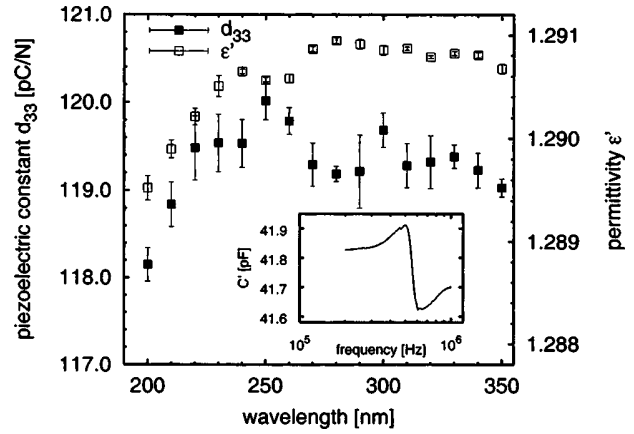


FIG. 3. Decrease of the piezoelectric d_{33} constant after UV irradiation. Each point is an average of four resonance scans after a 20 min irradiation at the respective wavelength. The inset shows a typical dielectric spectrum in the vicinity of the resonance.

plex numbers to allow for mechanical losses. For a free-standing film, the complex elastic stiffness c_{33} can be obtained from f_p and the sample density ρ via

$$f_p = \frac{1}{2h} \sqrt{\frac{c_{33}}{\rho}}, \quad (2)$$

and the piezoelectric coefficient d_{33} is given by

$$d_{33}^2 = \frac{k_x^2 \epsilon_r \epsilon_0}{c_{33}}. \quad (3)$$

Between 350 and 200 nm, the sample was irradiated at 10 nm intervals for 20 min each, and four resonance spectra were acquired at each wavelength. The quantities f_p , k_x , and ϵ_r were determined via a least squares fit, from which d_{33} was then calculated using Eq. (3) with an accuracy of better than 0.5 %. Figure 3 shows that the piezoelectric constant remained unchanged under irradiation down to 220 nm. However, successive irradiation at 210 and 200 nm reduced the piezoelectric effect by approximately 1%. Given the relatively large 20 nm monochromator bandwidth in this experiment, it is reasonable to assume that the charge associated with the 198 nm peak is solely responsible for the piezoelectric behavior (and is therefore trapped on the inner surfaces of the voids), while the 223 and 276 nm peaks correspond to charges at the external sample surfaces. No effect of UV irradiation on the resonance frequency (and hence, on the mechanical stiffness) was detected.

This result can be interpreted either as a partial discharge of the entire film, or as a complete discharge of a surface layer of thickness h_1 (Fig. 4). The latter interpretation appears more likely, since bulk discharge is prevented in part by the strong scattering of UV light in the polymer foam which effectively limits the optical penetration depth. Moreover, charge carriers released at greater depths cannot reach the electrodes due to their low mobility. Recent observations of photostimulated discharge in polyethylene terephthalate¹⁵ also indicate that quantitative bleaching occurred only for charges within approximately 3 μm of the surface. These effects are at the spatial resolution limit of acoustic space charge profiling techniques,⁶ but might be resolved by fast thermal wave or thermal pulse techniques.

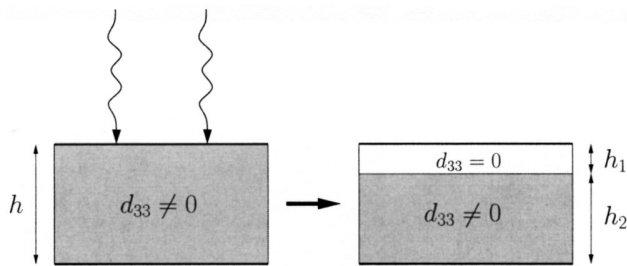


FIG. 4. Schematic view of the sample before and after UV irradiation. A thin surface layer has been completely discharged, while the remaining sample retains its space charge and piezoelectric properties.

In conclusion, three distinct deep charge trap levels at energies between 4.6 and 6.3 eV have been detected in cellular polypropylene films. Irradiation at specific wavelengths leads to a partly selective bleaching of individual trap levels. In addition, UV irradiation at wavelengths less than 210 nm decreases the effective piezoelectric coefficient of the material by partly discharging the sample. Investigation of UV irradiation at vacuum UV wavelengths is currently in preparation.

The authors gratefully acknowledge stimulating discussions and experimental support by M. Paajanen (VTT Processes, Tampere, Finland), as well as M. Wegener and W. Wirges (both University of Potsdam). The cooperation with

VTT was supported by the German Academic Exchange Service (DAAD) under Project No. 9803. F.C.G. would like to acknowledge financial support from PROMEP-SUPERA.

¹K. Kirjavainen, US Patent No. 4,654,546 (1987).

²J. Lekkala and M. Paajanen, in: *Proceedings, 10th International Symposium on Electrets*, edited by A. A. Konsta, A. Vassilikou-Dova, and K. Vartzeli-Nikaki (IEEE, Piscataway, NJ, 1999), pp. 743–746.

³M. Paajanen, J. Lekkala, and H. Välimäki, *IEEE Trans. Dielectr. Electr. Insul.* **8**, 629 (2001).

⁴M. Paajanen, M. Wegener, and R. Gerhard-Multhaupt, *J. Phys. D* **34**, 2482 (2001).

⁵J. F. Rabek, *Photodegradation of Polymers* (Springer, Heidelberg, 1995).

⁶*Electrets*, 3rd ed., edited by G. M. Sessler and R. Gerhard-Multhaupt (Laplacian, Morgan Hill, CA, 1999).

⁷M. Meunier and N. Quirke, *J. Chem. Phys.* **113**, 369 (2000).

⁸M. Meunier, N. Quirke, and A. Aslanides, *J. Chem. Phys.* **115**, 2876 (2001).

⁹J. D. Brodribb, D. O'Colmain, and D. M. Hughes, *J. Phys. D* **8**, 856 (1975).

¹⁰T. Oda, T. Utsumi, T. Kumano, and M. Itami, in *Proceedings, 5th International Conference on Electrets*, edited by G. M. Sessler and R. Gerhard-Multhaupt (IEEE, Piscataway, NJ, 1985), pp. 288–293.

¹¹T. Oda, T. Utsumi, and G. Matsubara, in *Proceedings, 6th International Symposium on Electrets*, edited by D. K. Das-Gupta and A. W. Pattullo (IEEE, Piscataway, NJ, 1988), pp. 142–146.

¹²G. S. Neuschwandtner, R. Schwödauier, M. Vieytes, S. Bauer-Gogonea, S. Bauer, J. Hillenbrand, R. Kressmann, G. M. Sessler, M. Paajanen, and J. Lekkala, *Appl. Phys. Lett.* **77**, 3827 (2000).

¹³“IEEE standard on piezoelectricity,” ANSI/IEEE Std. 176-1987, 1987.

¹⁴W. P. Mason, *Physical Acoustics* (Academic, New York, 1967), Vol. 1, part A.

¹⁵A. Mellinger, F. Camacho González, R. Gerhard-Multhaupt, L. F. Santos, and R. M. Faria, in *Proceedings, 11th International Symposium on Electrets*, edited by R. J. Fleming (IEEE, Piscataway, NJ, 2002), pp. 7–10.

Dielectric Resonance Spectroscopy: a Versatile Tool in the Quest for Better Piezoelectric Polymers

Axel Mellinger

Department of Physics
University of Potsdam, Am Neuen Palais 10,
14469 Potsdam, Germany

ABSTRACT

Piezoelectric polymers are widely used in sensor and actuator applications. Compared to ceramic materials, they have the advantage of mechanical flexibility and an acoustic impedance similar to those of water or air. Their electrical, electromechanical and mechanical properties can be investigated by analyzing piezoelectric resonances in their dielectric spectrum. Apart from its ability to reveal the high-frequency behavior of piezoelectric polymer films, this technique is appealing from a practical point of view because several important parameters can be measured with a single scan that only requires standard dielectric spectroscopy equipment commonly found in many laboratories. This article outlines the theoretical foundations of piezoelectric resonance, examines the experimental aspects, and reviews recent applications in the field of piezoelectric polymers.

Index Terms — piezoelectricity, piezoelectric resonances, piezoelectric coefficient, coupling factor, polypropylene, polyvinylidene fluoride, polyvinylidene fluoride-trifluoroethylene, polyamide, thickness extension resonance, shear mode, voided polymer, cellular polymer, porous polymer, space-charge electret, corona charging, dielectric spectroscopy.

1 INTRODUCTION

FOR many years, piezoelectric materials have been used in a wide range of sensor and actuator applications. Among these materials, piezoelectric polymers have the advantage of being usable in mechanically flexible sensors and actuators with large areas and various shapes as well as in transducers with good acoustical coupling to air or water. Furthermore these polymers are interesting because of their various microscopic mechanisms of piezoelectricity as well as pyro- and ferroelectricity. A polarization in the polymer results in breaking of the symmetry, which is a prerequisite for piezoelectric properties. Symmetry-breaking is observed in both polar polymers (usually non-porous) and in the new class of voided porous or cellular space charge electrets.

The basis of piezoelectricity in polar polymers is the orientation of molecular dipoles, e.g. a remanent polarization in ferroelectric domains or a frozen-in polarization in the glassy phase. Piezoelectricity occurs based on a change of the dipole density during application of mechanical stress or an electric field. The commercially most important example is polyvinylidene fluoride (PVDF), where piezoelectric properties were discovered more than thirty

years ago [1,2]. The structure of polymer chains, the different phases, the preparation and the orientation processes as well as the resulting properties have been well investigated in PVDF [3–5] and some of its copolymers, e.g. with trifluoroethylene (TrFE) and tetrafluoroethylene [4,6,7] or hexafluoropropylene P(VDF-HFP) [8–10]. Since their acoustic impedance is similar to that of water, these materials are widely used in ultrasound hydrophone probes [11,12] and have found their way into medical imaging at high frequencies up to 100 MHz [13,14].

Odd-numbered polyamides [15], several copolymers of vinylidene cyanide (VDCN) [16], polyureas [17], polyurethane [18], and polythioureas [19] are further examples for piezoelectric properties based on an orientation process of molecular dipoles. Recently, a new class of non-polar porous or cellular space charge electrets has received considerable attention in the literature [20]. Compared to PVDF, these materials are significantly more compressible, resulting in piezoelectric coefficients of several hundred pC/N and an acoustic impedance much closer to that of air, which makes them excellent candidates for use in loudspeakers and microphones [21,22]. Focusing devices, such as spherical sound generators or Fresnel zone and phase plates [23], are a particularly interesting application.

Manuscript received on 7 February 2003, in final form 16 July 2003.

The demand for materials with high piezoelectric coefficients and a broad operating temperature range from -25°C to at least 120°C has triggered a very active research, thus necessitating the availability of reliable experimental techniques to characterize the mechanical, electromechanical and electrical properties. Typically, sample characterization requires many separate experiments, which is not only time-consuming but also increases the risk of altering essential properties during measurement or transfer. Some experiments require accurate *in situ* methods for measuring the piezoelectric coefficient during UV irradiation or thermal treatment. A very versatile technique is the analysis of piezoelectric resonances in the dielectric spectrum. Compared to static or dynamic mechanical measurements or optical interferometry, dielectric spectroscopy has the advantage of yielding several important material parameters in a single measurement with readily available laboratory equipment, as long as the sample can be accessed under stress-free or certain limited mechanical boundary conditions. In a typical experiment, the theoretical expression for the frequency dependence of the complex capacitance $\tilde{C}(\omega)$ is fitted to the experimental data. From the fitted parameters, the mate-

rial parameters in the small signal limit are then easily calculated.

This paper provides an introduction into the theoretical and experimental aspects of measuring piezoelectric resonances. After a brief historical overview, the expressions for the complex sample capacitance as a function of frequency are derived in Section 3. This part also discusses how to incorporate various losses, and gives equations relating some key mechanical and electromechanical quantities to experimentally measured values. Section 4 compares dielectric resonance spectroscopy to other experimental techniques and outlines the analysis of dielectric resonance data. Finally, Section 5 discusses some recent applications of resonance spectroscopy in the field of piezoelectric polymers.

2 HISTORY OF PIEZOELECTRIC RESONANCES

Piezoelectricity in crystals was discovered in 1880 by the Curie brothers [24,25]. Perhaps the earliest report of a piezoelectric resonance can be found in the work of Nicolson [26] on the frequency dependence of the capacity, current and conductance of a rochelle salt crystal. At

Table 1. Summary of symbols used in this work; alternate symbols commonly found in the literature are also listed. Indices are within the following bounds: $i, j = 1 \dots 6$; $m, n = 1 \dots 3$.

Physical quantity	Symbol		SI unit
	This work	Other	
Elastic stiffness (Young's modulus, elastic modulus)	c_{ij}	C, Y, E	N m^{-2}
Heat capacity	c		$\text{J kg}^{-1} \cdot \text{K}^{-1}$
Complex capacitance	$\tilde{C} = C' - iC''$		$\text{F} = \text{CV}^{-1}$
Electric field	\mathbf{E}, E_m		V m^{-1}
Piezoelectric strain (or charge) coefficient	d_{mi}		$\text{CN}^{-1} = \text{mV}^{-1}$
Electric displacement	\mathbf{D}, D_m		Cm^{-2}
Piezoelectric stress coefficient	e_{mi}		Cm^{-2}
Piezoelectric voltage coefficient	g_{mi}		m^2C^{-1}
Gibbs free energy density	G	g	Jm^{-3}
Sample thickness	h	t	m
Inverse piezoelectric strain coefficient	h_{mi}		$\text{NC}^{-1} = \text{Vm}^{-1}$
Enthalpy density	H	h	Jm^{-3}
Electromechanical coupling factor	k_{ij}, k_p, k_t		1
Sample length	l		m
Pyroelectric coefficient	p_m		$\text{Cm}^{-2} \text{K}^{-1}$
Mechanical quality factor	Q_m		1
Elastic compliance	s_{ij}		$\text{m}^2 \text{N}^{-1}$
Entropy density	S	σ, s	$\text{JK}^{-1} \text{m}^{-3}$
Temperature	T	θ	K
Internal energy density	U	u	J m^{-3}
Speed of sound	v, v_m	c	m s^{-1}
Sample width	w		m
Admittance	$\tilde{Y} = G + iB$		$\text{S} = \Omega^{-1}$
Impedance	$\tilde{Z} = R + iX$		Ω
Thermal expansion coefficient	α_i		K^{-1}
Dielectric impermeability	β_{mn}		$\text{Vm A}^{-1} \text{s}^{-1}$
Dielectric constant	ϵ_{mn}		$\text{As V}^{-1} \text{m}^{-1}$
Poisson's ratio	ν	σ	1
Density	ρ		kg m^{-3}
Mechanical stress	$\boldsymbol{\sigma}, \sigma_i$	T, S, X	Nm^{-2}
Mechanical strain	$\boldsymbol{\tau}, \tau_i$	e, S, ϵ	1

that time (1919), the resonance curves were merely reported as an interesting phenomenon, but just three years later the first theoretical description of longitudinal oscillations in quartz rods was published by Cady [27] in an effort to develop radio frequency oscillators with high frequency stability. This description was later expanded by von Laue [28], who also included energy dissipation terms and was the first to note that the piezoelectric coefficient could be obtained from the measured resonance curves, thus laying the foundations of a versatile experimental technique. Much of the early history of piezoelectric materials and their applications are treated in Cady's book on piezoelectricity [29]. An in-depth treatment of piezoelectric materials, their behavior under oscillating electric fields and their corresponding equivalent circuits was published by Berlincourt et al. [30]. This description was later incorporated into the IEEE Standard on Piezoelectricity [31]. While piezoelectric resonances had become a well-established tool for the investigation of ceramic materials, the method was thought not to be applicable to polymer samples because of their small coupling factors and large mechanical losses. The first successful observation of resonances in films of polyvinylidene fluoride (PVDF) was reported by H. Ohigashi in 1976 [32]. Since then, dielectric resonance spectroscopy has been used extensively in the search for new and better polymeric transducer electrets.

3 THEORETICAL OVERVIEW

The physics of resonant vibrations in piezoelectric materials has been extensively covered in the literature [30,31]. Since some of these reviews may no longer be accessible to all readers, a brief introduction into the theory of length (LE) and thickness extension (TE) resonances will be given here. The approach largely follows that of Berlincourt et al. [30], with emphasis on the symmetries relevant in piezoelectric polymer materials.

3.1 CONSTITUENT EQUATIONS

Thermodynamically, piezoelectricity is commonly defined via the Gibbs free energy density

$$G = U - \tau_i \sigma_i - D_m E_m - ST; \quad i = 1 \dots 6, m = 1 \dots 3 \quad (1)$$

where U is the internal energy per unit volume, τ_i and σ_i are the components of the strain and stress tensors $\boldsymbol{\tau}$ and $\boldsymbol{\sigma}$, respectively, D_m and E_m are the components of the electric displacement \mathbf{D} and the electric field \mathbf{E} , S is the entropy per unit volume, and T is the temperature. Unless otherwise mentioned, repeated indices indicate summation throughout this paper. Unfortunately, the existing literature shows a confusing and sometimes ambiguous variety of notation for these physical quantities. Table 1 lists some of the commonly found symbols.

In their full tensorial form, stress and strain are represented by the 3×3 matrices σ_{pq} and τ_{pq} [33]. Figure 1

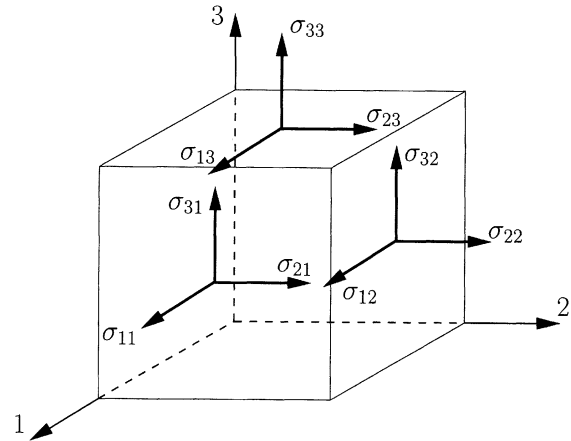


Figure 1. Components of the stress tensor shown on the three faces on a cube.

shows the 9 components of the stress tensor on the faces of a cube. The strain tensor is defined in terms of the displacements ξ_k along the x , y , and z axes by

$$\tau_{kl} = \frac{1}{2} \left(\frac{\partial \xi_l}{\partial x_k} + \frac{\partial \xi_k}{\partial x_l} \right); \quad k, l = 1 \dots 3 \quad (2)$$

Since both $\boldsymbol{\sigma}$ and $\boldsymbol{\tau}$ are symmetric tensors with only 6 independent elements, we shall use the simpler 1-dimensional Voigt notation, where $\boldsymbol{\sigma} = (\sigma_{11}, \sigma_{22}, \sigma_{33}, 2\sigma_{13}, 2\sigma_{23}, 2\sigma_{12})$ and $\boldsymbol{\tau} = (\tau_{11}, \tau_{22}, \tau_{33}, 2\tau_{13}, 2\tau_{23}, 2\tau_{12})$. The electric field \mathbf{E} and electric displacement \mathbf{D} , on the other hand, are vectors specified by three independent components: $\mathbf{E} = (E_1, E_2, E_3)$ and $\mathbf{D} = (D_1, D_2, D_3)$. From the differential

$$dG = -\tau_i d\sigma_i - D_m dE_m - SdT \quad (3)$$

it is evident that temperature is a free variable and G is well-suited for describing isothermal processes ($dT = 0$). Fast oscillation processes, however, are far from thermal equilibrium and should therefore be treated as an adiabatic process (constant entropy, $dS = 0$) described by the enthalpy

$$H = U - \tau_i \sigma_i - D_m E_m; \quad i = 1 \dots 6, m = 1 \dots 3. \quad (4)$$

The (adiabatic) piezoelectric strain coefficient d_{mi} is defined as the second derivative

$$d_{mi} = - \left(\frac{\partial^2 H}{\partial E_m \partial \sigma_i} \right)_S \quad (5)$$

where the subscript S denotes that entropy is kept constant. Since

$$dH = -\tau_i d\sigma_i - D_m dE_m + TdS \quad (6)$$

is a perfect differential, the derivatives can be taken in arbitrary order, so that

$$d_{mi} = \left(\frac{\partial D_m}{\partial \sigma_i} \right)_{E,S} = \left(\frac{\partial \tau_i}{\partial E_m} \right)_{\sigma,S} \quad (7)$$

where the $(\partial D_m / \partial \sigma_i)_{E,S}$ term describes the direct piezoelectric effect (an electrical displacement caused by mechanical stress) and the $(\partial \tau_i / \partial E_m)_{\sigma,S}$ term represents the inverse piezoelectric effect (a dimensional change caused by an electric field). Similarly, we obtain the elastic stiffness c_{ij} , the elastic compliance s_{ij} and the dielectric constant ϵ_{mi} via

$$c_{ij}^E = \left(\frac{\partial \sigma_i}{\partial \tau_j} \right)_{E,S} \quad (8)$$

$$s_{ij}^E = \left(\frac{\partial \tau_i}{\partial \sigma_j} \right)_{E,S} \quad (9)$$

and

$$\epsilon_{mn}^\sigma = \left(\frac{\partial D_m}{\partial E_n} \right)_{\sigma,S} \quad (10)$$

From the total derivatives

$$d\tau_i = \left(\frac{\partial \tau_i}{\partial \sigma_j} \right)_{E,S} d\sigma_j + \left(\frac{\partial \tau_i}{\partial E_m} \right)_{\sigma,S} dE_m + \left(\frac{\partial \tau_i}{\partial S} \right)_{\sigma,E} dS \quad (11)$$

and

$$dD_m = \left(\frac{\partial D_m}{\partial \sigma_j} \right)_{\tau,S} d\sigma_j + \left(\frac{\partial D_m}{\partial E_m} \right)_{\sigma,S} dE_m + \left(\frac{\partial D_m}{\partial S} \right)_{\sigma,\tau} dS \quad (12)$$

we thus obtain (in the linear approximation) the constituent equations

$$\tau_i = s_{ij}^E \sigma_j + (d^t)_{im} E_m \quad (13)$$

$$D_m = d_{mj} \sigma_j + \epsilon_{mn}^\sigma E_n, \quad (14)$$

where $(d^t)_{im}$ is the transpose of the piezoelectric strain coefficient in equation (5).

By substituting the total derivative of the entropy density

$$\begin{aligned} dS &= \left(\frac{\partial S}{\partial \sigma_i} \right)_{E,T} d\sigma_i + \left(\frac{\partial S}{\partial E_m} \right)_{\sigma,T} dE_m + \left(\frac{\partial S}{\partial T} \right)_{\sigma,E} dT \\ &= \alpha_i^E d\sigma_i + p_m^\sigma dE_m + \frac{\rho c^{E,\sigma}}{T} dT \end{aligned} \quad (15)$$

into equations (11) and (12), we can obtain the adiabatic material constants (denoted by a superscript S) in terms

of the isothermal ones (denoted by a superscript T)

$$s_{ij}^{E,S} = s_{ij}^{E,T} - \frac{\alpha_i^E \alpha_j^E T}{\rho c^{E,\sigma}} \quad (16)$$

$$d_{mi}^S = d_{mi}^T - \frac{\alpha_i^E p_m^\sigma T}{\rho c^{E,\sigma}} \quad (17)$$

$$\epsilon_{mn}^{\sigma,S} = \epsilon_{mn}^{\sigma,T} - \frac{p_m^\sigma p_n^\sigma T}{\rho c^{E,\sigma}} \quad (18)$$

here, α_i^E and p_m^σ are the thermal expansion and pyroelectric coefficients, respectively, and $\rho c^{E,\sigma}$ is the heat capacity per unit volume. In most practical cases, the difference between the adiabatic and isothermal quantities is small. In particular, the difference between the piezoelectric and dielectric constants vanishes in non-pyroelectric materials.

For certain sample geometries, it is advantageous to use τ and D as independent variables. This is done by starting with the internal energy per unit volume, given by

$$dU = \sigma_i d\tau_i + E_m dD_m + T dS \quad (19)$$

which leads to the constituent equations

$$\sigma_i = c_{ij}^D \tau_j - (h^t)_{in} D_n \quad (20)$$

$$E_m = -h_{mj} \tau_j + \beta_{mn}^\tau D_n \quad (21)$$

where the elastic stiffness c_{ij} , the inverse piezoelectric strain coefficient h_{mi} and the dielectric impermeability β_{mn} are defined by

$$c_{ij}^D = \left(\frac{\partial \sigma_i}{\partial \tau_j} \right)_{D,S} \quad (22)$$

$$h_{mi} = - \left(\frac{\partial \sigma_i}{\partial D_m} \right)_{\tau,S} = \left(\frac{\partial E_m}{\partial \tau_i} \right)_{D,S} \quad (23)$$

$$\beta_{mn}^\tau = \left(\frac{\partial E_m}{\partial D_n} \right)_{\tau,S} \quad (24)$$

For most crystal symmetries (with the exception of triclinic and monoclinic [30]), β is related to the more widely used permittivity ϵ through $\beta_{mm} = 1/\epsilon_{mm}$, since both quantities are diagonal. Two other piezoelectric coefficients are frequently used in the literature: the stress coefficient

$$e_{mi} = - \left(\frac{\partial \sigma_i}{\partial E_m} \right)_{\tau,S} = \left(\frac{\partial D_m}{\partial \sigma_i} \right)_{E,S} \quad (25)$$

and the voltage coefficient

$$g_{mi} = - \left(\frac{\partial E}{\partial \sigma_i} \right)_{D,S} = \left(\frac{\partial \tau_i}{\partial D_m} \right)_{\sigma,S} \quad (26)$$

The four piezoelectric coefficients are interrelated through the following equations

$$d_{mi} = \epsilon_{nm}^{\sigma} g_{ni} = e_{mj} s_{ji}^E \quad (27)$$

$$g_{mi} = \beta_{nm}^{\sigma} d_{ni} = h_{mj} s_{ji}^D \quad (28)$$

$$e_{mi} = \epsilon_{nm}^{\tau} h_{ni} = d_{mj} c_{ji}^E \quad (29)$$

$$h_{mi} = \beta_{nm}^{\tau} e_{ni} = g_{mj} c_{ji}^D \quad (30)$$

3.2 COUPLING FACTOR

Neglecting the thermal term and using equations (13)–(14), the internal energy of the system is

$$\begin{aligned} U &= \frac{1}{2} \tau_i \sigma_i + \frac{1}{2} D_m E_m \\ &= \underbrace{\frac{1}{2} \sigma_i s_{ij} \sigma_j}_{U_e} + 2 \cdot \underbrace{\frac{1}{2} E_m d_{mi} \sigma_i}_{U_m} + \underbrace{\frac{1}{2} E_m \epsilon_{mn} E_n}_{U_d} \end{aligned} \quad (31)$$

The coupling factor is defined as the ratio of the mutual elastic and dielectric energy U_m to the geometric mean of the elastic and dielectric self-energies U_e and U_d

$$k = \frac{U_m}{\sqrt{U_e U_d}} \quad (32)$$

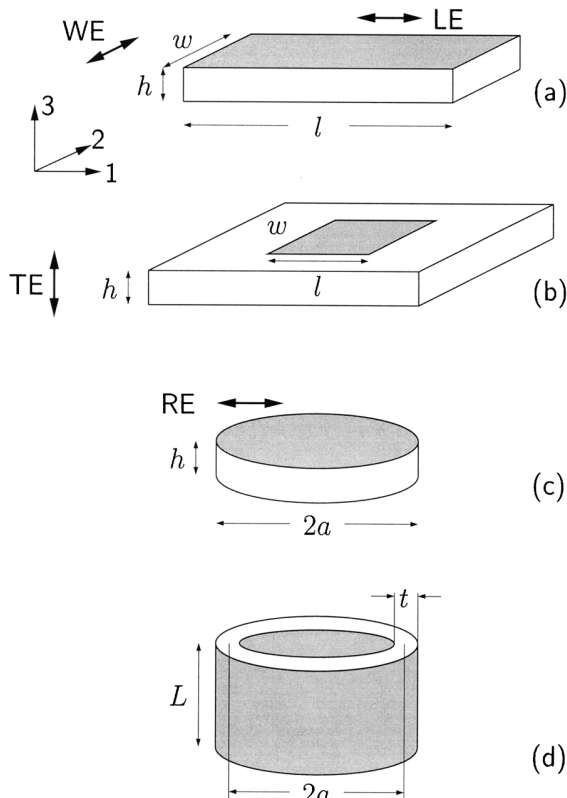


Figure 2. Important resonator geometries. a, Length- and width extender bar; b, laterally clamped thickness extension resonator; c, thin radial resonator; d, radially poled cylinder. The metal electrodes are indicated by the shaded areas.

An alternative definition of the coupling factor is based on the electromechanical energy conversion during a compression-expansion cycle. With the mechanical work W_1 and W shown in Figure 3, the coupling factor is defined as

$$k = \frac{W_1}{W_1 + W_2} \quad (33)$$

As shown in [31], this definition leads to the same results as equation (32).

In general, equation (31) is rather complicated due to the large number of tensor components. For piezoelectric resonances in polymer films, however, this number is greatly reduced by symmetry of the material, as well as the sample geometry. First, many poled piezoelectric polymers have a $C_{\infty m}$ (∞m) symmetry.¹ The first symbol refers to the Schönflies classification, the second (in parentheses) to the Hermann-Mauguin notation where the material constants are identical to that of the C_{6v} ($6mm$) crystal class. As shown in Table 2, there are only 5 independent elastic, 3 piezoelectric and 2 dielectric constants. Uniaxially stretched polymers belong to the C_{2v} ($mm2$) symmetry class, which exhibits 9 independent elastic, 5 piezoelectric and 3 dielectric constants.

The number of relevant material parameters may be further reduced by the sample geometry. For example, for a thin plate with metallized surfaces normal to the z or 3 direction (Figure 2a), the electric fields E_1 and E_2 vanish. If a stress is applied parallel to the x axis and the bar is

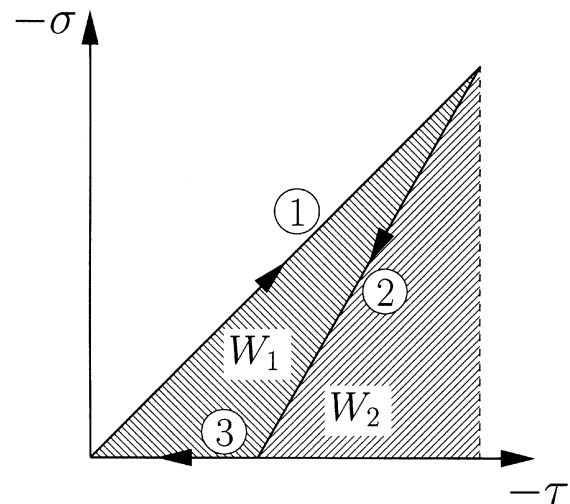


Figure 3. Stress-strain diagram showing the electromechanical energy conversion during a compression-expansion cycle. 1, compression under short-circuit conditions; 2, removal of mechanical stress with electric load connected; 3, short-circuiting. During compression, the energy $W_1 + W_2$ is stored in the sample. Upon expansion, the work W_1 is performed on the load [31].

¹The first symbol refers to the Schönflies classification, the second (in parentheses) to the Hermann-Mauguin notation.

shown later (see, e.g., equation (51)), the resonance or antiresonance frequency is inversely proportional to the relevant sample dimension. Since the thickness of most polymer films is considerably smaller than their lateral dimensions, the TE resonance occurs at significantly higher frequencies than, e.g., length- and width extension modes.

Under these assumptions, Newton's equation of motion for a wave propagating in the z direction of a thin film is

$$\rho \frac{\partial^2 \xi_3}{\partial t^2} dx dy dz = \frac{\partial \sigma_3}{\partial z} dx dy dz, \quad (44)$$

where ξ_3 is the displacement of a small volume element in the z direction and ρ is the density. As mentioned earlier, $\partial D/\partial z = 0$ in samples free of space charge. Using $\tau_3 = \partial \xi_3/\partial z$ and inserting the constituent equations for laterally clamped samples (20)–(21) we obtain

$$\frac{\partial^2 \xi_3}{\partial t^2} = \frac{c_{33}^D}{\rho} \frac{\partial^2 \xi_3}{\partial z^2} \quad (45)$$

For a harmonic excitation $D_3(z,t) = D_0 \exp(i\omega t)$ the differential equation is solved by

$$\xi_3(z,t) = \left(A \sin \frac{\omega z}{v_3^D} + B \cos \frac{\omega z}{v_3^D} \right) e^{i\omega t} \quad (46)$$

where

$$v_3^D = (c_{33}^D/\rho)^{1/2} \quad (47)$$

is the speed of sound in the z direction. For a free-standing sample the boundary condition ($\sigma_3 = 0$ at $z = 0, h$, where h is the sample thickness as shown in Figure 2b) applies. Since $\tau_3 = \partial \xi_3/\partial z$, we can use equation (20) to calculate A and B , obtaining

$$\tau_3 = \frac{h_{33}^2}{c_{33}^D} D_0 \left[\cos \frac{\omega z}{v_3^D} + \tan \frac{\omega h}{2v_3^D} \sin \frac{\omega z}{v_3^D} \right] \exp(i\omega t) \quad (48)$$

The electrical response of the piezoelectric sample is given by its impedance

$$Z = \frac{V_3}{I_3} = \frac{\int_0^h E_3 dz}{lw \dot{D}_3} \quad (49)$$

where V_3 is the voltage across the sample in the z direction and I_3 is the current in the same direction. Substituting equations (21) and (48) into (49) and converting to the complex capacitance $\tilde{C} = 1/(i\omega Z) = C' - iC''$, we finally obtain

$$\tilde{C}_{\text{TE}}(\omega) = \frac{\epsilon_{33}^T lw}{h} \frac{1}{1 - k_t^2 \frac{\tan(\omega/4f_{a,\text{TE}})}{\omega/4f_{a,\text{TE}}}} \quad (50)$$

where

$$f_{a,\text{TE}} = \frac{v_3^D}{2h} = \frac{1}{2h} \sqrt{\frac{c_{33}^D}{\rho}} \quad (51)$$

is the antiresonance frequency (at which, in the absence of losses, the reactance $X = \Im \tilde{Z} = 0$). Once $f_{a,\text{TE}}$ has been determined from the experimental spectrum, equation (51) can be used to calculate the elastic stiffness c_{33} .

When one of the sample faces is attached to a substrate, a different boundary condition ($\tau_3 = 0$ at $z = 0$, $\sigma_3 = 0$ at $z = h$) applies. In this case the complex capacitance is still described by equation (50); however, the antiresonance frequency is reduced by a factor of two

$$f_{a,\text{TE}}^{\text{cl}} = \frac{1}{4h} \sqrt{\frac{c_{33}^D}{\rho}} \quad (52)$$

3.3.2 LENGTH-EXTENSION RESONANCE

Let us now consider a thin bar with an electric field applied parallel to the z axis (Figure 2a). For a non-zero d_{31} piezoelectric coefficient this will cause a mechanical stress in the x direction. If the bar is free to cross-expand in the y and z directions, $\sigma_2 = \sigma_3 = \sigma_4 = \sigma_5 = \sigma_6 = 0$, which is why σ is chosen as one of the independent variables. Since the electroded faces form equipotential surfaces ($E = \text{const.}$) in the direction of motion, the electric field E is the natural choice for the other independent variable, so that equations (13)–(14) are the relevant constituent equations. Newton's equation of motion is equivalent to equation (44), with ξ_3 and $(\partial \sigma_3/\partial z)$ replaced by ξ_1 and $(\partial \sigma_1/\partial x)$, respectively. With $\tau_1 = \partial \xi_1/\partial x$ we obtain

$$\rho \frac{\partial^2 \xi_1}{\partial t^2} = \frac{1}{s_{11}^E} \frac{\partial^2 \xi_1}{\partial x^2} - \frac{d_{31}}{s_{11}^E} \frac{\partial E_3}{\partial x} \quad (53)$$

where the last term vanishes since the xy plane is an equipotential surface. For a harmonic excitation $E_3(t) = E_0 \exp(i\omega t)$ the solution $\xi_1(x,t)$ to this differential equation has the same functional form as equation (46), with v_3^D replaced by the speed of sound in the x direction

$$v_1^E = (\rho s_{11}^E)^{-1/2}. \quad (54)$$

As before, A and B are obtained from the boundary conditions $\sigma_1 = 0$ at $x = 0, l$ (where l is the sample length). The complex capacitance $\tilde{C}_{\text{LE}} = 1/(i\omega Z)$ is then given by

$$\begin{aligned} \tilde{C}_{\text{LE}}(\omega) &= \frac{I}{i\omega V} = \frac{\int_0^l \dot{D}_3 dx}{i\omega \int_0^h E_3 dz} \\ &= \frac{\epsilon_{33}^T lw}{h} \left\{ (1 - k_{31}^2) + k_{31}^2 \frac{\tan(\omega/4f_{r,\text{LE}})}{\omega/4f_{r,\text{LE}}} \right\} \quad (55) \end{aligned}$$

The impedance Z reaches a minimum at the resonance frequency

$$f_{r,LE} = \frac{v_1^E}{2l} = \frac{1}{2l\sqrt{\rho s_{11}^E}} \quad (56)$$

3.3.3 WIDTH-EXTENSION RESONANCE

Samples of significantly different length l and width w show both LE and width extension (WE) resonances that are separated in the spectrum by a factor of l/w . At first glance, one might expect that the complex capacitance is described by a relation completely analogous to (55). However, there is a subtle difference: since the resonance frequency for the WE resonator is higher than the LE resonance frequency, the sample can be considered clamped in the x direction, so that both σ_1 and σ_2 are generally non-zero, whereas $\sigma_3 = \sigma_4 = \sigma_5 = \sigma_6 = 0$. Consequently, the solution to the equation of motion is slightly different compared to the previous case of LE resonances [34]. The speed of sound in the y direction is

$$v_2^E = \left(\frac{s_{11}^E}{\rho(s_{11}^E s_{22}^E - (s_{12}^E)^2)} \right)^{1/2} \quad (57)$$

and the complex capacitance

$$\tilde{C}_{WE}(\omega) = \frac{\epsilon_{33}^\sigma l w}{h} (1 - k_{31}^2) \left\{ (1 - k_{WE}^2) + k_{WE}^2 \frac{\tan(\omega/4 f_{r,WE})}{\omega/4 f_{r,WE}} \right\} \quad (58)$$

where the WE resonance frequency and coupling factor are defined by

$$f_{r,WE} = \frac{v_2^E}{2w} \quad (59)$$

and

$$k_{WE}^2 = \frac{s_{11}^E}{(1 - k_{31}^2) \epsilon_{33}^\sigma (s_{11}^E s_{22}^E - s_{12}^E)} \left(d_{32} - \frac{s_{12}^E}{s_{11}^E} d_{31} \right)^2 \quad (60)$$

respectively.

3.3.4 RADIAL RESONATORS

A frequently used geometry is that of thin circular disks electroded on their major faces (Figure 2c). The equations of motion in cylindrical geometry were treated extensively by Mason [35] and summarized in the IEEE Standard on Piezoelectricity [31]. For brevity, only the final result will be presented here. The capacitance of a thin circular plate of radius a and thickness h is given by

$$\tilde{C}_R(\omega) = -\frac{\epsilon_{33}^p \pi a^2}{h} \left[\frac{2(k^P)^2}{1 - \nu - \Omega J_0(\Omega)/J_1(\Omega)} \right] \quad (61)$$

where J_0 and J_1 are the 0th and 1st order Bessel functions of the first kind,

$$\Omega = \frac{\omega a}{v^P} \quad (62)$$

and k^P is the planar radial coupling factor, related to the planar coupling factor defined in equation (36) by

$$(k^P)^2 = \frac{1 + \nu^E}{2} \left(\frac{k_p^2}{1 - k_p^2} \right) \quad (63)$$

Furthermore,

$$v^P = \sqrt{\frac{1}{\rho s_{11}^E [1 - (\nu^E)^2]}} \quad (64)$$

is the planar radial speed of sound (equal to v_2^E from equation (57) if $s_{11} = s_{22}$) and

$$\epsilon_{33}^p = \frac{-2d_{31}^2}{s_{11}^E - s_{12}^E} + \epsilon_{33}^\sigma \quad (65)$$

is the planar radial permittivity.

3.3.5 RADIALLY POLED CYLINDERS

Certain transducer applications, such as piezoelectric cables [36], use cylindrical shells, also known as radially poled cylinders (RPC). This resonator geometry, shown in Figure 2d, was first treated by Haskins and Walsh [37] and used in the calculation of material parameters by Tasker et al. [38]. This case is more complicated than the previously discussed geometries as coupling between the LE and the radial mode must be taken into account. The frequency dependence of the complex capacitance is given by

$$\tilde{C}_{RPC}(\omega) = \frac{2\pi a L \epsilon_{33}^\sigma}{t \alpha(\omega)} \left\{ k_{31}^2 \frac{[1 - (1 + \nu)\Omega^2]^2 \tan(\kappa L/2)}{1 - \Omega^2} \frac{\kappa L/2}{\kappa L/2} + 1 - k_{31}^2 - (1 + \nu)[(1 - \nu - 2k_{31}^2)\Omega^2] \right\} \quad (66)$$

with

$$\Omega = \frac{\omega a}{v} \quad (67)$$

$$\alpha(\omega) = 1 - (1 - \nu^2)\Omega^2 \quad (68)$$

and

$$\kappa = \frac{\omega}{v} \left[\frac{\alpha(\omega)}{1 - \Omega^2} \right]^{1/2} \quad (69)$$

Here, a is the radius of the cylinder (more precisely, the arithmetic mean of the inner and outer radius), t is its

wall thickness and L its height. To avoid coupling with other modes, the condition $t \leq a/10$ should be fulfilled.

3.3.6 THICKNESS SHEAR RESONANCE

Finally, we shall briefly consider the thickness shear (TS) mode. As shown in Figure 4, it is observed in thin samples electroded perpendicular to the poling direction. The derivation of the equations motion [39] is very similar to the case of thickness extension resonances and will not be repeated here. The capacitance is given by

$$\tilde{C}_{\text{TS}}(\omega) = \frac{\epsilon_{11}^{\tau} h w}{h} \frac{1}{1 - k_{15}^2 \frac{\tan(\omega/4f_{a,\text{TS}})}{\omega/4f_{a,\text{TS}}}} \quad (70)$$

where

$$k_{15}^2 = \frac{d_{15}^2}{\epsilon_{11}^{\tau} s_{44}^E} \quad (71)$$

is the shear coupling factor and

$$f_{a,\text{TS}} = \frac{v_3^D}{2h} = \frac{1}{2h} \sqrt{\frac{c_{55}^D}{\rho}} \quad (72)$$

is the TS antiresonance frequency.

3.4 LOSSES IN PIEZOELECTRIC POLYMERS

Materials subjected to a periodic mechanical or electrical stress exhibit some energy dissipation into heat. Mechanical losses may originate from molecular relaxation processes [40]. In polymers, the joint motion of the main chain and side groups at the glass transition temperature is generally referred to as the α relaxation, whereas processes involving shorter main chain segments or side groups only are known as β , γ , ... relaxations. If the participating molecular groups carry an electric dipole moment, there will be both mechanical and electrical energy dissipation.

The combined effect of mechanical, electromechanical and electrical losses were first described by Holland [41]

who calculated the power dissipation density

$$P_d = \frac{1}{2} \omega \Im(E \cdot D' + \sigma \cdot \tau') \quad (73)$$

where \Im denotes the imaginary part. By inserting the appropriate constituent equations (13)–(14) or (20)–(21), it was shown that P_d is proportional to the imaginary parts of s_{ij} , d_{mj} and ϵ_{mn} , which are commonly defined by

$$s_{ij} = s'_{ij} - i s''_{ij} \quad (74)$$

$$d_{mj} = d'_{mj} - i d''_{mj} \quad (75)$$

$$\epsilon_{mn} = \epsilon'_{mn} - i \epsilon''_{mn} \quad (76)$$

Certain restrictions are imposed on the values of the imaginary parts due to the requirement that power dissipation must always be positive. With a complex compliance s_{ij} (or stiffness c_{ij}), the resonance and antiresonance frequencies from equations (56) and (51), respectively, must also be complex, as well as the coupling constants k_{31} , k_{33} and k_t , defined in equations (35), (39) and (41), respectively.

3.5 A SAMPLE FREQUENCY SPECTRUM

To conclude this section, we shall examine the frequency spectrum of the complex capacitance in the vicinity of a TE resonance. Even though the discussion is based on a TE resonator, the general shape of the spectrum is similar for all geometries and modes discussed in this work.

The spectrum resulting from equation (50) is shown in Figure 5. At the antiresonance frequency $f_{a,\text{TE}}$, the real part of the capacitance C' exhibits a typical resonance shape, while C'' shows a loss peak. Also visible are odd-numbered higher harmonics. Even-numbered harmonics do not appear in the spectrum, since the symmetric motion in different regions of the sample cancels the electric response. The height of the loss peak is proportional to the square of coupling factor k_t , whereas its width is primarily determined by the imaginary part of the antiresonance frequency, and thus by the imaginary part c_{33}'' of the elastic stiffness. In materials with high mechanical losses the broadened line shape may lower the sensitivity and accuracy in determining the material parameters. In addition, high-loss samples generally require a *least squares*

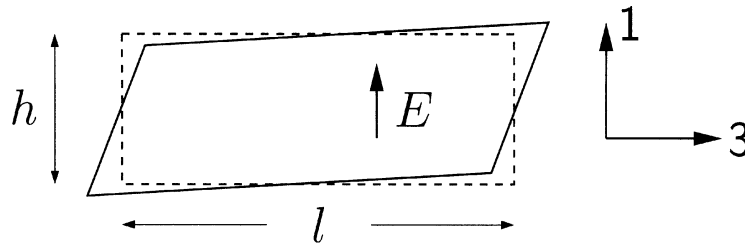


Figure 4. Schematic view of the thickness shear (TS) mode. The sample is poled in the z or 3 direction and electroded on the faces perpendicular to the x (1) axis.

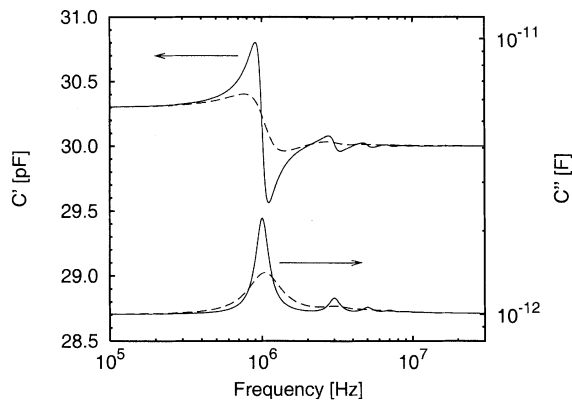


Figure 5. Calculated frequency dependence of C' and C'' for the TE resonance (equation (50)). A constant loss of $i10^{-12}$ F was added to the capacitance to simulate a frequency-independent dielectric loss. The parameters used in calculating the spectrum were: $(\epsilon_{33}^T l w/h) = 30.0$ pF, $k_t = 0.1$, $f_{a,TE} = (1.0 + 0.1i)$ MHz (solid lines) and $(1.0 + 0.3i)$ MHz (dashed lines).

fit data analysis (cf. Section 4.4) for obtaining accurate results.

4 EXPERIMENTAL TECHNIQUES

While the main focus of this review is on dielectric resonances, some other commonly used methods for measuring piezoelectric coefficients will be described in the following paragraphs.

4.1 STATIC AND DYNAMIC MECHANICAL MEASUREMENTS

To investigate piezoelectric properties, a variety of techniques have been described in the literature. In quasistatic [10,42] or dynamic measurements [43,44] of the direct piezoelectric coefficient, a mechanical force was applied to the samples and the resulting electrical signal was measured. To study the inverse piezoelectric properties a frequency-dependent electric field was applied and the vibration of the film was measured in either direct contact, using, e.g., atomic force microscopy [45] or a stylus profilometer [46], or without direct contact using an acoustical technique [21,22,47,48]. Some of these techniques impose a significant mechanical load on the sample, which can lead to deformations of samples with low elastic stiffness [43,49].

In addition to the above mentioned methods, several techniques based on the propagation of acoustic or thermal steps or waves have been developed to study the depth profile of d_{33} [50]. However, acoustic pulse- and step-wave methods are difficult to apply to porous and cellular electrets due to their large acoustic scattering.

4.2 INTERFEROMETERS

An all-optical technique that does not require a mechanical contact to the sample is the interferometric detection of changes in the sample thickness after applying an electric field, thus making use of the inverse piezoelectric effect. In typical polymer films with a thickness of 10 μm and d_{33} around 10 pm/V, application of moderate electric fields ($E \approx 1 \dots 10$ V/ μm) leads to a displacement of 1 nm at best, well below optical wavelengths. However, using a sinusoidal excitation and lock-in detection of the optical signal, displacements as small as a few pm can be detected. The d_{33} coefficient of PVDF was measured using a Twyman-Green or Michelson interferometer [51,52]. The effects of temperature drift are minimized in a Nomarski interferometer [53], where a part of the sample not exposed to the electric field serves as reference mirror. For films with rough surfaces the reflectivity must be improved by, e.g., attaching a reflective foil [43]. In addition to the piezoelectric coefficient, the electrostrictive properties can be obtained from the response at twice the excitation frequency [54].

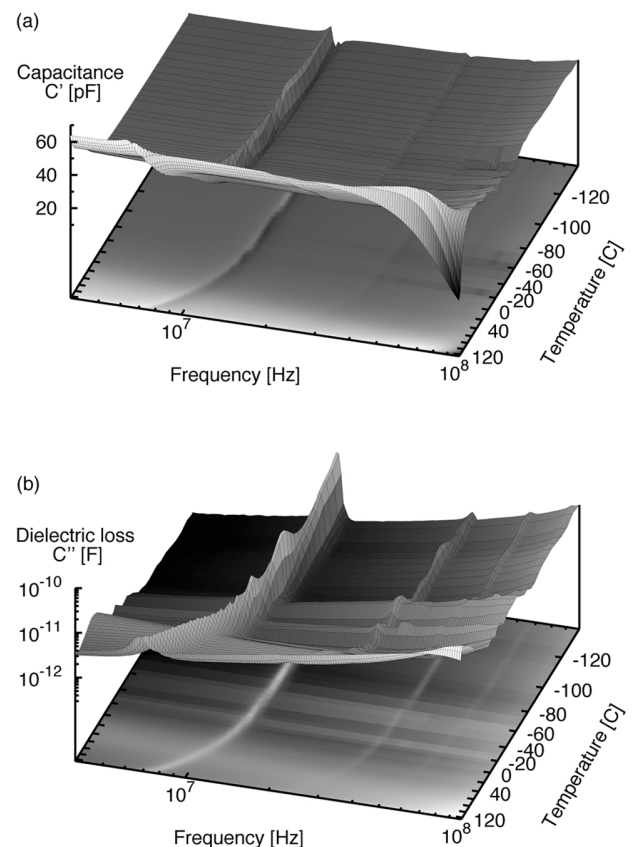


Figure 6. Temperature-frequency map of the real (a) and imaginary (b) capacitance near the thickness extension resonance of a commercial P(VDF-TrFE) copolymer film (Piezotech SA, thickness 110 μm). The plot shows the fundamental thickness extension resonance near 10 MHz, as well as the 3rd, 5th and (very weakly) the 7th harmonics. Above the glass transition temperature, the softening of the material leads to a decrease in the resonance frequency [88].

4.3 DIELECTRIC SPECTROSCOPY

Dielectric spectroscopy is a well-established research tool for investigating molecular dipole relaxations [55,56]. Typically, the real and imaginary capacitance of the sample are recorded over a broad range of frequencies stretching from the μHz range up to several GHz [57]. The same equipment can be used to study the piezoelectric resonances described in Section 3. Unlike molecular relaxations, where the full width at half maximum (FWHM) is at least 1.14 decades (for a pure Debye-type relaxation), resonance peaks are often much narrower, depending on the mechanical quality factor Q_m defined in equation (77). Therefore, a higher frequency resolution is required, so that $\Delta f/f \ll (1/Q_m)$. The thickness extension resonance typically occurs at frequencies between 100 kHz and 100 MHz, depending on the elastic stiffness and thickness of the sample, according to equation (51). Below 30 MHz, standard dielectric analyzers (such as LCR bridges and frequency response analyzers) can be used. At higher frequencies, stray capacitances and inductances significantly affect the accuracy of the measured impedance or capacitance. However, impedance analyzers measuring the complex reflection coefficient of a coaxial line terminated by the sample have been successfully used to study resonances around 100 MHz [58].

In contrast to mechanical or interferometric measurements, a single dielectric spectrum yields three important material parameters (elastic modulus or compliance, permittivity and electromechanical coupling factor), from which the piezoelectric coefficient can be deduced. Moreover, by acquiring dielectric spectra at different temperatures the temperature dependence of these parameters is easily obtained. As an example, Figure 6 shows the real and imaginary capacitance of a poly(vinylidene-trifluoroethylene) copolymer film as a function of both frequency and temperature.

Depending on the piezoelectric coefficient under investigation, different sample geometries must be used [32,59]. As shown in Figure 7, square or circular electrodes with an area between 1 and 3 cm^2 are commonly utilized for measuring d_{33} or e_{33} via TE resonances. Narrow strips are suitable for analyzing LE and WE resonances, yielding d_{31} and d_{32} . However, care must be taken to ensure the absence of mode coupling [60]. A length-to-width ratio of 8 is often considered sufficient to separate the LE and

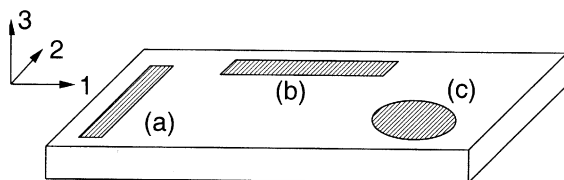


Figure 7. Electrode geometries for measuring d_{31} , d_{32} (a and b) and d_{33} piezoelectric coefficients (c) [32].

WE modes [61], although higher harmonics of the LE mode could affect the WE resonance in materials with a high mechanical quality factor Q_m .

Often there is a preferential direction in the polymer (such as the draw axis for uniaxially stretched films) along which the electrodes should be oriented. The evaporated electrodes should have sufficient thickness to minimize their resistance. Otherwise, this resistance, together with the sample capacitance, will give rise to a Debye relaxation spectrum at high frequencies, leading to a substantial increase in the dielectric loss and reducing the overall sensitivity to detect small piezoelectric resonances. Special care should be taken to ensure a uniform sample thickness across the electroded area. Non-uniformities will lead to a dampened and broadened resonance spectrum, resulting in underestimated coupling factors k_t or k_{31} .

A potential disadvantage of the resonance method is its lower sensitivity compared to the previously discussed mechanical and interferometric techniques. This is due to the fact that the resonance amplitude is proportional to the square of the coupling factor (cf. equations (50) and (55)) and hence (according to equations (35), (39) and (41)) to the square of the piezoelectric coefficient. For small coefficients, the height of the resonance profile will therefore approach the resolution limit of the dielectric spectrometer, especially in the presence of high mechanical losses. Nevertheless, values as low as 2 pC/N have been successfully observed [61]. Ohigashi [32] estimated that piezoelectric resonances can be observed and analyzed if the quantity $k^2 Q_m$ is larger than approx. 0.005. Here, Q_m represents the mechanical quality factor given by

$$Q_m = (\tan \delta_m)^{-1} = \frac{c'}{c''} \quad (77)$$

where $\tan \delta_m$ is the mechanical loss tangent and c' and c'' are the real and imaginary parts of the elastic stiffness.

4.4 ANALYSIS OF DIELECTRIC RESONANCE DATA

The dielectric measurement yields the real and imaginary components of the impedance \tilde{Z} , admittance \tilde{Y} or capacitance \tilde{C} . The former quantities are commonly used in electrical engineering, while the latter (or the permittivity, which for a parallel plate capacitor with an electrode area A is related to \tilde{C} via $\tilde{C} = \epsilon_{33} A/h$) is the preferred representation in dielectric spectroscopy, since there is no inherent frequency dependence in \tilde{C} , whereas both

$$\tilde{Y} = i\omega\tilde{C} \quad (78)$$

and

$$\tilde{Z} = (i\omega\tilde{C})^{-1} \quad (79)$$

are frequency-dependent even in the absence of molecular relaxations or resonances.

4.4.1 NON-REGRESSION TECHNIQUES

From the experimental data, the material parameters k , c (or s) and d (or e) can be calculated in several ways. Often, the parallel and series resonance frequencies f_p and f_s (defined as the frequencies where the real parts of the impedance \tilde{Z} and admittance \tilde{Y} have a maximum, respectively) are used for this purpose. For example, the impedance of a TE resonator is obtained from equations (50) and (79) as

$$\tilde{Z}_{TE}(\omega) = \frac{h}{i\omega\epsilon_{33}lw} \left[1 - k_t^2 \frac{\tan(\omega/4f_{a,TE})}{\omega/4f_{a,TE}} \right] \quad (80)$$

so that

$$k_t^2 = \frac{\pi f_s}{2 f_p} \tan\left(\frac{\pi f_p - f_s}{2 f_p}\right) \quad (81)$$

The elastic stiffness is readily obtained from equation (51) if both sample thickness and density are known. This method is recommended in the IEEE Std. 176-1987 [31], and is applicable to materials with small losses. Other approaches, such as the modified f_p and f_s approach by Sherrit et al. [62] or the iterative method by Smits [63,64] have been more successful in incorporating small losses, but still fail to obtain accurate material parameters from materials with higher dielectric losses, as was clearly shown in a careful comparison of different analysis methods by Kwok et al. [65].

4.4.2 NON-LINEAR LEAST SQUARES REGRESSION

Comparing the results for a number of different materials (among them two polymers, PVDF and P(VDF-TrFE)), the authors of the previously mentioned study [65] concluded that a direct non-linear *least squares* fit of the experimental data to the functional form of, e.g., equations (80) or (50) yields the most accurate results, and also can take into account the frequency dependence of ϵ_{33} and the dielectric loss δ_e defined by

$$\tan \delta_e = \frac{\epsilon_{33}''}{\epsilon_{33}'} \quad (82)$$

For example, when the resonance frequency lies in the vicinity of a molecular relaxation, it may be necessary to include the contribution from dipole relaxation in the form of, e.g., a Havriliak-Negami term [56]

$$\epsilon(\omega) = \epsilon_\infty + \frac{\Delta\epsilon}{\{1 + (i\omega\tau)^\alpha\}^\beta} \quad (83)$$

where $\Delta\epsilon$ is the relaxation strength and α and β are phenomenological shape parameters. Moreover, this method can handle large mechanical losses (as shown by, e.g., the analysis of porous Teflon[®] AF films [66]) and does

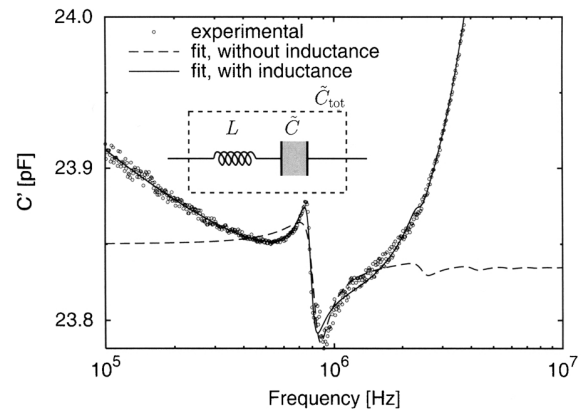


Figure 8. Experimental and fitted dielectric spectrum of a cellular PP sample. The dashed curve results from a fit of equation (84) to the measured data; the solid curve was obtained with the modifications to equation (84) described in the text. The inset shows the equivalent circuit described by equation (85).

not depend on arbitrary choices of a reference frequency. Since many programming languages and least squares fitting routines are designed to work with real numbers only, Kwok et al. separated equation (80) into its real and imaginary part by neglecting mechanical losses higher than second order. However, a number of recent software packages, such as the freely available GNU PLOT [67] have a built-in capability to handle complex numbers in their fitting routine. In this case, equations (50) or (80) can be used directly to obtain the relevant material parameters. As the real and imaginary part of the complex capacitance $\tilde{C}(\omega)$ are related through the Kramers-Kronig transform, it suffices to fit either $C'(\omega)$ or $C''(\omega)$ to the experimental data. Fitting the latter often requires augmenting equation (50) with an additional parameter $-iC_{loss}$ to allow for a background of frequency-independent loss.

To demonstrate the flexibility of non-linear regression techniques, we shall examine the case of a cellular polypropylene sample (cf. Section 5.2.1). The dielectric spectrum near the TE resonance was recorded with a HP 4192A impedance analyzer at room temperature. Due to the constraints of the experimental setup, the connecting wires had a non-negligible inductance of approx. 0.7 μ H, leading to a sharp rise in the real part of the sample capacitance C' above 2 MHz as seen in Figure 8. In addition, the off-resonance value of C' is slightly frequency-dependent, as visible in the spectrum towards the low frequency end. Initially, the real part of the equation

$$\tilde{C}_{TE}(\omega) = \frac{C_0}{1 - k_t^2 \frac{\tan(\omega/4f_{a,TE})}{\omega/4f_{a,TE}}} \quad (84)$$

was fitted to the experimental data in the frequency range between 500 and 2000 kHz, with the fit parameters C_0 (real), $f_{a,TE}$ and k_t (both complex). As shown by the

dashed curve in Figure 8, agreement with the experimental data was only fair. A significant improvement was obtained with two modifications:

- A frequency-dependent C_0 , as described by the polynomial

$$C_0(\omega) = C_{00} \left\{ 1 + a \log_{10} \left(\frac{\omega}{2\pi \Re f_{a,TE}} \right) + b \left[\log_{10} \left(\frac{\omega}{2\pi \Re f_{a,TE}} \right) \right]^2 \right\}$$

with the phenomenological parameters a and b . The terms were chosen so that $C_0(\omega) = C_{00}$ when the frequency $(\omega/2\pi)$ equals the real part $\Re f_{a,TE}$ of the anti-resonance frequency.

- Inductance was taken into account by calculating the effective capacitance

$$\tilde{C}_{\text{tot}}(\omega) = \frac{1}{-\omega^2 L + \tilde{C}_{\text{TE}}(\omega)^{-1}} \quad (85)$$

of an inductor in series with the sample capacitor, as depicted in the inset of Figure 8.

With equation (85) as the new model function and a frequency-dependent C_0 , there is good agreement between the solid curve and the experimental data across the entire recorded frequency range. The remaining deviation around 900 kHz most likely results from a non-uniform sample thickness, thus stressing the need for high-quality samples.

4.4.3 EQUIVALENT CIRCUITS

Even though a least squares fit is the method of choice for obtaining material parameters, it is sometimes advantageous (particularly for transducer applications) to describe the dielectric spectrum in terms of lumped circuit models. The widely used Van Dyke circuit model [31] shown in Figure 9a has four real circuit parameters. This is insufficient to model the dielectric function (50) of a piezoelectric resonance which has three complex parameters (ϵ_{33} , c_{33} and k_t) and hence six independent material constants. Recently, Sherrit et al. [68] successfully approximated the piezoelectric resonance spectrum using a circuit with three complex elements shown in Figure 9b. Their work gives conversion formulae between the lumped constants and the material parameters.

4.5 OTHER EXPERIMENTAL TECHNIQUES

Although most dielectric spectroscopy experiments are carried out in the frequency domain, experiments can and have also been performed in the time domain [55]. Therefore it is not surprising that time-domain techniques have

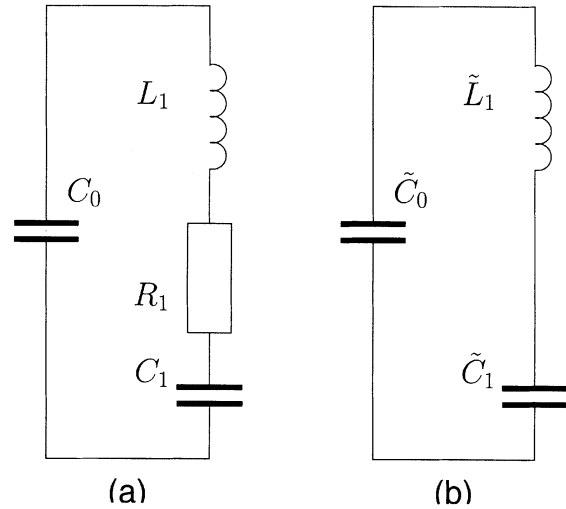


Figure 9. Lumped circuit models. a, Van Dyke model, where all circuit elements are real; b, Butterworth circuit model with complex circuit elements [68].

been successfully used to study the piezoelectric properties of polymer films. When the opaque surface of a polymer sample is instantaneously heated by a fast laser pulse (duration ≤ 10 ns), dampened oscillations are observed in the short-circuit current, as shown in Figure 10 [69]. Care must be taken, though, to separate the piezoelectric from the pyroelectric contribution [70].

One limitation of the piezoelectric resonance technique is the fact that the elastic and piezoelectric material parameters can only be determined at a fixed frequency which depends on the dimensions and elastic stiffness of the sample. In most cases, however, this is not a major concern since they exhibit only a weak frequency dependence [71]. For samples with low mechanical losses, the frequency dependence of the capacitance in the vicinity of higher odd-numbered harmonics may be used to obtain these parameters at a number of different frequencies from the same data. When the frequency dependence is a major concern, several samples with different width or thickness must be analyzed. In addition, other techniques such as surface acoustic waves (SAW) have successfully been used to determine material parameters at several frequencies for a single sample [71,72].

5 POLYMER MATERIALS

5.1 POLAR POLYMERS

5.1.1 POLY(VINYLIDENE FLUORIDE) AND ITS COPOLYMERS

As mentioned earlier, the first report of piezoelectric resonances in polymer materials was in Ohigashi's work on PVDF [32]. The dielectric spectra were recorded in a cryostat at temperatures between -170 and 100°C . Using different sample geometries, the author was able to mea-

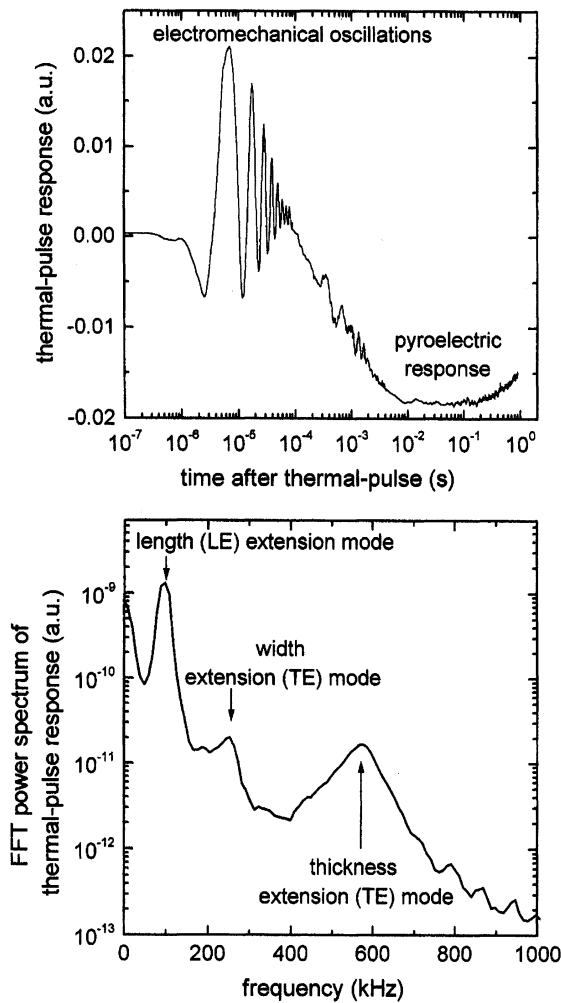


Figure 10. Thermal pulse response of a charged cellular polypropylene film. Top: time domain signal; bottom: frequency domain response (fast Fourier transform of time domain signal). The transient signal shows oscillations from TE, LE and WE resonances, as well as a pyroelectric contribution [69].

sure the temperature dependence of the piezoelectric coefficients e_{31} , e_{33} , d_{31} and d_{33} , as well as of the elastic constants s_{11} and c_{33} and the coupling factors k_{31} , k_{33} and k_{22} . While k_{33} remained at a constant value of 0.19 over a wide range of temperatures, k_{31} exhibited a strong increase above the glass transition temperature at approx. -40°C . Since LE resonances parallel to the y or z axis were very weak for PVDF stretched uniaxially in the x direction, k_{32} and d_{32} were determined from samples cut at various angles θ with the x axis. The effective piezoelectric coefficient $d_{31'}$ and elastic compliance $s_{11'E}$ are expressed by

$$d_{31'} = d_{31} \cos^2\theta + d_{32} \sin^2\theta \quad (86)$$

and

$$s_{11'E} = s_{11}^E \cos^4\theta + s_{22}^E \sin^4\theta + (2s_{12}^E + s_{16}^E) \sin^2\theta \cos^2\theta. \quad (87)$$

A similar study, combined with quasistatic and interferometric measurements was done by Schewe [73], who used a lumped-circuit approach rather than hand-matching the material parameters.

Copolymerization of trifluoroethylene with vinylidene fluoride produces a random copolymer with piezoelectric properties similar to PVDF. However, P(VDF-TrFE) is ferroelectric directly after extrusion from the melt and does not require stretching. Also, it exhibits a Curie temperature which depends on the TrFE content (unlike PVDF, which melts before reaching the Curie temperature). Generally, the piezoelectric coefficients and coupling constants are slightly larger than those found in PVDF [74]. Even higher values were observed by Omote et al. in "single crystalline" P(VDF-TrFE) formed by crystallization of uniaxially stretched films under stress-free conditions [75]. The effects of electrode clamping on commercial P(VDF-TrFE) tiles was studied by Sherrit et al. who compared the TE resonance spectra of flexible copolymer films to those of sandwich tiles with stiff electrodes [76]. They reported lower values of c_{33}^D and h_{33} , as well as a slight increase in ϵ_{33}^r , although they point out that these are only effective material constants for the copolymer-electrode system.

Other shapes besides the usual planar geometries may also be investigated with the resonance technique. Wegener and Gerhard-Multhaupt [36] studied the poling behavior of commercial piezoelectric polymer cables made of a P(VDF-TrFE) layer between an inner and outer conductor (Figure 11). The resonance spectra acquired at different temperatures are shown in Figure 12. For cables poled under optimized conditions, only a weak decrease in d_{33} was observed between 30 and 120°C , indicating a thermal stability similar to that of P(VDF-TrFE) films.

In addition to pure polymer films, ceramic-polymer composites such as lead zirconate titanate (PZT)/PVDF-TrFE have been widely used in medical ultrasound imaging. Due to their complex geometry, coupling between different modes of vibration must be taken into account [77,78].

5.1.2 ODD-NUMBERED POLYAMIDES

Another class of ferroelectric polymers with great promise for transducer applications are odd-numbered polyamides [4], also known under their trade name Nylon[®]. While they do not yet offer the same piezoelectric coefficients as PVDF and its copolymers, they can be

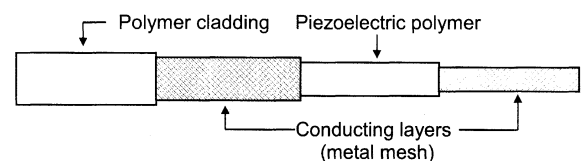


Figure 11. Schematic view of a piezoelectric polymer cable [36].

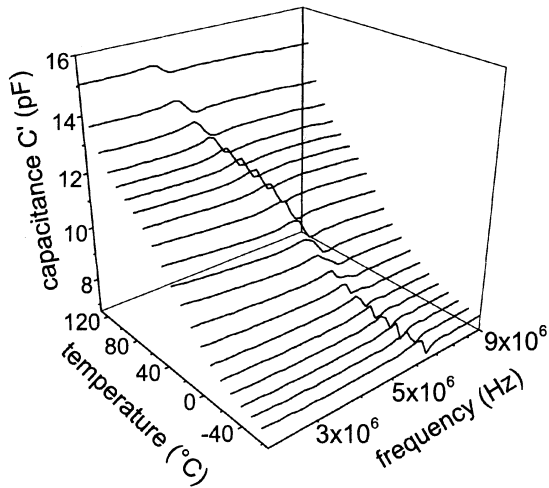


Figure 12. Frequency-temperature map of the capacitance C' for a commercial piezoelectric polymer cable. The TE resonance frequency shifts from 5.2 MHz at 30°C to 3.6 MHz at 120°C [36].

used at temperatures in excess of 200°C without significant degradation. The highest d_{33} values were reported for films prepared by melt-quenching in ice water and subsequent uniaxial stretching. Resonance spectroscopy was successfully applied to study the behavior of k_t and Q_m in both polyamide 7 and polyamide 11 at temperatures between 20 and 160°C [79]. With a value of about 0.11, the coupling factor k_t was lower than in PVDF, but stable up to 160°C. Also, the lower mechanical quality factor (8 in polyamide 7 and polyamide 11 compared to 25 in PVDF-TrFE) offers a greater bandwidth for transducer applications in an aqueous environment. Due to its higher remanent polarization, the coupling factor of polyamide 7 was expected to be higher than that of polyamide 11. This was not observed, although the authors note that an uneven film thickness could have affected the accuracy of the experiment. Very recently, Frübing et al. reported a mechanical quality factor of 11.5 in their own study of melt-quenched, cold-drawn polyamide 77 [80], which appears to confirm the importance of thickness uniformity. They also reported a piezoelectric coefficient of 5.3 pC/N at room temperature, which rapidly dropped to 3.8 pC after 30 min of annealing at 170°C, but remained unchanged upon further annealing. This decrease was attributed to a thermally unstable rigid amorphous phase which manifests itself in the dielectric spectrum through an α , relaxation above 90°C.

5.2 POROUS AND CELLULAR ELECTRET POLYMERS

In recent years, a new group of non-polar porous or cellular space charge electrets has received much attention in basic research as well as for transducer applications [20]. In contrast to polar non-porous polymers, they contain no microscopic dipoles. Instead, symmetry break-

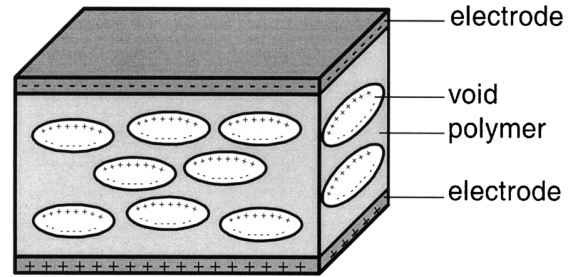


Figure 13. Schematic cross-section of a cellular polypropylene film. The charged voids act as macroscopic dipoles. Their flat shape gives rise to a low elastic stiffness c_{33} perpendicular to the film plane.

ing occurs on a macroscopic scale, resulting from charge separation inside the voids and trapping at the internal surfaces of the cellular structure (cf. Figure 13). The change in dipole moment upon application of a mechanical stress on the polymer surfaces gives rise to the (quasi-) piezoelectric behavior of these materials. Several examples will be discussed in this section.

5.2.1 CELLULAR POLYPROPYLENE

In cellular PP, which has become commercially available in recent years [81], a layer of biaxially stretched PP foam with a thickness between 30 and 120 μm is sandwiched between thin, non-porous PP films. The lens-like voids in the inner layer are between 10 and 100 μm long, but only a few μm thick, resulting in a substantial anisotropy in the elastic stiffness [61]. While the in-plane stiffness does not substantially differ from that of the compact polymer, the c_{33} elastic stiffness is only 2.2 MPa. Several types of PP foams with different thickness and void sizes have been developed by VTT Processes (formerly VTT Chemical Technology) [82].

The cellular PP films are electrically charged in a corona discharge, where the high electric field leads to Paschen breakdown inside the voids. This was recently demonstrated by recording the electroluminescence during charging using a bipolar poling field [46]. The assumed charging process of the internal surfaces was proved by imaging the charge distribution in obliquely cut cross sections of a charged film using a scanning electron microscope [83]. For the most sensitive HS01 type of cellular PP, electrical charging with a point-to-plane corona charging technique at normal atmosphere and room temperature yields quasistatic and dynamic d_{33} coefficients of 250 pC/N and 140 pC/N, respectively [59,84]. These values are around ten times higher than the piezoelectric activity found in PVDF, and can be enhanced up to 790 pC/N if the samples are treated in dielectric gases during or before corona charging [85]. The high d_{33} coefficients are the result of the low elastic modulus in the z direction. Since $e_{33} \approx d_{33}c_{33}$ (cf. equation (42)), it is evident from Table 3 that even though the stress coefficient e_{33} is 2–3

Table 3. Material parameters of different piezoelectric and quasi-piezoelectric polymers at room temperature, measured with the piezoelectric resonance technique.

	Polar			Non-polar	
	PVDF ¹	PVDF-TrFE ²	Polyamide 11 ³	Cellular PP ⁴	Porous Teflon [®] AF ⁵
s_{11} (10^{-9} m ² /N)	0.25	0.036		1.1	
s_{22} (10^{-9} m ² /N)	0.23	0.16		0.56	
c_{33} (10^6 N/m ²)	9470	11000	(4100–500i)	2.2	(0.17–0.26i)
k_{31}	0.161	0.15		0.018	
k_{32}	0.03	0.12		0.018	
k_t	0.205	0.292	0.11	0.06	0.1
d_{31} (pC/N)	27.9	7		2	
d_{32} (pC/N)	4.8	12			
d_{33} (pC/N)	–17.4	–38	7.6	140	600
e_{31} (mC/m ²)	110	140			
e_{32} (mC/m ²)	20	72			
e_{33} (mC/m ²)	–165	–185	31	0.31	0.24
ϵ_3/ϵ_0	7.7	5.5	2.2	1.23	

¹ From [32] (UO-2 film at 25°C).

² "Single crystalline" film at 295 K, from [75].

³ Calculated from Tables 2 and 3 in [79].

⁴ HS01 type, from [59].

⁵ From [66].

orders of magnitude smaller than in PVDF copolymers and polyamide, this is more than compensated by the lower c_{33} value. The anisotropic stretching conditions are reflected by a significant difference between the compliances s_{11} and s_{22} (cf. Table 3).

While the cellular PP films have been shown to retain their (quasi-)piezoelectric properties at temperatures up to 50°C, higher ambient temperatures lead to a rapid decrease in d_{33} [82]. Thermally stimulated current (TSC) experiments have indicated that the loss of sensitivity can be attributed to the detrapping of space charges from the air/PP interfaces in the voids.

Piezoelectric resonances were first studied in cellular PP by Neugschwandtner et al., who observed LE and TE resonances separated in frequency by only a factor of three (Figure 14). This is significantly less than one might expect based on the different dimensions along the x and z axes. For samples with a width of 4 mm and a thickness of 70 μ m, the resonance frequencies should be separated by more than a factor of 50, according to equations (51) and (56). Thus, the experimental result is a clear indication of the strongly anisotropic elastic modulus.

The different origin of (quasi-)piezoelectricity in polar polymers with oriented dipoles and in non-polar cellular space charge electrets also results in differences in their other electrical properties. To this date, none of the cellular or porous electrets exhibits a significant d_{31} coefficient or relevant pyroelectric properties. Thus, the use of the d_{33} effect is possible without having to separate these contributions.

Dielectric resonance spectroscopy is very sensitive to small changes in the (quasi-) piezoelectric coefficient. This high accuracy was recently used to detect the ultraviolet (UV)-induced 1% reduction of d_{33} in cellular PP [49]. PP

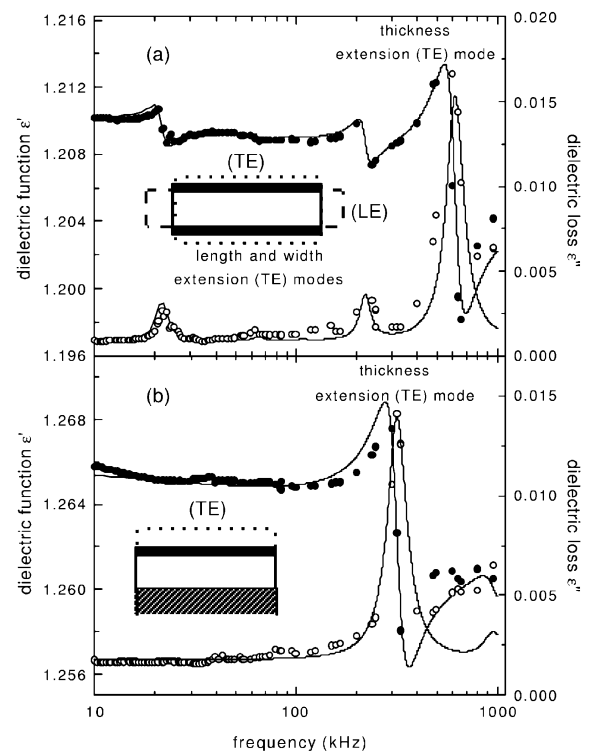


Figure 14. Dielectric function of a cellular polypropylene sample. a, mechanically free; b, clamped [61].

foam shows three distinct peaks (276, 223 and 198 nm) in its photostimulated discharge spectrum, which were interpreted as pertaining to deep charge traps. Figure 15 shows the decay of d_{33} during a 3.5 h irradiation at 200 nm [86]. During UV exposure, the spectra were acquired repeatedly in 5 min intervals. Unlike mechanical static or dy-

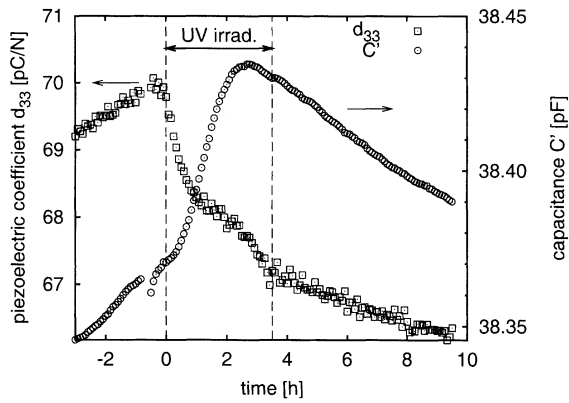


Figure 15. 4% reduction of the d_{33} coefficient in cellular polypropylene observed during a 3.5 h exposure to UV radiation at 200 nm. The low elastic stiffness of the material gives rise to a gradual thickness (and hence capacitance) drift of approx. 0.2% [86].

dynamic measurements, the piezoelectric resonance method imposes very little mechanical stress on the sample, thus avoiding inelastic deformation of the soft material.

5.2.2 POROUS TEFLON® AF

A relatively new member of the family of PTFE copolymers is the amorphous Teflon® AF. In addition to its low dielectric losses and high optical transmission, it is soluble in perfluorocarbons and hydrofluoroethers. Thin films can thus be prepared through a variety of solvent-based coating techniques. Porous Teflon® AF films were prepared from a solution of Teflon® AF 1600 resin in Fluorinert® FC-77 (3M) using a doctor-blade technique on a substrate heated above the boiling point of the solvent [66]. The evaporating solvent leaves a voided film with open pores, a thickness of 3...10 μm and a density of approx. 500 kg/m^3 , which was subsequently sealed with a non-porous Teflon® AF 1600 layer. The dielectric loss spectrum in Figure 16 shows a very broad resonance peak at a temperature-independent frequency of about 60 kHz.

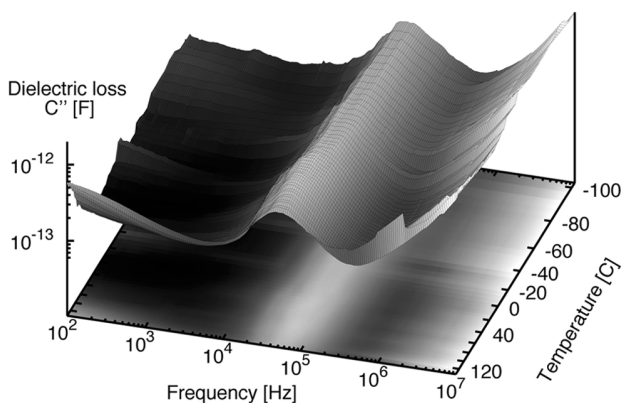


Figure 16. Dielectric loss (C'') of a 55 μm porous Teflon® AF 2400/non-porous Teflon® AF 1600 sandwich film, recorded as a function of frequency at different temperatures. (From [66].)

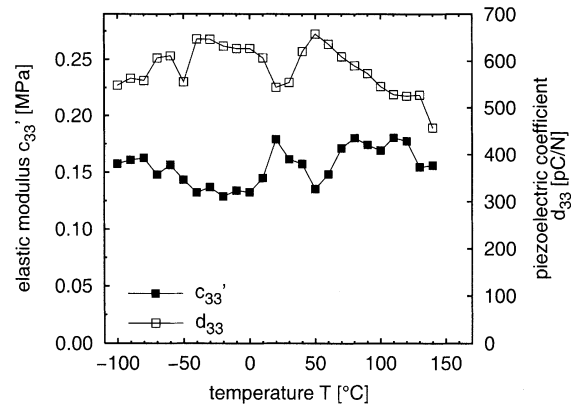


Figure 17. Temperature dependence of the elastic stiffness c'_{33} and the piezoelectric constant d_{33} of the same porous Teflon® AF sample as in Figure 16 [66].

Fitting equation (50) to the experimental data yielded a piezoelectric coefficient of $d_{33} \approx 600$ pC/N with only a slight temperature dependence. As shown in Figure 17, the piezoelectric effect is thermally stable up to 120°C, approx. 40°C below the glass transition temperature of Teflon® AF 1600. Note the very low elastic stiffness of about 150 kPa, which is only slightly larger than the bulk modulus of air. Dielectric spectroscopy experiments carried out at different pressures [66] have nevertheless confirmed that the observed stiffness results from the morphology of the polymer rather than air trapped inside the voids.

5.2.3 COMPOSITE MATERIALS

Porous polymers have also been combined with non-porous polymer layers in order to increase the piezoelectric response. In these composite materials, the softer porous layer performs the same function as the air gap in an electret condenser microphone. In a composite consisting of charged layers of porous PTFE and non-porous FEP, a piezoelectric coefficient of 150 pC/N was obtained at a resonance frequency of 160 kHz [87].

To summarize this section, Table 3 lists some important material parameters of the polymers discussed in this paper. For further information on piezoelectric polymers, the reader is referred to the reviews of Eberle et al. [5] and Gerhard-Mulhaupt [20] and Nalwa's comprehensive book on ferroelectric polymers [4].

6 CONCLUSIONS

DIELECTRIC spectroscopy has become an important tool for investigating the properties of piezoelectric polymers. While PVDF and its copolymers are already being used in many commercial applications, there is very active research in finding materials with higher piezoelectric constants. Closed-cell charge-storing polymer foams such as cellular PP are an attractive choice at

temperatures below 50°C, if the temperature dependence of its material parameters can be taken into account. New fluoropolymer-based foams offer a high degree of thermal stability with piezoelectric constants of up to 600 pC/N. As charge storage at the microscopic level is rather poorly understood at present, efforts are underway for a comprehensive investigation, combining optical, electrical and mechanical techniques. As part of this approach the piezoelectric resonance technique is particularly well-suited for *in situ* studies of elastic and piezoelectric material parameters.

ACKNOWLEDGMENTS

The author wishes to thank S. Bauer (Johannes Kepler University, Linz, Austria), R. Gerhard-Multhaupt, P. Frübing and M. Wegener (all University of Potsdam, Germany) for stimulating discussions and A. Pucher and W. Wirges for their experimental support.

REFERENCES

- [1] H. Kawai, "The piezoelectricity of poly(vinylidene fluoride)", *Jpn. J. Appl. Phys.*, Vol. 8, pp. 975–977, 1969.
- [2] E. Fukada, "History and recent progress in piezoelectric polymers", *IEEE Trans. Ultrason., Ferroelect., Freq. Contr.*, Vol. 47, no. 6, pp. 1277–1290, 2000.
- [3] T. Furukawa, "Structure and properties of ferroelectric polymers", *Key Engineering Materials*, Vol. 92–93, pp. 15–30, 1994.
- [4] H. Nalwa, Ed., *Ferroelectric Polymers*, New York, Marcel Dekker Inc., 1995.
- [5] G. Eberle, H. Schmidt, B. Dehlen, and W. Eisenmenger, "Piezoelectric polymer electrets", in *Electrets*, 3rd ed., R. Gerhard-Multhaupt, Ed., Morgan Hill, CA, Laplacian Press, Vol. 2, ch. 11, pp. 81–128, 1999.
- [6] F. Baltá Calleja, A. González Arche, T. A. Ezquerro, C. Santa Cruz, F. Batallán, B. Frick, and E. López Cabarcos, "Structure and properties of ferroelectric copolymers of poly(vinylidene fluoride)", in *Adv. Polym. Sci.*, H.-G. Zachmann, Ed., Vol. 108, pp. 1–48, 1993.
- [7] N. Koizumi, "Ferroelectric behavior and related physical properties of some copolymers of vinylidene fluoride", in *Key Engineering Materials*, D. K. Das-Gupta, Ed., Vol. 92–93, pp. 161–180, 1994.
- [8] X. Lu, A. Schirokauer, and J. Scheinbeim, "Giant electrostrictive response in poly(vinylidene fluoride-hexafluoropropylene) copolymers", *IEEE Trans. Ultrason., Ferroelect. Freq. Contr.*, Vol. 47, pp. 1291–1295, 2000.
- [9] A. C. Jayasuriya and J. I. Scheinbeim, "Ferroelectric behavior in solvent cast poly(vinylidene fluoride/hexafluoropropylene) copolymer films", *Appl. Surf. Sci.*, Vol. 175, pp. 386–390, 2001.
- [10] W. Künstler, M. Wegener, M. Seiss, and R. Gerhard-Multhaupt, "Preparation and assessment of piezo- and pyroelectric poly(vinylidene fluoride-hexafluoropropylene) copolymer films", *Appl. Phys. A*, Vol. 73, pp. 641–645, 2001.
- [11] P. A. Howie and H. R. Gallantree, "Transducer applications of PVDF", *IEEE Intern. Ultrasonics Sympos.*, Piscataway, NJ, IEEE Service Center, pp. 566–569, 1983.
- [12] R. H. Tancrell, D. T. Wilson, and D. Ricketts, "Properties of PVDF for sonar", *IEEE Intern. Ultrasonics Sympos.*, Piscataway, NJ, IEEE Service Center, pp. 624–629, 1985.
- [13] F. S. Foster, K. A. Harasiewicz, and M. D. Sherar, "A history of medical and biological imaging with polyvinylidene fluoride (PVDF) transducers", *IEEE Trans. Ultrason., Ferroelect., Freq. Contr.*, Vol. 47, pp. 1363–1371, 2000.
- [14] G. R. Harris, R. C. Preston, and A. S. DeReggi, "The impact of piezoelectric PVDF on medical ultrasound exposure measurements, standards, and regulations", *IEEE Trans. Ultrason., Ferroelect., Freq. Contr.*, Vol. 47, pp. 1321–1335, 2000.
- [15] B. Newman, J. Scheinbeim, J. Lee, and Y. Takase, "A new class of ferroelectric polymers, the odd-numbered nylons", *Ferroelectrics*, Vol. 127, pp. 229–234, 1992.
- [16] S. Miyata, M. Yoshikawa, S. Tasaka, and M. Ko, "Piezoelectricity revealed in the copolymer of vinylidene cyanide and vinyl acetate", *Polym. J.*, Vol. 12, pp. 857–860, 1980.
- [17] S. Tasaka, T. Shouko, and N. Inagaki, "Ferroelectric polarization reversal in polyureas with odd number of CH₂ groups", *Jpn. J. Appl. Phys.*, Vol. 31, pp. L1086–L1088, 1992.
- [18] S. Tasaka, T. Shouko, K. Asami, and N. Inagaki, "Ferroelectric behavior in aliphatic polyurethanes", *Jpn. J. Appl. Phys.*, Vol. 33, pp. 1376–1379, 1994.
- [19] S. Tasaka, K. Ohishi, and N. Inagaki, "Ferroelectric behavior in aliphatic polythioureas", *Ferroelectrics*, pp. 203–210, 1995.
- [20] R. Gerhard-Multhaupt, "Less can be more: Holes in polymers lead to a new paradigm of piezoelectric materials for electret transducers", *IEEE Trans. Dielectr. Electr. Insul.*, Vol. 9, pp. 850–859, 2002.
- [21] J. Backman, "Audio applications of electrothermomechanical film (ETMF)", *J. Audio Eng. Soc.*, Vol. 38, pp. 364–371, 1990.
- [22] J. Backman and M. Karjalainen, "Audio and ultrasonic transducers based on electrothermomechanical film (ETMF)", *IEEE Intern. Conf. Acoustics, Speech, and Signal Processing*, Vol. 2, Piscataway, NJ, IEEE Service Center, pp. 1173–1176, 1990.
- [23] H. Hoislbauer, R. Schwödianer, S. Bauer-Gogonea, and S. Bauer, "Patterned piezoelectricity in charged, cellular polymers for air-borne ultrasound devices", *IEEE 11th Intern. Sympos. Electrets*, Piscataway, NJ, IEEE Service Center, pp. 58–61, 2002.
- [24] J. Curie and P. Curie, "Développement par compression de l'électricité polaire dans les cristaux hémihédres à faces inclinées", *Bull. Soc. Min. France*, pp. 90–93, 1880.
- [25] J. Curie and P. Curie, in *Comptes rendus hebdomadaires des séances de l'académie des sciences*, Vol. 91. Paris: Gauthier-Villars, pp. 294–295, 1880.
- [26] A. M. Nicolson, "The piezo electric effect in the composite rochelle salt crystal", *AIEE Transactions*, Vol. 38, pp. 1467–1485, 1919.
- [27] W. G. Cady, "Theory of longitudinal vibrations of viscous rods", *Phys. Rev. Lett.*, Vol. 19, pp. 1–6, 1922.
- [28] M. v. Laue, "Piezoelektrisch erzwungene Schwingungen von Quarzstäben", *Z. für Physik*, Vol. 34, pp. 347–361, 1925.
- [29] W. G. Cady, *Piezoelectricity*, Dover Publications, 1962.
- [30] D. A. Berlincourt, D. R. Currand, and H. Jaffe, "Piezoelectric and piezomagnetic materials", in *Physical Acoustics*, W. P. Mason, Ed., New York, Academic, Vol. I, Pt. A, 1967.
- [31] "IEEE standard on piezoelectricity", *ANSI/IEEE Std. 176-1987*, 1987.
- [32] H. Ohigashi, "Electromechanical properties of polarized polyvinylidene fluoride films as studied by the piezoelectric resonance method", *J. Appl. Phys.*, Vol. 47, pp. 949–955, 1976.
- [33] I. M. Ward and D. W. Hadley, *An introduction to the mechanical properties of solid polymers*. Chichester, UK, John Wiley & Sons, 1993.
- [34] H. Salhofer, "Breitbandige dielektrische Resonanzspektroskopie an piezoelektrischen Polymeren", *Diploma Thesis* (in German), unpublished, Johannes Kepler Universität, Linz, Austria, 2002.
- [35] W. P. Mason, "Electrostrictive effect in barium titanate ceramics", *Phys. Rev.*, Vol. 74, pp. 1134–1147, 1948.
- [36] M. Wegener and R. Gerhard-Multhaupt, "Electric poling and electromechanical characterization of 0.1 mm thick sensor films and 0.2 mm thick cable layers from piezoelectric poly(vinylidene fluoride-trifluoroethylene)", *IEEE Trans. Ultrason., Ferroelect., Freq. Contr.*, Vol. 50, pp. 921–931, 2003.
- [37] J. F. Haskins and J. L. Walsh, "Vibrations of ferroelectric cylindrical shells with transverse isotropy", *J. Acoust. Soc. Amer.*, vol. 29, pp. 729–734, 1957.

- [38] R. Tasker, M. Lukas, M. Sayer, and S. Sherrit, "Techniques to determine the complex material constants of spherical and cylindrical ring resonators", IEEE International Ultrasonics Symposium, Piscataway, NJ, IEEE Service Center, pp. 987–990, 1999.
- [39] N. Aurelle, D. Roche, C. Richard, and P. Gonnard, "Sample aspect ratio influence on the shear coefficients measurements of a piezoelectric bar", IEEE International Symposium on Applications of Ferroelectrics, pp. 162–165, 1994.
- [40] G. R. Strobl, *The Physics of Polymers*, 2nd ed., Berlin, Springer, 1997.
- [41] R. Holland, "Representation of dielectric, elastic and piezoelectric losses by complex coefficients", IEEE Trans. Sonics Ultrason., Vol. 14, pp. 18–20, 1967.
- [42] W. Künstler, Z. Xia, T. Weinhold, A. Pucher, and R. Gerhard-Multhaupt, "Piezoelectricity of porous polytetrafluoroethylene single- and multiple-film electrets containing high charge densities of both polarities", Appl. Phys. A, Vol. 70, pp. 5–8, 2000.
- [43] R. Kressmann, "Linear and non-linear piezoelectric response of charged cellular polypropylene", J. Appl. Phys., Vol. 90, pp. 3489–3496, 2001.
- [44] M. Paajanen, J. Leikkala, and K. Kirjavainen, "Electromechanical film (EMFi)—a new multipurpose electret material", Sensors and Actuators, Vol. 84, pp. 95–102, 2000.
- [45] J. Peltonen, M. Paajanen, and J. Leikkala, "Determination of the actuator sensitivity of electromechanical polypropylene films by atomic force microscopy", J. Appl. Phys., Vol. 88, pp. 4789–4793, 2000.
- [46] M. Lindner, S. Bauer-Gogonea, and S. Bauer, "Dielectric barrier microdischarges: mechanism for the charging of cellular piezoelectric polymers", J. Appl. Phys., Vol. 91, pp. 5283–5287, 2002.
- [47] R. Gerhard-Multhaupt, W. Künstler, T. Görne, A. Pucher, T. Weinhold, M. Seiss, Z. Xia, A. Wedel, and R. Danz, "Porous PTFE space-charge electrets for piezoelectric applications", IEEE Trans. Dielectr. Electr. Insul., Vol. 7, pp. 480–488, 2000.
- [48] R. Kressmann, "New piezoelectric polymer for air-borne and water-borne sound transducers", J. Acoust. Soc. Am., Vol. 109, pp. 1412–1416, 2001.
- [49] A. Mellinger, F. Camacho González, and R. Gerhard-Multhaupt, "Ultraviolet-induced discharge currents and reduction of the piezoelectric coefficient in cellular polypropylene films", Appl. Phys. Lett., Vol. 82, pp. 254–256, 2003.
- [50] G. M. Sessler, "Distribution and transport of charge in polymers", *Electrets*, 3rd ed., R. Gerhard-Multhaupt, Ed., Morgan Hill, CA, Laplacian Press, Vol. 2, ch. 10, pp. 41–80, 1999.
- [51] R. G. Kepler and R. A. Anderson, "Piezoelectricity and pyroelectricity in polyvinylidene fluoride", J. Appl. Phys., Vol. 49, pp. 4490–4494, 1978.
- [52] T. Furukawa and N. Seo, "Electrostriction as the origin of piezoelectricity in ferroelectric polymers", Jpn. J. Appl. Phys. 1, Vol. 29, pp. 675–680, 1990.
- [53] H.-J. Winkelhahn, H. H. Winter, and D. Neher, "Piezoelectricity and electrostriction of dye-doped polymer electrets", Appl. Phys. Lett., Vol. 64, pp. 1347–1349, 1994.
- [54] I. L. Guy and Z. Zheng, "Piezoelectricity and electrostriction in ferroelectric polymers", Ferroelectrics, Vol. 264, pp. 1691–1696, 2001.
- [55] A. K. Jonscher, *Dielectric Relaxation in Solids*. London, Chelsea Dielectrics Press, 1983.
- [56] S. Havriliak, Jr. and S. J. Havriliak, *Dielectric and Mechanical Relaxation in Materials*. Munich, Germany, Hanser, 1997.
- [57] A. Schönhal, F. Kremer, and E. Schlosser, "Scaling of the α -relaxation in low-molecular-weight glass-forming liquids and polymers", Phys. Rev. Lett., Vol. 67, p. 999, 1991.
- [58] E. Markiewicz, J. Kulek, and Cz. Pawlaczyk, "Simple electric equivalent circuit method to determine piezoelectric and elastic properties of piezoelectric polymer film", IEEE Trans. Dielectr. Electr. Insul., Vol. 6, pp. 304–308, 1999.
- [59] G. S. Neugschwandtner, R. Schwödiauer, S. Bauer-Gogonea, S. Bauer, M. Paajanen, and J. Leikkala, "Piezo- and pyroelectricity of a polymer-foam space-charge electret", J. Appl. Phys., Vol. 89, pp. 4503–4511, 2001.
- [60] H. L. W. Chan and I. L. Guy, "Piezoelectric ceramic/polymer composites for high frequency applications", Key Engineering Materials, Vol. 92, p. 275, 1994.
- [61] G. S. Neugschwandtner, R. Schwödiauer, M. Vieytes, S. Bauer-Gogonea, S. Bauer, J. Hillenbrand, R. Kressmann, G. M. Sessler, M. Paajanen, and J. Leikkala, "Large and broadband piezoelectricity in smart polymer-foam space-charge electrets", Appl. Phys. Lett., Vol. 77, pp. 3827–3829, 2000.
- [62] S. Sherrit, H. D. Wiederick, and B. K. Mukherjee, "Non-iterative evaluation of the real and imaginary material constants of piezoelectric resonators", Ferroelectrics, Vol. 134, pp. 111–119, 1992.
- [63] J. G. Smits, "Iterative method for accurate determination of the real and imaginary parts of the materials coefficients of piezoelectric ceramics", IEEE Trans. Sonics Ultrason., Vol. 23, pp. 393–402, 1976.
- [64] J. G. Smits, "High accuracy determination of real and imaginary parts of elastic, piezoelectric and dielectric constants of ferroelectric PLZT (11/55/45) ceramics with iterative method", Ferroelectrics, Vol. 64, pp. 275–291, 1985.
- [65] K. W. Kwok, H. L. W. Chan, and C. L. Choy, "Evaluation of the material parameters of piezoelectric materials by various methods", IEEE Trans. Ultrason., Ferroelect., Freq. Contr., Vol. 44, pp. 733–743, 1997.
- [66] A. Mellinger, M. Wegener, W. Wirges, and R. Gerhard-Multhaupt, "Dynamic piezoelectricity in sandwich porous/nonporous amorphous fluoropolymer films", Appl. Phys. Lett., Vol. 79, pp. 1852–1854, 2001.
- [67] "Gnuplot 3.7.1", Available for download from www.gnuplot.info.
- [68] S. Sherrit, H. D. Wiederick, B. K. Mukherjee, and M. Sayer, "An accurate equivalent circuit for the unloaded piezoelectric vibrator in the thickness mode", J. Phys. D: Appl. Phys., Vol. 30, pp. 2354–2363, 1997.
- [69] R. Schwödiauer, G. S. Neugschwandtner, K. Schratlbauer, M. Lindner, M. Vieytes, S. Bauer-Gogonea, and S. Bauer, "Preparation and characterization of novel piezoelectric and pyroelectric polymer electrets", IEEE Trans. Dielectr. Electr. Insul., Vol. 7, pp. 578–586, 2000.
- [70] Y. Takahashi, K. Hiraoka, and T. Furukawa, "Time evolution of laser-induced pyroelectric responses in a VDF/TrFE copolymer", IEEE Trans. Dielectr. Electr. Insul., Vol. 5, pp. 957–960, 1998.
- [71] Y. Roh, V. V. Varadan, and V. K. Varadan, "Characterization of all the elastic, dielectric, and piezoelectric constants of uniaxially oriented poled PVDF films", IEEE Trans. Ultrason., Ferroelect., Freq. Contr., Vol. 49, pp. 836–847, 2002.
- [72] G. Kovacs, G. Trattnig, and E. Langer, "Accurate determination of material constants of piezoelectric crystals from SAW velocity measurements", IEEE Intern. Ultrasonics Sympos., Piscataway, NJ, IEEE Service Center, pp. 269–272, 1988.
- [73] H. Schewe, "Piezoelectricity of uniaxially oriented polyvinylidene fluoride", IEEE Intern. Ultrasonics Sympos., Piscataway, NJ, IEEE Service Center, pp. 519–524, 1982.
- [74] T. Furukawa, "Structure and functional properties of ferroelectric polymers", Adv. Coll. Interf. Sci., Vol. 71–72, pp. 183–208, 1997.
- [75] K. Omote, H. Ohigashi, and K. Koga, "Temperature dependence of elastic, dielectric, and piezoelectric properties of 'single crystalline' films of vinylidene fluoride trifluoroethylene copolymer", J. Appl. Phys., Vol. 81, pp. 2760–2768, 1997.
- [76] S. Sherrit, H. D. Wiederick, B. K. Mukherjee, and D. F. Jones, "The effects of electrode clamping on poly(vinylidene fluoride-trifluoroethylene) copolymer tiles", Ferroelectrics, Vol. 171, pp. 313–320, 1995.
- [77] K. W. Kwok, H. L. W. Chan, and C. L. Choy, "Lead zirconate titanate/poly(vinylidene fluoride-trifluoroethylene) 1-3 composites for ultrasonic transducer applications", IEEE Trans. Ultrason., Ferroelect., Freq. Contr., Vol. 46, pp. 626–637, 1999.
- [78] J. S. Hornsby and D. K. Das-Gupta, "Finite-difference modeling of piezoelectric composite transducers", J. Appl. Phys., Vol. 87, pp. 467–473, 2000.
- [79] L. F. Brown, J. L. Mason, M. L. Klinkenborg, J. I. Scheinbeim, and B. A. Newman, "Ferroelectric Nylon materials and their

- feasibility for ultrasound transducers", IEEE Trans. Ultrason., Ferroelect., Freq. Contr., Vol. 44, pp. 1049–1059, 1997.
- [80] P. Frübing, A. Kremmer, W. Neumann, R. Gerhard-Multhaupt, and I. L. Guy, "Dielectric relaxation of polyamide 11 in relation to piezo- and pyroelectricity", IEEE Trans. Diel. Electr. Insul. (in press).
- [81] K. Kirjavainen, "Electromechanical film and procedure for manufacturing same", US Patent No. 4,654,546, 1987.
- [82] J. Lekkala and M. Paajanen, "EMFi—new electret material for sensors and actuators", IEEE 10th International Symposium on Electrets, A. A. Konsta, A. Vassilikou-Dova, and K. Vartzeli-Nikaki, Eds., Piscataway, NJ, IEEE Service Center, pp. 743–746, 1999.
- [83] J. Hillenbrand and G. Sessler, "Piezoelectric properties of polypropylene/air and poly(vinylidene fluoride)/air composites", IEEE Conf. Electr. Insul. Dielectr. Phenomena (CEIDP), pp. 161–165, 2000.
- [84] M. Paajanen, H. Välimäki, and J. Lekkala, "Modelling the electromechanical film (EMFi)", J. of Electrostatics, Vol. 48, pp. 193–204, 2000.
- [85] M. Paajanen, M. Wegener, and R. Gerhard-Multhaupt, "Understanding the role of the gas in the voids during corona charging of cellular electret films—a way to enhance their piezoelectricity", J. Phys. D: Appl. Phys., Vol. 34, pp. 2482–2488, 2001.
- [86] A. Mellinger, F. Camacho González, and R. Gerhard-Multhaupt, "Photostimulated discharge in electret polymers: an alternative approach for investigating deep traps", IEEE Trans. Diel. Electr. Insul., (in press).
- [87] S. Bauer, S. Bauer-Gogonea, M. Dansachmüller, and R. Schwödiauer, "Charge in heterogeneous materials: a new route for piezoelectricity", 4th Intern. Conf. Electric Charges in Non-Conductive Materials, Paris, France, Société Française du Vide, Paris, pp. 124–131, 2001.
- [88] A. Mellinger, unpublished results, 2001.



Axel Mellinger was born in Munich, Germany, in 1967. He studied physics at the Technical University in Munich, where he obtained the diploma degree in 1992 and the Ph.D. degree in 1995 at the Max Planck Institute for Extraterrestrial Physics in Garching, Germany. Subsequently He held a two-year post-doctoral position at University of California, Berkeley, USA in the Department of Chemistry, where he investigated the reaction dynamics of the ketene molecule. Since December 1997 he is a staff member at the University of Potsdam, Germany. His present work focuses on charge storage mechanisms in polymer electrets, optically induced charge-detrapping, and the study of piezoelectric resonances in charged polymer foams.

Photostimulated Discharge in Electret Polymers: an Alternative Approach for Investigating Deep Traps

Axel Mellinger, Francisco Camacho González and Reimund Gerhard-Multhaupt

Department of Physics
University of Potsdam, Am Neuen Palais 10,
14469 Potsdam, Germany

ABSTRACT

The stability of space charge in electrets such as polytetrafluoroethylene (PTFE), polyethylene terephthalate (PETP) and polypropylene (PP) under ultraviolet irradiation has been investigated using photostimulated discharge spectroscopy. While only weak discharge currents were observed in PTFE coated with semitransparent gold electrodes, up to 15 pA/cm^2 were found in PETP around the UV absorption edge near 310 nm. Space charge profiles obtained with the piezoelectrically generated pressure step method indicate that near-surface charges were almost completely removed. In PP foam, recent findings of a UV-reduced d_{33} coefficient were confirmed for exposure times of up to 3.5 h, and a discharge peak at 200 nm could be assigned to the charges stored on the surfaces of the voids. The unique morphology and the (quasi-)piezoelectric properties of cellular PP make it a role model for the future investigation of charge storage in electrets.

Index Terms — Electret polymers, photostimulated discharge, polytetrafluoroethylene, polyethylene terephthalate, polypropylene, UV spectroscopy, piezoelectricity, piezoelectric resonances, piezoelectric coefficient, thickness extension resonance, voided polymer, cellular polymer, porous polymer, space-charge electret, corona charging, dielectric spectroscopy.

1 INTRODUCTION

SINCE the invention of the electret condenser microphone [1] space-charge electrets have played an important part in a variety of commercial applications [2,3]. Their unique property is their capability to store space charge near the surface or in the bulk for long periods of time. In particular, polytetrafluoroethylene (PTFE) and its copolymers (often known under their trade names Teflon® TFE, FEP, PFA and AF) have been shown to have excellent charge-retention properties. Other examples of space-charge electret polymers include polyethylene terephthalate (PETP), cycloolefin copolymers, polyethylene and polypropylene (PP). The latter has received considerable attention in the last few years, following the development of electromechanical transducers based on polypropylene electret foams [4].

Despite the widespread applications of space charge electrets, the microscopic mechanisms of charge storage are still poorly understood. For PTFE and its copolymers, it is generally accepted that charges generated by a room-temperature corona discharge are stored in relatively shallow

traps, while either charging at elevated temperature or exposure to a mono-energetic electron beam at room temperature produces deeper traps, resulting in a higher thermal stability [2]. Space charge profiles in PTFE and FEP obtained by the piezoelectrically generated pressure step (PPS) method indicate that shallow traps are located near the surface, whereas deeper traps are distributed homogeneously in the bulk [5]. In the same work, space charge densities of up to 2500 C/m^3 were reported.

Thermally stimulated discharge (TSD) experiments yielded trap depths between 0.5 and 1.5 eV [6]. However, this does not fully explain the exceptional long-term stability of space charge electrets. Deep chemical traps with depths between 3 and 8 eV, comparable to the bond strengths between the constituent atoms could be the stabilizing factor. A recent molecular modeling approach [7] highlighted the role of chemical impurities in creating deep ($>1 \text{ eV}$) chemical traps.

One promising method for studying the electric and dielectric processes in solids is optical excitation (photostimulated discharge, PSD), where trapped charge carriers are released by irradiating the sample with monochromatic light. Initial PSD (also named photostimulated cur-

Manuscript received on 4 February 2003, in final form 10 July 2003.

rent, PSC) experiments on organic materials were performed by Brodribb et al. in the early 1970s [8]. Compared with thermal methods, PSD offers a substantially improved energy resolution over a wide range of trap depths and allows direct and accurate observation of trapping phenomena. The changing temperature in TSD experiments, on the other hand, causes a modification of the trap center environment, due to the formation or release of kinks in the polymer chain, and molecular movements of both the main chain (“repetition”) and the side-groups (“wet-dog effect” [9]).

Photostimulated detrapping currents in Teflon® FEP were reported by Oda et al. [10], who inferred the presence of a single trapping level at 4.9 eV. Positive bias voltages led to a substantial enhancement of the detrapping current, and current reversal was observed at elevated temperatures. The spectra showed a monotonically increasing current at wavelengths shorter than 255 nm. In a subsequent paper [11], it was concluded that an indirect process (charge injection from the electrodes) rather than direct detrapping is the principal mechanism through which the photocurrent is generated.

In polystyrene, Crine et al. [12] observed positive photocurrents of about 0.1 pA/cm² which they attributed to photogeneration of charge carriers under an applied electric field. Their experimental results could be quantitatively described with the Onsager model [13]. They explicitly excluded the possibility of photoinjection (based on the almost field-independent energy threshold for photocurrent generation) and charge detrapping. However, photogeneration requires a significant absorption cross section, which is not found in PTFE at wavelengths above 200 nm. Photoconduction in PTFE was observed at energies above 8.4 eV [14], with holes being the dominant carriers.

2 EXPERIMENT

Samples of PTFE (Plastpolymer, St. Petersburg), PETP (Wolfen, Germany, or Mylar® brand, DuPont Teijin Films) and cellular polypropylene (PP, VTT Processes) were rinsed in isopropanol and charged either with a monoenergetic electron beam [15] (electron energy 1–20 keV) or in a point-to-plane corona discharge at ±15 kV with an air gap of 4 cm and a grid voltage of ±2 kV. The resulting space charge distribution was monitored by means of the piezoelectrically generated pressure step

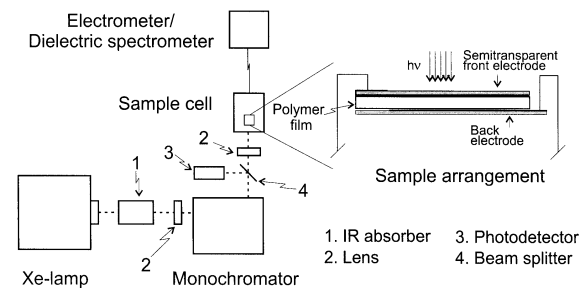


Figure 1. Experimental setup for measuring photostimulated discharge currents.

(PPS) method [5] under short-circuit conditions with a resolution of approx. 2 μm. By varying the charging parameters (i.e., electron energy or sample temperature), it was possible to selectively produce either a surface or a bulk charge (Table 1). The samples were either directly coated with semitransparent electrodes ($d \approx 15$ nm) or sandwiched between quartz plates with similar coatings.

As shown in Figure 1, the films were subsequently irradiated with monochromatic light (bandwidth 4 nm) generated by a 1000 W Hg-Xe or a 450 W Xe arc lamp (Oriol) and a monochromator (Photon Technology International) equipped with a UV-enhanced grating (blaze angle for 250 nm). A small portion of the light was split off by a beam-splitter and focused onto a UV-sensitive photodiode (Hamamatsu S1336-BQ). At the sample position, the photon flux density at 400 nm was about 1.3×10^{15} cm⁻² s⁻¹. Figure 2 shows a comparison of the 450 W Xe arc lamp spectrum with the extraterrestrial air mass zero (AM0) [16] and the terrestrial air mass 1.5 (AM 1.5) solar spectra [17]. Near 200 nm, the irradiance of the lamp spectrum matches that of the AM0 solar spectrum. The short-circuit photostimulated discharge current was measured with a Keithley 6517A electrometer while the UV light was scanned from longer to shorter wavelengths at a rate of 120 nm/min. In the following sections, a photocurrent flowing from the illuminated electrode to the electrometer is regarded as positive, as indicated in Figure 10.

In order to verify that the samples were not significantly heated during irradiation, the surface temperature was measured using a resistive bolometer [18]. As shown in Figure 3, the increase in temperature was less than 0.1 K between 600 and 400 nm. Below 400 nm, the temperature changes were even smaller, due to the lower incident flux.

Table 1. PTFE charging parameters and charge distributions.

Method	Voltage [kV]		Beam Energy [keV]	Temp. [°C]	Remarks
	point	grid			
corona	±15	±2	—	20	surface charge
corona	+15	+2	—	200	stable positive volume charge
el. beam	—	—	20	20	charge layer at $x \approx 5$ μm

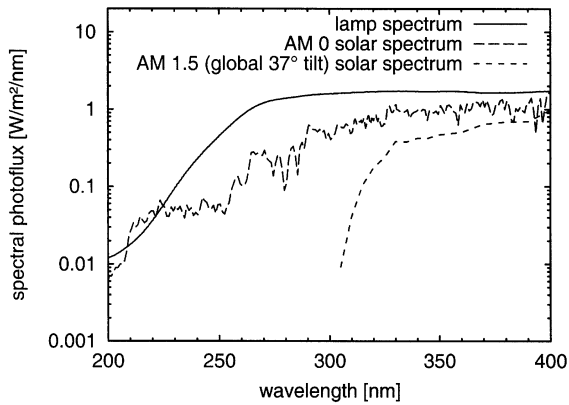


Figure 2. Comparison of the 450 W Xe arc lamp irradiance with the extraterrestrial air mass zero (AM0) [16] and the terrestrial air mass 1.5 (AM1.5) solar spectrum [17]. Near 200 nm, which is the most effective wavelength for altering the (quasi-)piezoelectric properties of cellular PP films, the irradiance in the lamp spectrum nearly matches the AM0 flux.

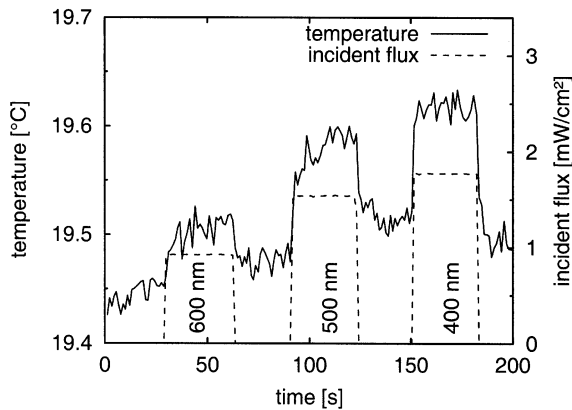


Figure 3. Bolometrically measured surface temperature of a cellular polypropylene film during irradiation at different wavelengths. No significant heating of the sample surface was observed.

Dielectric measurements were performed using a Novo-control ALPHA high-resolution dielectric analyzer with a modified open sample holder where the samples could be exposed to UV light. For the measurement of piezoelectric resonances, the films were mounted in a way that allowed free vibrations in the thickness direction.

3 RESULTS AND DISCUSSION

3.1 POLYTETRAFLUOROETHYLENE

The photocurrent spectra of gold-coated and uncoated samples are shown in Figure 4a. Both corona- and electron beam-charged PTFE show a monotonically rising photocurrent at wavelengths shorter than 270 nm. This signal can be bleached by prolonged illumination (15–60 min) at 240 nm. As will be shown later, the strong photocurrent observed for uncoated films (with pressed-on electrodes) can be explained by the external photoeffect.

Samples coated with 15 nm of gold show a greatly reduced photocurrent due to the absence of the external photoeffect. The residual current can be attributed to the detrapping of bulk charges from traps with a depth of 4.6 eV, in good agreement with the results of Oda [10]. An interesting question is whether charges injected either through a pressed-on or an evaporated electrode can lead to charge compensation or detrapping in the polymer bulk. If internal charge compensation occurs, this process is not necessarily accompanied by external currents. To address this question, samples of corona-charged PTFE ($T = 200^\circ\text{C}$), coated with semitransparent gold electrodes on both sides, were irradiated at 240 nm for 50 min and the PPS charge profiles compared before and after irradiation. As shown in Figure 4b, charging at elevated temperature results in an asymmetric charge profile with the centroid of positive bulk charge displaced towards the back of the sample ($18\ \mu\text{m}$). Negative compensation charges are located near the front ($0\ \mu\text{m}$) and back surfaces. After bleaching at 240 nm, part of the charge was removed from the bulk. Detrapping of near-surface charges could also occur, but cannot be confirmed at this stage, since the

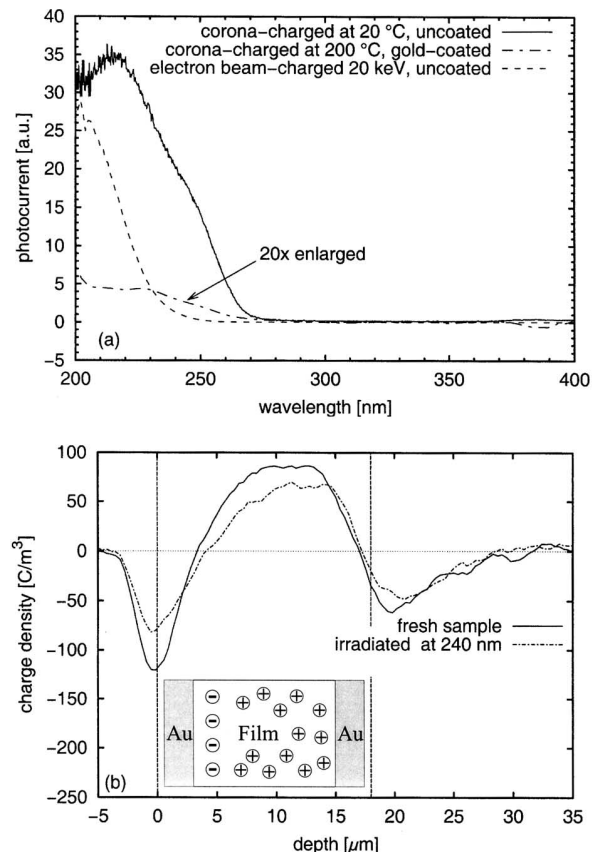


Figure 4. a, UV-flux normalized PSD spectra of an $18\ \mu\text{m}$ PTFE film, acquired at a scan rate of 120 nm/min. Sample charging as listed in Table 1; b, Space charge profiles of a gold-coated PTFE film corona-charged at 200°C before and after irradiation at 240 nm. The inset shows the schematic charge distribution in the sample.

PPS method cannot distinguish between near-surface charges (in the polymer) and compensation charges on the metal electrodes. The inset of the figure shows the schematic representation of the charge distribution in the sample.

3.2 POLYETHYLENE TEREPHTHALATE

Figure 5 shows the photo-stimulated discharge spectrum of a 16 μm PETP film negatively corona-charged at room temperature. To prevent premature removal of the surface charge, an asymmetric electrode arrangement was chosen, as depicted in the inset. The sample was coated with a semitransparent Cu electrode, which was connected to the grounded anode during the charging process. The spectrum shows a single broadened peak (peak current density -15 pA/cm^2) near 305 nm, equivalent to a trap depth of 4.1 eV. After 12 min of irradiation at 303 nm (shown in Figure 6a), the photocurrent peak decreases substantially, while its centroid is red-shifted to 310 nm. The residual peak can be permanently bleached by irradiation with 310 nm light. As with PTFE, the transient nature of the photocurrent indicates the presence of a charge detrapping mechanism, rather than photoinduced conductivity. The onset of the photocurrent coincides with the optical absorption edge of PETP, resulting from a transition derived from the $^1A_{1g} \rightarrow ^1B_{2u}$ (1L_b) benzene transition [19]. This suggests that trapped charges are either associated with aromatic groups on the polymer chain or that detrapping is an indirect process, where, in a first step, photon absorption leads to the generation of an exciton, which is dissociated by the internal electric field. The charges resulting from the dissociated exciton could then neutralize or detrapp charges located at other positions along the polymer chain. The fact that preferential bleaching was observed when the sample was irradiated at

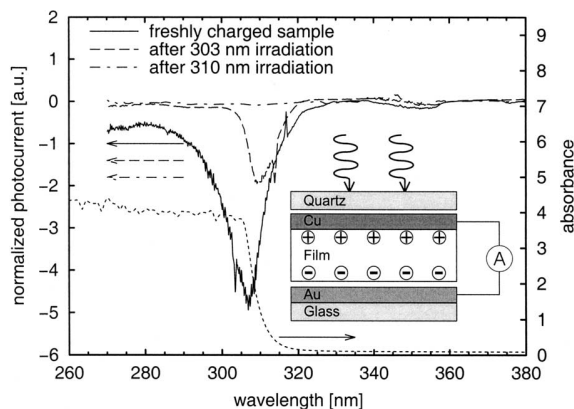


Figure 5. UV-flux normalized PSD spectrum of corona-charged PETP immediately after corona-charging and after optical bleaching at 303 and 310 nm. The peak current density near 305 nm was approx. -15 pA/cm^2 . Bleaching times were 720 and 780 s, respectively (Figure 6a). The dotted curve shows the UV absorption spectrum. The inset shows the electrode arrangement and orientation of the sample.

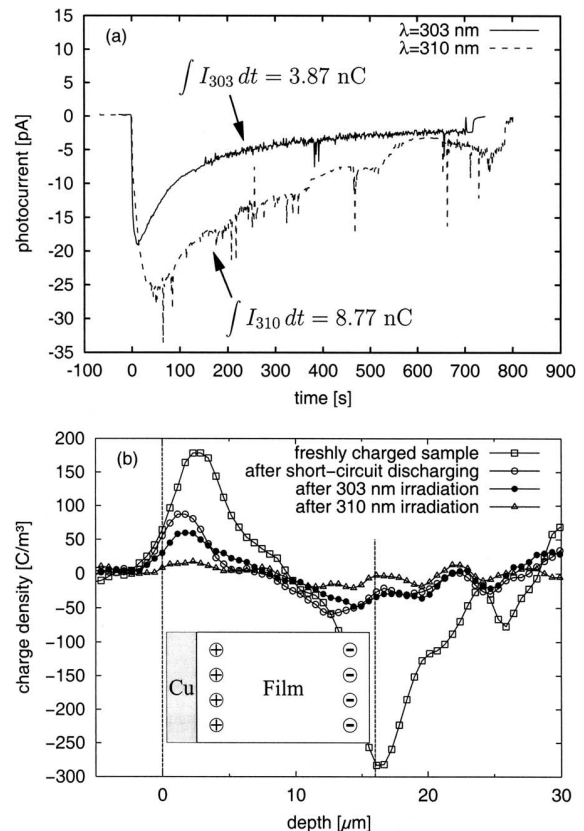


Figure 6. a, Discharge current distribution; b, charge density distribution. 16 μm PETP film corona-charged for 1 min at room temperature ($V_{\text{needle}} = -12 \text{ kV}$). Total integrated discharge current is 12.6 nC. During the PPS measurement, the uncoated surface was covered with an uncharged PETP layer of the same thickness in order to protect the surface charge. The space charge density is given by the derivative of the electric displacement. The schematic charge distribution is shown in the inset.

303 nm gives some support to the first point of view, since only a direct process would allow state-selective detrapping.

As shown in Figure 6a, the integrated discharge current amounts to a total charge of 12.6 nC. Independent information on the removed charge can be obtained from PPS measurements before and after bleaching, depicted in Figure 6b. To protect the surface charge, the uncoated side was covered with an uncharged PETP layer of the same thickness (16 μm). All space charge is located near the surfaces, at depths of 3 μm or less. After the freshly charged sample was connected to the electrometer, an initial decay of surface charge was observed for approximately 1 h. Subsequent irradiation at 303 and 310 nm removed almost all surface charge. Only a slight decrease in surface charge was found after irradiation at 303 nm while nearly complete depletion is seen after exposure to 310 nm light. This can be explained by the different optical penetration depth, which is a factor of 2.5 larger at 310 nm according to the UV absorption spectrum shown in

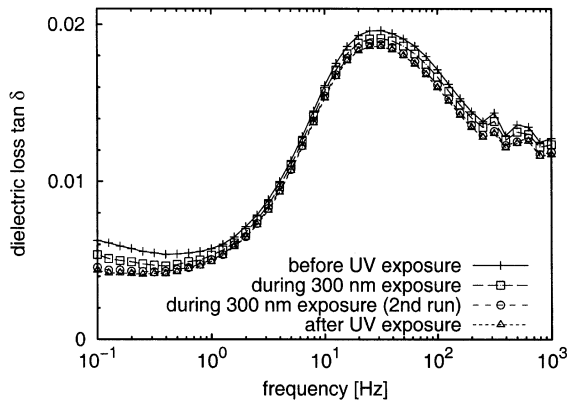


Figure 7. Dielectric loss of a 23 μm PETP film before, during and after UV irradiation at 300 nm. Each UV exposure lasted 10 min.

Figure 5. With a sample area of 4 cm^2 , the charge removed by optical bleaching is found to be 240 nC, nearly 20 times larger than the integrated discharge current. Apparently, most of the detrapped negative charges recombine internally with their positive counterparts, without causing an external current.

The detrapping of charge carriers during UV irradiation at room temperature can also be detected as a change in the low-frequency loss of the dielectric loss spectrum (Figure 7). The increased losses for charged PETP are not accompanied by a substantial increase in the permittivity ϵ' . This is in contrast to recent measurements above 130°C, where an increase both in ϵ' and the dielectric loss $\tan \delta$ was attributed to electrode polarization [20]. Since the time scale for charge detrapping is similar to the duration of a dielectric frequency scan, this method cannot capture the dynamics of charge detrapping. Dielectric spectroscopy in the time domain usually requires shorter data acquisition times, but at the expense of a lower signal-to-noise ratio [21].

3.3 POLYPROPYLENE

Transducers based on cellular polypropylene have recently become commercially available [4]. In this material, a high external field (often generated in a corona discharge) leads to electric breakdown inside the voids, followed by charge separation and trapping of the charges on the surfaces of the voids. Unlike traditional piezoelectric polymers (such as polyvinylidene fluoride), the electromechanical response is caused by stress-induced changes of macroscopic dipoles formed by the trapped charges. Using a gas expansion treatment, (quasi-)piezoelectric d_{33} coefficients of up to 790 pC/N have been reported [22]. In Figure 8, the PSD spectrum of a 70 μm cellular PP film shows three peaks near 280, 230 and 200 nm, corresponding to trap depths of 4.6, 5.6 and 6.3 eV, respectively. Preferential bleaching of the peaks was observed after irradiating the sample with one of these

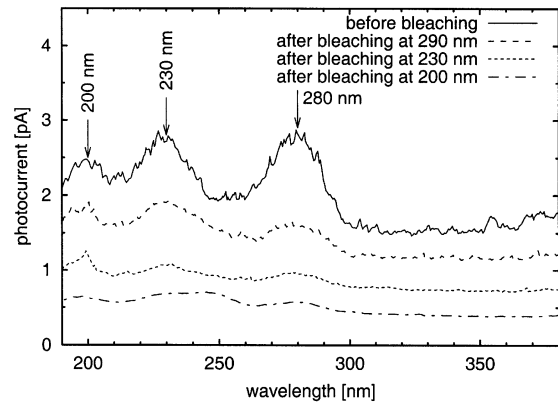


Figure 8. Photostimulated discharge spectra of cellular PP film. Three trap levels are readily visible in the spectra. For clarity, the traces have been shifted along the vertical axis.

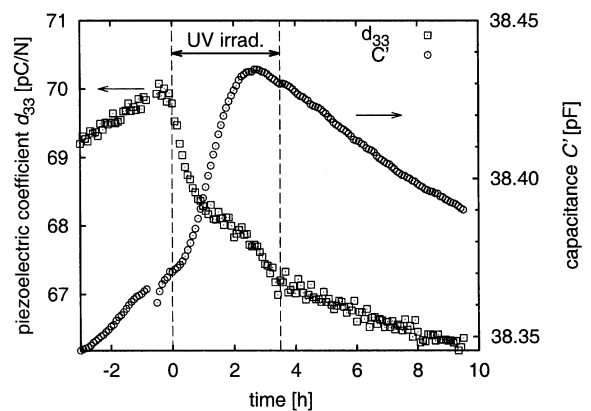


Figure 9. Decay of the d_{33} coefficient in cellular polypropylene (nominal thickness 70 μm) during a 3.5 h UV irradiation at 200 nm. d_{33} is reduced by 4%, while the low elastic stiffness of the material gives rise to a gradual thickness (and hence capacitance) drift of approx. 0.2%.

wavelengths. Recently, it was possible to measure a 1% decrease in d_{33} after irradiation at 210 and 200 nm, whereas irradiation at wavelengths above 210 nm left d_{33} unchanged [23]. In this work, we present additional long-exposure data (Figure 9) showing a 4% reduction of d_{33} after irradiating the film for 3.5 h at 200 nm. The piezoelectric coefficient was measured by recording the dielectric spectrum in the vicinity of the thickness-extension resonance [24,25]. Compared to quasistatic or dynamic mechanical methods, this technique imposes very little mechanical stress on the sample, thereby eliminating errors caused by inelastic deformation of the polymer foam. During the UV exposure, the spectra were acquired repeatedly in 5 min intervals. The experimental spectra were fitted to the expression [26,27]

$$C'(\omega) = \frac{\epsilon_r \epsilon_0 A}{h} \Re \left\{ \left(1 - k_t^2 \frac{\tan(\omega/4f_p)}{(\omega/4f_p)} \right)^{-1} \right\} \quad (1)$$

where \Re denotes the real part, ϵ_r is the relative permittivity of the sample, A and h are the electroded sample area and thickness, respectively, k_t is the electromechanical coupling factor, and f_p is the parallel resonance frequency. Both k_t and f_p must be treated as complex numbers to allow for mechanical losses. The elastic stiffness c_{33} and the piezoelectric coefficient d_{33} were then obtained via

$$c_{33} = \rho(2hf_p)^2 \tag{2}$$

and

$$d_{33}^2 = \frac{k_t^2 \epsilon_r \epsilon_0}{c_{33}} \tag{3}$$

where ρ is the sample density. As the elastic stiffness in the z direction is only 2.2 MPa, PP foam exhibits some creep after being mounted in the sample holder of the dielectric spectrometer. This is evident from the drift in capacitance (reflecting a change in thickness) as well as the gradual change in d_{33} before and after UV irradiation (Figure 9). It should be noted that the UV-induced decay of d_{33} appears to be an approximately linear function of time, so that a substantial decrease may be expected after exposure times of 24 h or more. The fact that d_{33} is unaffected by exposure to wavelengths longer than 210 nm [23] indicates that only the 6.3 eV traps are linked to the piezoelectric behavior and must therefore correspond to charges trapped on the inner surfaces of the voids. The other two levels at 4.6 and 5.6 eV are most likely associated with surface traps located on the non-cellular cover layers.

Near 200 nm, which is the most effective wavelength for altering the piezoelectric properties of cellular PP films, the irradiance in the lamp spectrum nearly matches the AM0 flux (Figure 2). Therefore, adequate UV protection would be required for using this material in a space environment. However, no adverse effects of the terrestrial UV radiation (AM 1.5 spectrum in Figure 2) are expected besides the well-known photodegradation of PP [28].

3.4 PROBABLE ADDITIONAL MECHANISMS OF PHOTOSTIMULATED DISCHARGING

3.4.1 CONTRIBUTION OF EXTERNAL PHOTOEFFECT

Part of the photocurrent of the uncoated samples can be related to the external photoeffect. This was demonstrated by recording the PSD spectrum of a corona-charged PTFE film (-15 kV/ -2 kV, 25°C , 5 min) sandwiched between a gold-coated glass plate and an aluminum-coated quartz plate, as shown in Figure 10. As is evident in Figure 11, the threshold for the onset of the photocurrent is approx. 360 nm (3.4 eV) when the positive

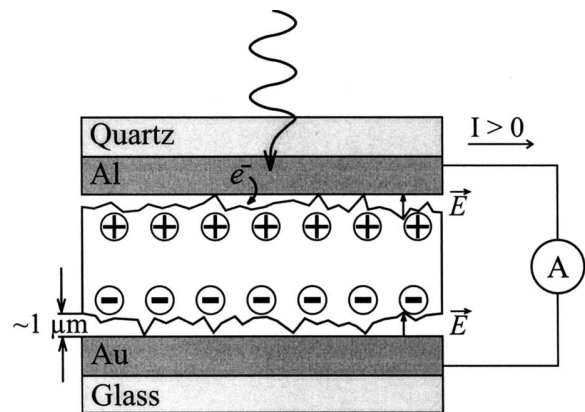


Figure 10. Schematic view of a polymer film with pressed-on Au and Al electrodes and surface charges.

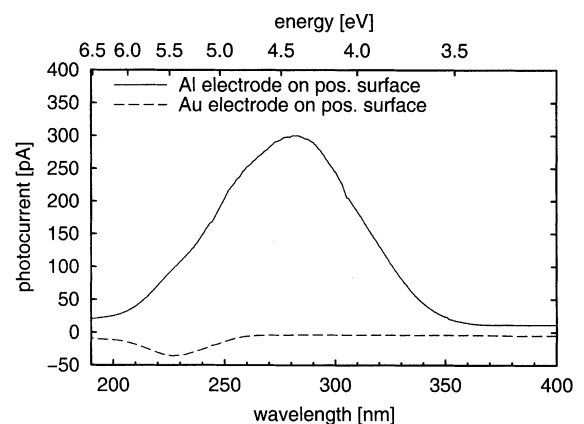


Figure 11. PSD spectra of PTFE film (18 μm), corona-charged ($V_{\text{needle}} = -15$ kV, $V_{\text{grid}} = -2$ kV, 25°C , 5 min.) sandwiched between pressed-on Al and Au electrodes, as shown in Figure 10. In both cases, the UV exposure was through the semitransparent Al electrode.

side of the sample (which was facing the ground electrode in the corona discharge) faces the aluminum electrode and 260 nm (4.9 eV) for the positive sample surface facing the gold electrode. Due to the surface roughness, small air gaps form between the sample surface and the pressed-on electrodes. At the electrode facing the positive surface of the PTFE film, electrons emitted through the external photoeffect are accelerated towards the sample, neutralizing the positive surface charge. Since PTFE is transparent to wavelengths longer than 170 nm (the band gap is reported to be 7.7 eV [29]), this mechanism can occur at either the front or back electrode, provided the respective sample surface is positively biased against the electrode. The photocurrent threshold is given by the work function of the electrode material, which is 4.28 eV (290 nm) for aluminum and 5.1 eV (243 nm) for gold. In conclusion, the external photoeffect must be taken into account only when using pressed-on electrodes at wavelengths below 260 nm.

3.4.2 INTERNAL ELECTRIC FIELD AND EXCITON RECOMBINATION

A tentative model for the photostimulated current of PETP is based on exciton dissociation in the internal electric field generated by the presence of space charge. From the experimentally obtained charge profile, the electric field can be calculated according to [30]

$$E(x') = -\frac{1}{\epsilon_r \epsilon_0} \left(\hat{\sigma}_1 - \int_0^{x'} \rho(x) dx \right) \quad (4)$$

with $\hat{\sigma}_1 = 1/s \int_0^s (s-x)\rho(x)dx$. Here, s is the sample thickness, and $\rho(x)$ is the charge density. The internal electric field, determined from equation (4), resembles that obtained from the PPS measurement, provided that ϵ_r is constant throughout the sample. However, the boundary conditions of the internal electric field are different from those of the PPS measurements. For PPS measurements, the compensation charge, which is found in the electrodes, contributes to the signal. This yields an electric displacement of $0 \mu\text{C}/\text{cm}^2$ at the front surface ($x = 0 \mu\text{m}$). On the other hand, the calculation of the internal electric field does not consider the compensation charge.

Figure 12 shows the electric field inside the PETP film before the first bleaching. The coated side of the sample corresponds to $x = 0 \mu\text{m}$, as shown in the inset of Figure 6b. In the bulk, the internal electric field is approx. $5 \text{ V}/\mu\text{m}$. The Onsager theory [13] of geminate recombination gives the probability ($f(r, \theta)$) that a charge pair will escape geminate recombination and dissociate under the influence of an electric field in an isotropic system

$$f(r, \theta) = \exp(-A) \exp(-B) \sum_{m=0}^{\infty} \sum_{n=0}^{\infty} \frac{A^m}{m!} \frac{B^{m+n}}{(m+n)!} \quad (5)$$

with $A = 2q/r$, $B = \beta r(1 + \cos \theta)$, $q \equiv e^2/8\pi\epsilon_0 kT$, $\beta \equiv eE/2kT$. Here, r is the initial separation distance between the oppositely charged carriers. θ is the angle between

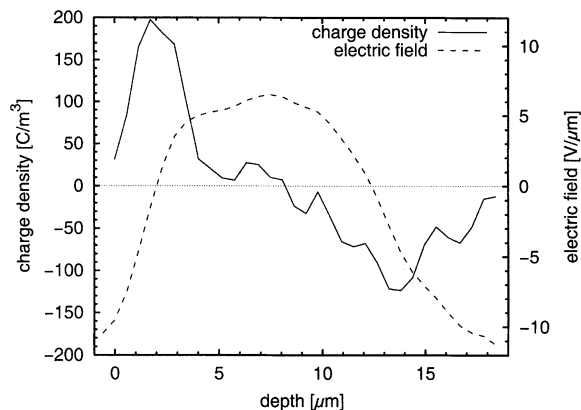


Figure 12. Calculation of electric field inside the PETP film. The charge density corresponds to the PPS signal after short-circuit discharging and before the first bleaching of the sample in the Figure 6b.

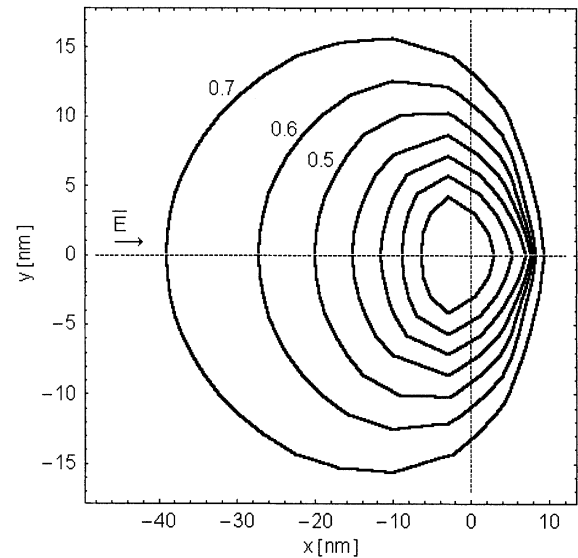


Figure 13. Contours of the geminate recombination escape probability $f(r, \theta)$ as a function of electron-hole separation. $\epsilon = 4$, $T = 300 \text{ K}$ ($\approx 27^\circ\text{C}$) and $E = 5 \text{ V}/\mu\text{m}$. The electron is placed at the origin.

the radius vector r and the electric field vector E . The contours of $f(r, \theta)$ calculated for an electric field of $5 \text{ V}/\mu\text{m}$ are shown in Figure 13. It can be seen that an initial separation of approx. 9.5 nm between an electron and its parent ion results in a probability as high as 0.7 to escape geminate recombination.

The negative photocurrent peak in the PETP films coincides with the optical absorption edge (Figure 5), related to the ${}^1A_{1g} \rightarrow {}^1B_{2u}$ (1L_b) transition of the aromatic group. In this way, it is probable that excitons are generated and become free carriers or recombine due to the high electric field. The interaction of excitons and trapped charge leads to a change in the charge distribution and further annihilation of trapped charge.

3.5 CHARGE STABILITY AND THERMALLY STIMULATED DISCHARGE EXPERIMENTS

All three polymers investigated in the present work show signatures of deep traps with depths between 4 and 6.3 eV . This is in contrast to most thermally stimulated discharge experiments [6,31], where trap depths between 0.5 and 1.5 eV were reported. However, these experiments reflect the activation energy for chain motion (the so-called α process) rather than direct detrapping of injected charges. Thermally stimulated currents may result from charges either shaken off from chain segments (well-known in the literature under the term “wet dog effect” [9]) or charges transported to the sample surface. Charge transport by molecular chains has recently been verified in PETP [20]. Therefore, PSD and TSD experiments should be considered as complementary methods highlighting different physical processes.

4 CONCLUSIONS

PHOTOSTIMULATED discharge spectroscopy in combination with depth-resolved space charge measurements has been used to obtain data on trap depths in various charge-storing polymer electrets. Only a weak discharge current was found in PTFE, whereas individual trapping levels could be observed in PETP and cellular PP. In the latter, the reduction of the piezoelectric coefficient under UV irradiation was also studied. A trap level near 6.3 eV could be assigned to charges located inside the voids.

ACKNOWLEDGMENTS

The authors gratefully acknowledge partial support from the PROBRAL program (CAPES/DAAD) and from the European Community within the GROWTH project DURASMART. Our thanks go to L. F. Santos and R. M. Faria (Instituto de Física de São Carlos, Universidade de São Paulo, Brazil) and W. Wirges (Universität Potsdam, Germany) for their experimental support and many stimulating discussions. The cellular PP samples were kindly provided by M. Paajanen of VTT Processes in Tampere, Finland. F.C.G. acknowledges financial support from PROMEP-SUPERA (Mexico).

REFERENCES

- [1] G. M. Sessler and J. E. West, "Self-biased Condenser Microphone with High Capacitance", *J. Acoust. Soc.*, Vol. 34, pp. 1787–1788, 1962.
- [2] R. Kressmann, G. Sessler, and P. Günther, "Space Charge Electrets", in *Electrets*, 3rd ed., R. Gerhard-Multhaupt, Ed., Morgan Hill, CA, Laplacian Press, Vol. 2, ch. 9, pp. 1–40, 1999.
- [3] V. N. Kestelman, L. S. Pinchuk, and V. A. Goldade, *Electrets in Engineering. Fundamentals and Applications*, 1st ed., Norwell, Massachusetts, Kluwer Academic Publishers, 2000.
- [4] M. Paajanen, H. Välimäki, and J. Lekkala, "Modelling the Electro-mechanical Film (EMFi)", *J. of Electrostatics*, Vol. 48, pp. 193–204, 2000.
- [5] R. Gerhard-Multhaupt, W. Künstler, G. Eberle, W. Eisenmenger, and G. Yang, "High Space-charge Densities in the Bulk of Fluoropolymer Electrets Detected with Piezoelectrically Generated Pressure Steps", *Space Charge in Solid Dielectrics*, pp. 123–132, 1997.
- [6] H. von Seggern, "Isothermal and Thermally Stimulated Current Studies of Positively Corona Charged (Teflon FEP) Polyfluoroethylene-propylene", *J. Appl. Phys.*, Vol. 52, pp. 4081–4085, 1981.
- [7] M. Meunier, N. Quirke, and A. Aslanides, "Molecular Modeling of Electron Traps in Polymer Insulators: Chemical Defects and Impurities", *J. Chem. Phys.*, Vol. 115, pp. 2876–2881, 2001.
- [8] J. D. Brodribb, D. M. Hughes, and T. J. Lewis, "The Energy Spectrum of Traps in Insulators by Photon-induced Current Spectroscopy", in *Electrets: Charge Storage and Transport in Dielectrics*, M. Perlman, Ed., 177–187, 1972.
- [9] M. Kryszewski, J. Ulanski, J. K. Jezka, and M. Zieliński, "Chain and Carrier Mobility in Polymer Systems as Investigated by Thermally Stimulated Current Techniques", *Polymer Bull.*, Vol. 8, pp. 187–192, 1982.
- [10] T. Oda, T. Utsumi, T. Kumano, and M. Itami, "Observation of Photo-stimulated Detrapping Currents of FEP Teflon Electrets", *IEEE 5th Intern. Conf. Electrets*, G. M. Sessler and R. Gerhard-Multhaupt, Eds., Piscataway, NJ, IEEE Service Center, pp. 288–293, 1985.
- [11] T. Oda, T. Utsumi, and G. Matsubara, "Observation of UV Photo-stimulated Currents of Teflon Electrets", *IEEE 6th Intern. Sympos. Electrets*, D. K. Das-Gupta and A. W. Pattullo, Eds., Piscataway, NJ, IEEE Service Center, pp. 142–146, 1988.
- [12] J. P. Crine and A. Yelon, "Photogeneration and Transport of Carriers in Atactic Polystyrene", *J. Appl. Phys.*, Vol. 51, pp. 2106–2114, 1980.
- [13] L. Onsager, "Initial Recombination of Ions", *Phys. Rev.*, Vol. 54, pp. 554–557, 1938.
- [14] M. Yun, K. Yoshino, Y. Inuishi, and M. Kawatsu, "Photoconduction in Polytetrafluoroethylene Induced by Vacuum-ultraviolet Light", *Jpn. J. Appl. Phys.*, Vol. 21, pp. 1592–1595, 1982.
- [15] B. Gross, "Radiation-induced Charge Storage and Polarization Effects", in *Electrets*, 3rd ed., G. M. Sessler, Ed., Morgan Hill, CA, Laplacian Press, Vol. 1, ch. 4, pp. 217–284, 1999.
- [16] C. Wehrli, "Extraterrestrial Solar Spectrum", *Physikalisch-Meteorologisches Observatorium and World Radiation Center, Davos Dorf, Switzerland, Publication 615*, 1985.
- [17] "Standard Tables for References Solar Spectral Irradiance at Air Mass 1.5: Direct Normal and Hemispherical for a 37° Tilted Surface," ASTM, Document G159-98, 1999.
- [18] R. Emmerich, S. Bauer, and B. Ploss, "Temperature Distribution in a Film Heated with a Laser Spot: Theory and Measurement", *Appl. Phys. A*, Vol. 54, pp. 334–339, 1992.
- [19] J. P. LaFemina and G. Arjavalingam, "Photophysics of Poly(ethylene terephthalate): Ultraviolet Absorption and Emission", *J. Phys. Chem.*, Vol. 95, pp. 984–988, 1991.
- [20] E. Neagu, P. Pissis, and L. Apekis, "Electrical Conductivity Effects in Polyethylene Terephthalate Films", *J. Appl. Phys.*, Vol. 87, pp. 2914–2922, 2000.
- [21] A. K. Jonscher, *Dielectric Relaxation in Solids*, London, Chelsea Dielectrics Press, 1983.
- [22] M. Paajanen, M. Wegener, and R. Gerhard-Multhaupt, "Understanding the Role of the Gas in the Voids during Corona Charging of Cellular Electret Films—a Way to Enhance their Piezoelectricity", *J. Phys. D: Appl. Phys.*, Vol. 34, pp. 2482–2488, 2001.
- [23] A. Mellinger, F. Camacho González, and R. Gerhard-Multhaupt, "Ultraviolet-induced Discharge Currents and Reduction of the Piezoelectric Coefficient in Cellular Polypropylene Films", *Appl. Phys. Lett.*, Vol. 82, pp. 254–256, 2003.
- [24] G. S. Neugschwandtner, R. Schwödiauer, M. Vieytes, S. Bauer-Gogonea, S. Bauer, J. Hillenbrand, R. Kressmann, G. M. Sessler, M. Paajanen, and J. Lekkala, "Large and Broadband Piezoelectricity in Smart Polymer-foam Space-charge Electrets", *Appl. Phys. Lett.*, Vol. 77, pp. 3827–3829, 2000.
- [25] A. Mellinger, M. Wegener, W. Wirges, and R. Gerhard-Multhaupt, "Thermally Stable Dynamic Piezoelectricity in Sandwich Films of Porous and Nonporous Amorphous Fluoropolymer", *Appl. Phys. Lett.*, Vol. 79, pp. 1852–1854, 2001.
- [26] "IEEE Standard on Piezoelectricity," ANSI/IEEE Std. 176-1987, 1987.
- [27] D. A. Berlincourt, D. R. Currand, and H. Jaffe, "Piezoelectric and Piezomagnetic Materials", in *Physical Acoustics*, W. P. Mason, Ed., New York, Academic, Vol. I, Pt. A, pp. 168–269, 1967.
- [28] J. F. Rabek, *Photodegradation of Polymers*, Heidelberg, Springer, 1995.
- [29] K. Seki, H. Tanaka, T. Ohta, Y. Aoki, A. Imamura, H. Fujimoto, H. Yamamoto, and H. Inokuchi, "Electronic Structure of Poly(tetrafluoroethylene) Studied by UPS, VUV Absorption, and Band Calculations", *Physica Scripta*, Vol. 41, pp. 167–171, 1990.
- [30] G. M. Sessler, "Physical Principles of Electrets", in *Electrets*, 3rd ed., G. M. Sessler, Ed., Morgan Hill, CA, Laplacian Press, Vol. 1, ch. 2, pp. 13–80, 1999.
- [31] J. van Turnhout, "Thermally Stimulated Discharge of Electrets", in *Electrets*, 3rd ed., G. M. Sessler, Ed., Morgan Hill, CA, Laplacian Press, Vol. 1, ch. 3, pp. 81–215, 1999.

This paper is based on a presentation given at the 11th IEEE International Symposium on Electrets, Melbourne, Australia, 1-3 October 2002.



Axel Mellinger was born in Munich, Germany, in 1967. He studied physics at the Technical University in Munich, where he obtained the diploma and the Ph.D. degrees in 1992 and 1995, respectively. He held a two-year post-doctoral position at UC Berkeley in the Department of Chemistry, where he investigated the reaction dynamics of the ketene molecule. Since December 1997 he is a staff member at the University of Potsdam, Germany. His present work focuses on charge storage mechanisms in polymer electrets, optically induced charge-detrapping, and the study of piezoelectric resonances in charged polymer foams.



Francisco Camacho González was born in Mexico City in 1972. He received the Bachelor and M.Sc. degrees in electrical engineering from the National Polytechnic Institute of Mexico. In 2002, he received the M.Sc. degree in Polymer Science jointly from the University of Potsdam and the Free University, Humboldt University, and Technical University in Berlin, with a thesis on photostimulated discharge of polymeric electrets. He is currently a Ph.D. student at the University of Potsdam. His research interests include mechanisms of charge retention and depletion, as well as molecular electro-mechanical and optical processes in polymeric electrets.



Reimund Gerhard-Multhaupt (F⁹³) was born on 31 May 1952 in Heidelberg, Germany. He studied mathematics and physics and received the Diplom-Physiker (Dipl.-Phys.) and Doktor-Ingenieur (Dr.-Ing.) degrees from the Technical University of Darmstadt in 1978 and 1984, respectively. In addition, he earned the highest German university degree, the habilitation (Dr.rer.nat.habil.), from the University of Potsdam in 1992. In 1978/79, he was a Research Fellow at the Collège Militaire Royal in Saint-Jean, Québec, Canada. From 1979 until 1981, he was employed as Research Assistant at the German Polymer Institute, and from 1980 until 1985 as Staff Scientist at the Technical University, both in Darmstadt, Germany, where he worked mainly in the field of polymer electrets and their applications. In 1981, 1982 and 1983, Dr. Gerhard-Multhaupt spent one month each year as Exchange Visitor at AT&T Bell Laboratories in Murray Hill, New Jersey, USA. In 1985, he joined the Heinrich-Hertz Institute for Communications Engineering in Berlin, Germany, as Scientist and Manager of several consecutive research projects on light-valve projection devices for high-definition television and on nonlinear optical polymers. From 1992 until 1994 he was a Lecturer in the Materials Science Department of the Technical University of Berlin. In 1994, he was appointed Associate Professor for Sensorics at the University of Potsdam, Germany. He became a Professor of Applied Condensed-Matter Physics at his university in 1997. From 1997 until 2000, he was Head of the Department of Physics in Potsdam. The research of his group in the area of soft-matter physics is mainly dedicated to the electret properties of non-porous and porous polymers and composites, in particular with respect to dipole-orientation and space-charge phenomena, ferro-, pyro- and piezoelectric behavior, and piezo- or pyroelectric transducer applications. In addition, there are research activities on physics of musical instruments, especially organ pipes. In 1985, Dr. Gerhard-Multhaupt served as Symposium Secretary of the IEEE-sponsored Fifth International Symposium on Electrets (ISE 5) in Heidelberg, Germany, and in 1991, as Co-Chairman of ISE 7 in Berlin, Germany. Since 2001, he has been a Digest Editor of the IEEE Dielectrics and Electrical Insulation Society (DEIS) and member of the Executive Committee of the Conference on Electrical Insulation and Dielectric Phenomena (CEIDP). He is a member of the German (DPG), European (EPS) and American (APS) Physical Societies, of the Association of German Electrical Engineers (VDE) and its Information Technology Society (ITG), and of the Berlin-Brandenburg Society of Polymer Research. He was recipient of a 1988 Best-Paper Award from the Information Technology Society (ITG) in the Association of German Electrical Engineers (VDE), of a Silver medal from the Foundation Werner-von-Siemens-Ring in 1989 and of the first prize of the Technology Transfer Award 2001 from the Technology Foundation Brandenburg.

Unbiased iterative reconstruction of polarization and space-charge profiles from thermal-wave experiments

Axel Mellinger

Department of Physics, University of Potsdam, Am Neuen Palais 10,
D-14469 Potsdam, Germany

E-mail: axm@rz.uni-potsdam.de

Received 6 November 2003, in final form 18 May 2004

Published 16 June 2004

Online at stacks.iop.org/MST/15/1347

doi:10.1088/0957-0233/15/7/017

Abstract

The thermal-wave technique or laser-intensity modulation method is an important tool for the non-destructive probing of space-charge and polarization profiles in electrets. Analysing the experimental data requires solving a Fredholm integral equation which is known to be an ill-conditioned problem. This paper presents an iterative approach that is capable of reconstructing inherently unsmooth distributions. The deviations from the true profiles are slightly smaller than those obtained with Tikhonov regularization, while the computational burden is not a limiting factor on modern personal computers. The optimum number of iterations is estimated using the randomized generalized cross-validation technique. Results are shown for a number of model distributions, as well as for experimental data from a layered polyvinylidene fluoride film sandwich.

Keywords: pyroelectric coefficient, space charge density, laser-intensity modulation method (LIMM), thermal waves, dielectric materials, space charge electrets, polarization depth profiles

1. Introduction

A key problem in electret research is the non-destructive measurement of polarization and space-charge profiles [1]. During the past two decades, several techniques have been developed to probe dielectric materials with a thickness ranging from a few μm to several mm. They all rely on the propagation of acoustic or thermal waves through the sample, where they cause a space- and time-dependent compression or expansion, leading to an electrical response under short-circuit conditions. Thermal waves may also cause an electrical response due to temperature-dependent polarization and permittivity. Acoustic techniques use the propagation of a pressure pulse or step, generated either with a quartz crystal (*pressure-step propagation method*, PPS [2]) or through the absorption of a short laser pulse (*laser-induced pressure-pulse method*, LIPP [3]). Alternatively, the acoustic response to a voltage pulse applied between the sample electrodes has been recorded with a piezoelectric transducer

(*pulsed electroacoustic method*, PEA [4]). While acoustic techniques have the advantage of nearly uniform resolution throughout the sample, it is difficult and costly to achieve a resolution better than approx. $1\ \mu\text{m}$, as both the pulse generation and detection equipment must have risetimes in the sub-ns range. Moreover, acoustic-pulse and pressure-step methods are difficult to apply to porous and cellular electrets due to their large acoustic scattering.

Thermal techniques, on the other hand, use the diffusion process of a thermal pulse or thermal wave in order to locally change the density and/or the dielectric constant. In addition, a pyroelectric current results in the presence of a temperature-dependent polarization. The *thermal pulse method* was first demonstrated in 1975 [5], while the *thermal wave method* was introduced in 1981 [6]. The latter is also known as the *laser-intensity modulation method* (LIMM), since the periodic heating is usually performed with an intensity-modulated laser beam. With heat diffusion being a slower process than the propagation of sound waves, the time resolution requirements

for the apparatus are less demanding. Conversely, with fast detection techniques, a spatial resolution of less than 1 μm is easily achieved [7]. A key advantage of the all-optical LIMM technique is its ability to investigate samples without requiring a mechanical contact. This is an important feature for, e.g., the study of soft polymer foams [8] which are easily deformed upon application of a mechanical stress [9]. Very recently, an in-depth review on thermal techniques was given by Bauer and Bauer-Gogonea [10].

Unlike with acoustic techniques, the electrical response of the sample to a thermal pulse, step or wave is not a simple function of the polarization or space-charge distribution, and sophisticated deconvolution methods must be used to solve the ill-conditioned problem of reconstructing the profile of the internal electric field [11]. In the following sections, we present an unbiased method for reconstructing distributions penetrating deep into the sample without requiring the extra constraints (e.g., smoothness) necessary with the widely used regularization techniques [12].

2. Theory

The propagation of the thermal wave in the sample is described by the heat-conduction equation

$$D \frac{\partial^2 T(z, t)}{\partial z^2} = \frac{\partial T(z, t)}{\partial t}, \quad (1)$$

where $T(z, t)$ is the temperature and D is the thermal diffusivity of the material. For thin samples, a one-dimensional analysis is usually sufficient, as shown by Emmerich *et al* [13] and Lang [14]. For polymer films with evaporated metal electrodes, only the polymer itself needs to be considered, as the electrodes are usually 2–3 orders of magnitude thinner than the polymer film. If the sinusoidally modulated light is absorbed at $z = 0$, the boundary conditions are [15]

$$\eta j_{\sim} e^{i\omega t} - G_0 T = -\kappa \left. \frac{\partial T}{\partial z} \right|_{z=0} \quad (2)$$

and

$$G_d = \kappa \left. \frac{\partial T}{\partial z} \right|_{z=d}, \quad (3)$$

where G_0 and G_d are the heat loss coefficients at the front and rear surface, κ is the thermal conductivity of the sample and $\eta j_{\sim} e^{i\omega t}$ is the absorbed power per unit area. For a free-standing film, both G_0 and G_d can usually be neglected, whereas samples thermally connected to a substrate may exhibit a substantial heat loss G_d . Under these conditions, equation (1) is solved by [15, 16]

$$T(z, t) = T_{\sim}(k, z) e^{i\omega t} \\ = \frac{\eta j_{\sim} \cosh[k(d-z)] + \frac{G_d}{\kappa k} \sinh[k(d-z)]}{\kappa k \left(1 + \frac{G_0 G_d}{\kappa^2 k^2}\right) \sinh(kd) + \frac{G_0 + G_d}{\kappa k} \cosh(kd)}, \quad (4)$$

where the complex thermal wave vector is given by

$$k = (1+i) \sqrt{\frac{\omega}{2D}}. \quad (5)$$

In the presence of a polarization p or space-charge ρ , the thermal wave in a sample with an electrode area A gives rise to the current [1]

$$I_{\sim}(\omega) = \frac{i\omega A}{d} \int_0^d g(z) T_{\sim}(k, z) dz, \quad (6)$$

with the distribution function

$$g(z) = (\alpha_{\epsilon} - \alpha_x) \int_0^z \rho(\xi) d\xi + p(z), \quad (7)$$

where α_{ϵ} is the temperature coefficient of the permittivity, α_x is the thermal expansion coefficient and $p(z)$ is the pyroelectric coefficient.

The key problem in the analysis of LIMM data is the reconstruction of the distribution function $g(z)$ from the experimentally observed frequency spectrum $I_{\sim}(\omega)$. The LIMM equation (6) is a Fredholm integral equation of the first kind, for which the finding of a solution is an ill-conditioned problem [17]. Within the experimental errors, the observed current $I_{\sim}(\omega)$ can result from an infinite number of distributions $g(z)$, most of which are strongly oscillating functions. Over the past 15 years, a number of techniques have been applied to obtain a unique solution of the LIMM equation [11]. Two widely used methods are the scanning-function method [18] and Tikhonov regularization [12, 19]. The former approach is an approximation applicable at frequencies where the penetration depth

$$z_r = \sqrt{2D/\omega} \quad (8)$$

is small compared to the sample thickness d . The approximate distribution is then given by

$$g_a(z_r) \approx \frac{\kappa d}{\eta j_{\sim} A D} [\text{Re } I_{\sim}(\omega) - \text{Im } I_{\sim}(\omega)]. \quad (9)$$

While highly effective in probing the surface region, this technique provides little information about the polarization or charge distribution in the bulk of the sample. Tikhonov regularization, on the other hand, has proven to be capable of extracting this information [20, 21]. A solution for $g(z)$ is obtained by minimizing the expression

$$\chi_r^2 = \sum_v \left| \frac{I(\omega_v)_{\text{exp}} - I(\omega_v)_{\text{calc}}}{\sigma_v} \right|^2 + \lambda \int_0^d \left| \frac{d^2 g(z)}{dz^2} \right|^2 dz, \quad (10)$$

where σ_v is the estimated error of the current at the frequency ω_v and λ is the regularization parameter. Finding the optimum value of λ is a non-trivial problem [19]. Recently, a new technique based on a combination of polynomial expansion and regularization was presented [11, 22].

A potential disadvantage of regularization methods is their bias towards smooth solutions, as imposed by the second term in equation (10). For sandwiched systems consisting of layers with different polarization, as well as for polymer films with injected space-charge layers, this often leads to an excessively smoothed reconstruction of $g(z)$.

In the quest for unbiased deconvolution techniques, one finds numerous examples in the field of digital image processing [23]. Here, the task is to restore blurred images with a known point-spread function (PSF). Interest in these techniques arose particularly after the launch of the

Hubble Space Telescope with its primary mirror suffering from spherical aberration. Several iterative methods are commonly used today [24]. While some of these, such as *Lucy–Richardson* or *maximum entropy* deconvolution, make specific use of the positivity of digital images, and are thus not applicable for reconstructing polarization profiles, the unregularized ‘steepest descent’ method (also known as van Cittert’s method [25] and Landweber iteration [26]) gives promising results in deconvolving L IMM measurements on samples with discontinuous polarization profiles.

First, using the trapezoid rule [17], the L IMM equation (6) is written as a system of linear equations:

$$I_{v,\text{calc}} = \sum_{\mu=0}^M R_{v\mu} g_{\mu}; \quad v = 0, \dots, N, \quad (11)$$

where

$$R_{v\mu} = i\omega \frac{A}{d} T_{\sim}(k_v, z_{\mu}) \times \begin{cases} (z_{\mu+1} - z_{\mu})/2; & \mu = 0 \\ (z_{\mu+1} - z_{\mu-1})/2; & 1 \leq \mu \leq M-1 \\ (z_{\mu} - z_{\mu-1})/2; & \mu = M \end{cases} \quad (12)$$

and

$$k_v = (1 + i)\sqrt{\omega_v/2D}. \quad (13)$$

M and N are the number of data points in the spatial and frequency domains, respectively. To take the higher resolution of L IMM near the surface into account, a logarithmic spacing is adopted for the z coordinate:

$$\log z_{\mu} = \log z_0 + \frac{\mu}{M}(\log z_M - \log z_0). \quad (14)$$

The *maximum-likelihood* solution is the one minimizing the expression

$$\chi^2[\mathbf{g}] = \sum_v \left| \frac{I_{v,\text{exp}} - \sum_{\mu=0}^M R_{v\mu} g_{\mu}}{\sigma_v} \right|^2, \quad (15)$$

which can be written in matrix notation as

$$\chi^2[\mathbf{g}] = (\mathbf{b} - \mathbf{A}\mathbf{g})^{\dagger}(\mathbf{b} - \mathbf{A}\mathbf{g}), \quad (16)$$

where the superscript \dagger denotes the transpose, complex conjugate matrix, $A_{v\mu} = R_{v\mu}/\sigma_v$ and $b_v = I_v/\sigma_v$. Van Cittert’s method is based on doing small steps in g_{μ} space in the direction opposite to the gradient $\nabla_{\mathbf{g}}\chi^2$. If $\mathbf{g}^{(n)}$ is the solution after n iterations, the next step is given by

$$\begin{aligned} \mathbf{g}^{(n+1)} &= \text{Re} \left\{ \mathbf{g}^{(n)} - \frac{\beta^{(n)}}{2} \nabla_{\mathbf{g}} \chi^2[\mathbf{g}^{(n)}] \right\} \\ &= \text{Re} \left\{ \mathbf{g}^{(n)} - \beta^{(n)} (\mathbf{A}^{\dagger} \mathbf{A} \mathbf{g}^{(n)} - \mathbf{A}^{\dagger} \mathbf{b}) \right\}, \end{aligned} \quad (17)$$

where Re denotes the real part. For $n \rightarrow \infty$ and a sufficiently small step size $\beta^{(n)}$, this scheme has been shown to converge to the solution that minimizes χ^2 [23]. In the present work, convergence was ensured by replacing $\beta^{(n)}$ with $\beta^{(n)}/2$ until $\chi^2[\mathbf{g}^{(n+1)}] < \chi^2[\mathbf{g}^{(n)}]$, while $\beta^{(n+1)} = 2\beta^{(n)}$ after each successful iteration step. The initial distribution $\mathbf{g}^{(0)}$ was obtained by interpolating the result of the scanning-function method [18] (cf equation (9)) with a smoothing cubic spline [27]. A schematic flow diagram is shown in figure 1.

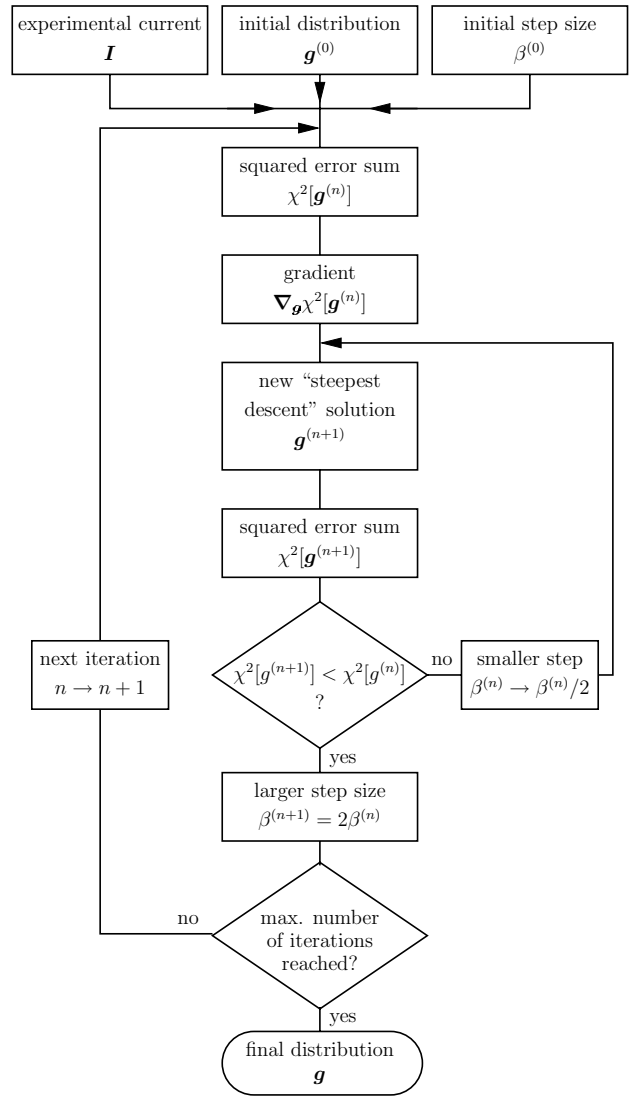


Figure 1. Schematic flow diagram of the iteration scheme.

3. Results and discussion

To demonstrate the effectiveness of the new iterative scheme, the algorithm was applied to several model polarization distributions $g(z)$, shown as dotted lines in figure 2:

- A bimorph (two layers of equal thickness with opposite polarization) [28, 29].
- A poled sheet sandwiched between two unpoled layers [28].
- A ‘ramp distribution’ of the electric field, resulting from a homogeneous space-charge density with compensation charges at both electrodes [30].

For a free-standing film ($G_0 = G_d = 0$), the frequency spectrum of the short-circuit current was then calculated using equation (11) and the diffusivity $D = 6.09 \times 10^{-8} \text{ m}^2 \text{ s}^{-1}$ of polyvinylidene fluoride (PVDF). $M = 500$ and $N = 80$ data points were used in the spatial and frequency domains, respectively. The latter resulted from the adopted frequency

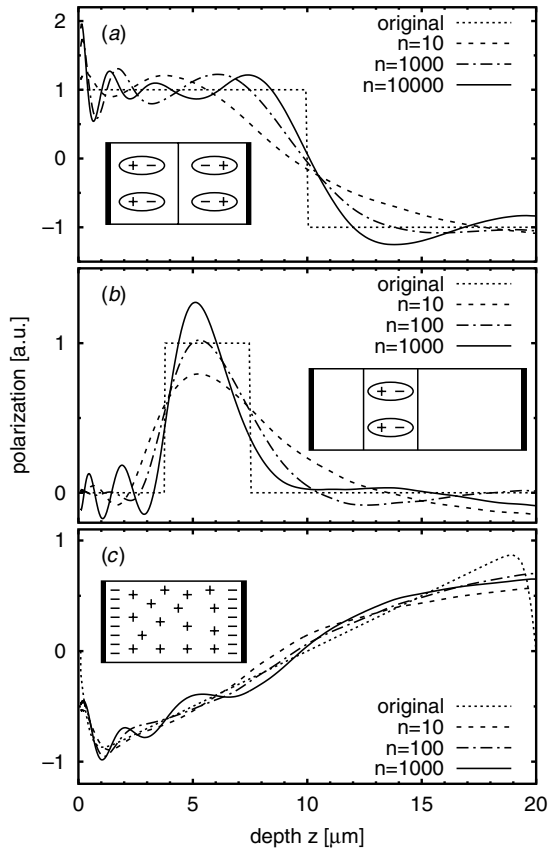


Figure 2. Iterative solution of the LIMM equation using synthetic distributions. (a) Bimorph, (b) poled layer, (c) uniform space-charge density with compensation charges at the electrodes. The insets show the schematic layer structure.

range of 10 Hz to 100 kHz with 20 data points per decade, which represents typical experimental conditions. At 10 Hz, the penetration depth $(2D/\omega)^{1/2}$ of the thermal wave is significantly larger than the assumed film thickness of 20 μm , while 100 kHz represents the upper frequency limit of many commercial lock-in amplifiers. To simulate experimental conditions, two random-noise contributions with a Gaussian distribution were added:

- standard deviation of 2% of the signal strength (to simulate fluctuations in the laser intensity), and
- standard deviation of 5 pA (to simulate background noise).

As an example, figure 3 shows the calculated current spectrum for a bimorph sample. All calculations were carried out with Octave [31] programs on a 1.5 GHz Intel® Pentium 4 personal computer. The typical execution speed was ten iterations per second.

The reconstructed profiles are shown in figure 2 for different numbers of iterations. Initially, the curves converge to the true profile, but develop increasing artefacts for higher n . It is therefore essential that the iteration process be stopped before achieving full convergence. To compare the reconstructed profile g_μ against the original distribution $g_\mu^{(\text{orig})}$ (shown as dotted lines in figure 2), the quantity

$$\psi^2 = \sum_{\mu=0}^M \left[\frac{z_\mu}{z_M} (g_\mu - g_\mu^{(\text{orig})}) \right]^2 \quad (18)$$

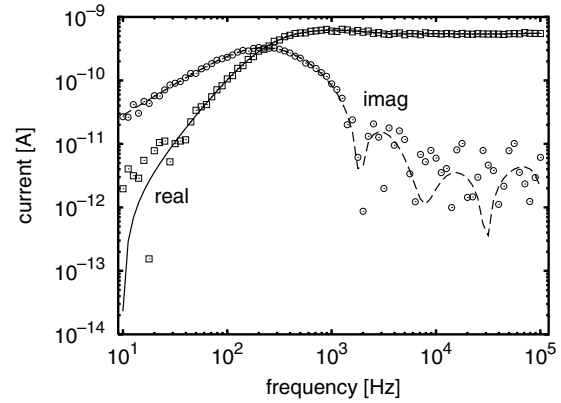


Figure 3. Calculated frequency spectrum of the pyroelectric current for a bimorph sample. The open squares and circles show the real and imaginary parts of the current calculated from the distribution plotted in figure 2(a) with additional Gaussian noise (see text for details). The solid and dashed lines represent the current calculated from the reconstructed profile after 10 000 iterations.

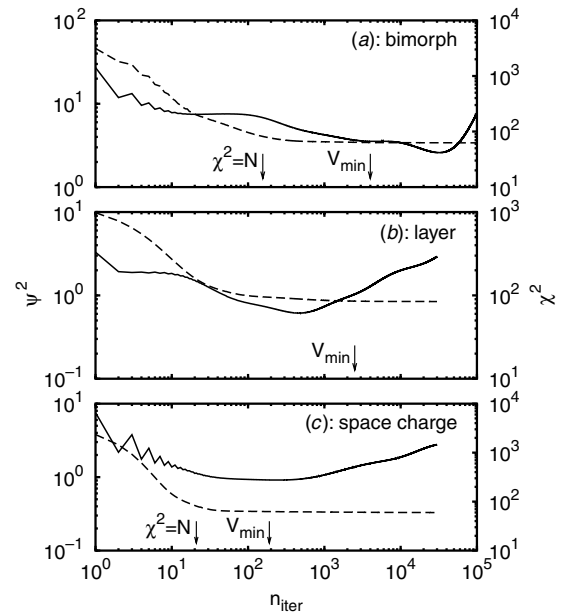


Figure 4. Squared error sums for the polarization profile (ψ^2 , solid lines) and the pyroelectric current (χ^2 , dashed lines) versus number of iterations. The arrows indicate the termination points given by the two methods discussed in the text: $\chi^2 = N$ (not reached in case (b)) and the minimum of $V(n)$ defined in equation (19) and depicted in figure 5.

was used as a figure-of-merit. Here, the error differences are scaled with the factor z_μ/z_M in order to assign equal weights to all depths, even though the z_μ values are scaled logarithmically according to equation (14). The dependence of ψ^2 and χ^2 on the number of iterations is shown in figure 4. Evidently, the optimum number of iterations n_{opt} (where ψ^2 reaches a minimum) is very different for the three model profiles. Reconstructing the bimorph profile required approx. 4400 iteration steps, whereas for the space-charge profile, ψ^2 was minimized after only 200 iterations. Obviously, ψ^2 cannot be calculated from experimental data, since the true polarization profile is unknown. Even though the broad

minima of ψ^2 indicate that the choice of n is not very critical, a formal termination criterion is required.

If the experimental error σ_v of each data point is known, χ^2 can be calculated from equation (15). One way to determine σ_v is to perform a series of measurements at fixed frequency and calculate the standard deviation. For large N and a Gaussian error distribution of the $N + 1$ individual data points, the expectation value of (15) is $\chi^2 = N + 1 \approx N$ [17], which can be used as a stopping condition. This method of using *a priori* information is often referred to as Morozov's discrepancy principle [32]. In practice, however, the termination value of n depends rather critically on the assumed experimental errors, since χ^2 becomes almost constant for large n , as shown in figure 4. If the experimental error is underestimated, χ^2 will be too large and may not reach the termination value $\chi^2 = N$ at all (cf figure 4(b)). On the other hand, overestimated errors lead to a premature termination of the iteration loop, resulting in excessively smoothed polarization profiles.

A method that does not depend on *a priori* information is the randomized generalized cross-validation (RGCV) technique [33]. It is based on the principle that the optimal solution should predict missing data points [32]. Iteration is stopped when the function

$$V(n) = \frac{\|\mathbf{b} - \mathbf{A}\mathbf{g}^{(n)}\|^2}{\|\text{Tr}(\mathbf{I} - \mathbf{F}^{(n)})\|^2} \quad (19)$$

reaches a minimum, where \mathbf{I} is the identity matrix, and the $(N + 1) \times (N + 1)$ matrix $\mathbf{F}^{(n)}$ is defined by¹

$$\mathbf{F}^{(n)}\mathbf{b} = \mathbf{A}\mathbf{g}^{(n)}. \quad (20)$$

As shown in [33], the denominator of equation (19) can be evaluated using a *Monte Carlo* approach by introducing a vector \mathbf{u} of $v = 0, \dots, N$ independent samples of a random variable U with zero mean and a variance of one. In addition, a vector $\mathbf{w}^{(n)}$ of length $M + 1$ is defined via

$$\mathbf{F}^{(n)}\mathbf{u} = \mathbf{A}\mathbf{w}^{(n)}. \quad (21)$$

By comparing equations (20) and (21) we conclude that $\mathbf{w}^{(n)}$ can be obtained from \mathbf{u} through the same iterative process that is used to extract the distribution $\mathbf{g}^{(n)}$ from the experimental data \mathbf{b} :

$$\mathbf{w}^{(n+1)} = \mathbf{w}^{(n)} - \beta^{(n)}(\mathbf{A}^\dagger \mathbf{A}\mathbf{w}^{(n)} - \mathbf{A}^\dagger \mathbf{u}). \quad (22)$$

The initial value $\mathbf{w}^{(0)}$ is set equal to the null vector. With these definitions, the denominator of equation (19) is given by

$$\|\text{Tr}(\mathbf{I} - \mathbf{F}^{(n)})\|^2 = \|\mathbf{u}^\dagger \mathbf{u} - \mathbf{u}^\dagger \mathbf{A}\mathbf{w}^{(n)}\|^2 \quad (23)$$

As shown in figure 5, $V(n)$ is a function with a shallow minimum. The minima are also indicated in figure 4; they fall within one order of magnitude of n_{opt} in all three cases. Thus, RGCV is more robust than the *a priori* technique based on the values of χ^2 .

Figure 6 shows the Tikhonov regularization results for the same profiles used in figure 2. A larger regularization parameter λ results in smoother curves. The optimum value for λ can be determined from figure 7, where the deviation ψ^2 from the true profiles is plotted versus λ . A comparison with the iterative results in figure 4 shows that the minima of ψ^2 are

¹ While the calculation of \mathbf{A} and \mathbf{b} according to equations (15) and (16) requires numerical values for σ_v , the minimum of $V(n)$ is independent of the chosen σ_v .

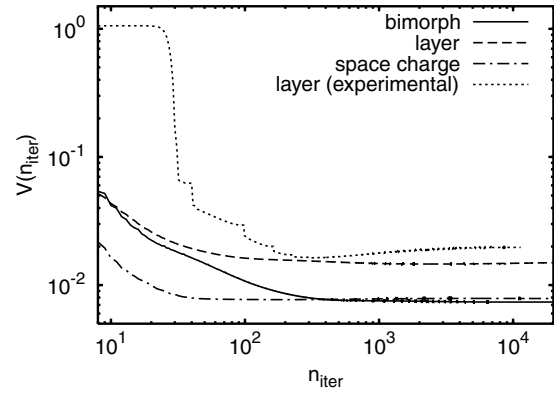


Figure 5. Plot of $V(n)$ defined in equation (19) for the three synthetic distributions of figure 2 and the experimental data of figure 8. All four curves exhibit a (in some cases very shallow) minimum.

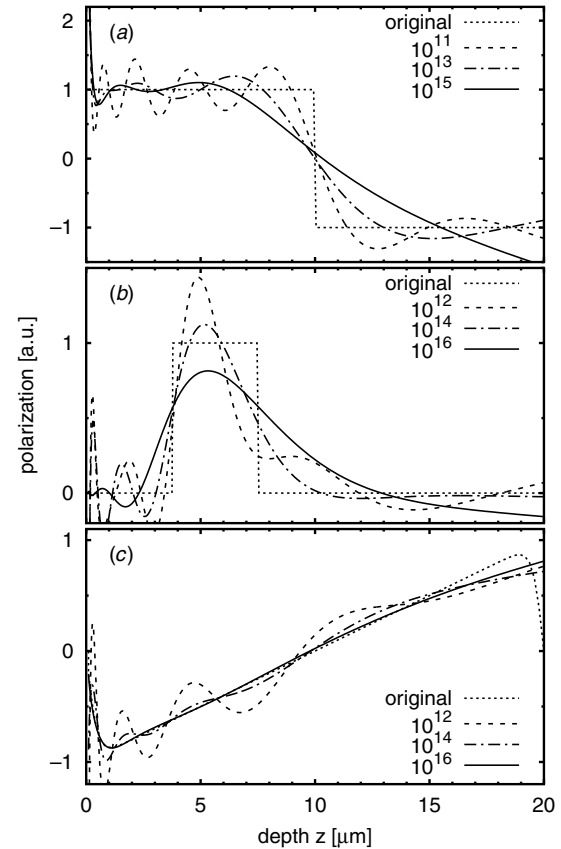


Figure 6. Reconstruction of the same distributions as in figure 2 using Tikhonov regularization with different values of λ (cf equation (10)). (a) Bimorph, (b) poled layer, (c) uniform space-charge density.

slightly larger than those obtained using van Cittert iterations. Therefore, Tikhonov regularization can, in principle, extract a similar amount of information from the experimental current spectrum as the iterative approach. However, choosing the optimum regularization parameter is a critical and complex task [19], and is prone to yielding excessively smoothed profiles. On the other hand, the iterative solution rapidly stabilizes after 10–100 iterations, with a very gradual build-up of artefacts.

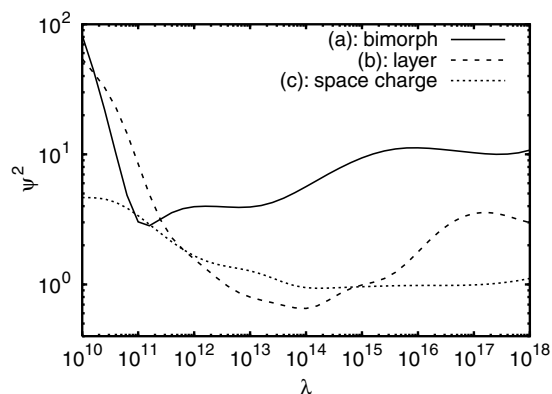


Figure 7. Dependence of ψ^2 on the regularization parameter λ . The minima of ψ^2 are slightly larger than those obtained iteratively.

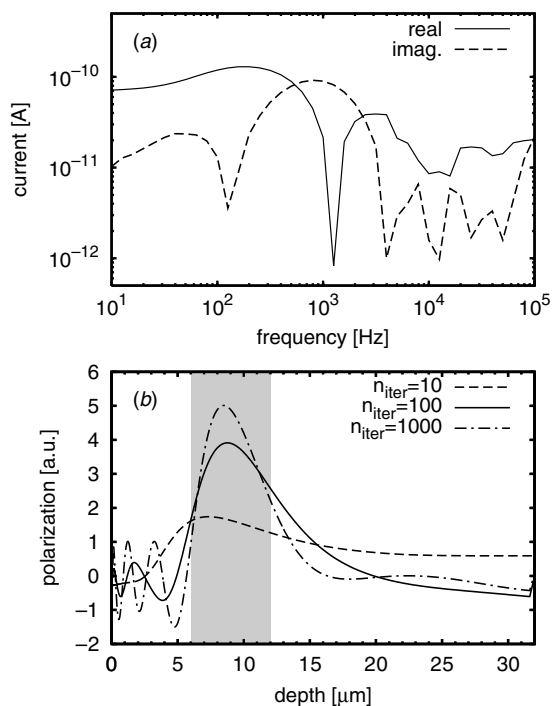


Figure 8. Experimental current spectrum (a) and reconstructed polarization profile (b) of a poled $6\ \mu\text{m}$ PVDF film, sandwiched between $6\ \mu\text{m}$ and $20\ \mu\text{m}$ unpoled PVDF layers. The shaded region indicates the poled layer. The RGCV termination condition according to equation (19) is $n = 320$ (cf figure 5).

The application of the iteration technique to the experimental current spectrum of a $32\ \mu\text{m}$ PVDF stack (one poled $6\ \mu\text{m}$ film sandwiched between $6\ \mu\text{m}$ and $20\ \mu\text{m}$ layers of unpoled PVDF) is shown in figure 8. Even though the current spectrum is perturbed by thermoelastic resonances in the free-standing sample around $10\ \text{kHz}$, the width of the poled layer is reconstructed correctly.

4. Conclusions

The ill-conditioned LIMM equation has been solved using an iterative scheme based on van Cittert's method. Simulations for various polarization and space-charge profiles showed optimum agreement with the true distributions after 90 to

7000 iterations, depending on the profile shape. The deviation from the true profiles was slightly lower than in the case of Tikhonov regularization with an optimized regularization parameter. Due to the very gradual build-up of artefacts, the number of iterations needed for the optimum solution is not a critical parameter. Its value can be estimated using the randomized generalized cross-validation (RGCV) technique. The iterative approach complements the scanning-function technique, which does not produce artefacts but (due to its reliance on a high-frequency approximation of the temperature distribution) gives accurate results near the surface only. Compared to regularization, a potential drawback is the longer computation time, although this is usually not a limiting issue on today's fast personal computers. Moreover, convergence could be accelerated with a more sophisticated minimization strategy, using, e.g., conjugate gradients [17].

Acknowledgments

The author gratefully acknowledges stimulating discussions with Reimund Gerhard-Multhaupt and Enis Tuncer (both University of Potsdam, Germany) and Sidney B Lang (Ben-Gurion University of the Negev, Beer Sheva, Israel).

References

- [1] Sessler G M 1999 Distribution and transport of charge in polymers *Electrets* 3rd edn, vol 2, ed R Gerhard-Multhaupt (Morgan Hill, CA: Laplacian Press) chapter 10 pp 41–80
- [2] Eisenmenger W and Haardt M 1982 Observation of charge compensated polarization zones in polyvinylidene fluoride (PVDF) films by piezoelectric acoustic step-wave response *Solid State Commun.* **41** 917–20
- [3] Sessler G M, West J E and Gerhard R 1982 High-resolution laser-pulse method for measuring space charge distributions in electrets *Phys. Rev. Lett.* **48** 563–6
- [4] Takada T, Maeno T and Kushibe H 1985 An electric stress pulse technique for the measurement of charges in a plastic plate irradiated by an electron beam *Proc. 5th Int. Symp. Electrets* ed G M Sessler and R Gerhard-Multhaupt (Piscataway, NJ: IEEE Service Center) pp 450–5
- [5] Collins R 1975 Distribution of charge in electrets *Appl. Phys. Lett.* **26** 675–7
- [6] Lang S B and Das-Gupta D K 1981 A technique for determining the polarization distribution in thin polymer electrets using periodic heating *Ferroelectrics* **39** 1249–52
- [7] Ploss B 2002 The resolution of thermal profiling techniques *Proc. 11th Int. Symp. on Electrets* (Piscataway, NJ: IEEE Service Center) pp 177–80
- [8] van Turnhout J, Staal R E, Wübbenhorst M and de Haan P H 1999 Distribution and stability of charges in porous polypropylene films *Proc. 10th Int. Symp. on Electrets* (Piscataway, NJ: IEEE Service Center) pp 785–8
- [9] Mellinger A, Camacho González F and Gerhard-Multhaupt R 2003 Ultraviolet-induced discharge currents and reduction of the piezoelectric coefficient in cellular polypropylene films *Appl. Phys. Lett.* **82** 254–6
- [10] Bauer S and Bauer-Gogonea S 2003 Current practice in space charge and polarization profile measurements using thermal techniques *IEEE Trans. Dielectr. Electr. Insul.* **10** 883–902
- [11] Lang S B 2004 Laser intensity modulation method (LIMM): review of the fundamentals and a new method for data analysis *IEEE Trans. Dielectr. Electr. Insul.* **11** 3–12
- [12] Tikhonov A N, Goncharkii A V, Stepanov V V and Kochikov I V 1987 Ill-posed image processing problems *Sov. Phys.—Dokl.* **32** 456–8

- [13] Emmerich R, Bauer S and Ploss B 1992 Temperature distribution in a film heated with a laser spot: Theory and measurement *Appl. Phys. A* **54** 334–9
- [14] Lang S B 2001 Two-dimensional thermal analysis of thin-film pyroelectric infrared detectors *Ferroelectrics* **258** 297–302
- [15] Ploss B, Bauer S and Bon C 1991 Measurement of the thermal diffusivity of thin films with bolometers and with pyroelectric temperature sensors *Ferroelectrics* **118** 435–50
- [16] Bloß P and Schäfer H 1994 Investigations of polarization profiles in multilayer systems by using the laser intensity modulation method *Rev. Sci. Instrum.* **65** 1541–50
- [17] Press W H, Teukolsky S A, Vetterling W T and Flannery B P 1992 *Numerical Recipes in C* 2nd edn (Cambridge: Cambridge University Press)
- [18] Ploss B, Emmerich R and Bauer S 1992 Thermal wave probing of pyroelectric distributions in the surface region of ferroelectric materials: a new method for the analysis *J. Appl. Phys.* **72** 5363–70
- [19] Weese J 1992 A reliable and fast method for the solution of fredholm integral equations of the first kind based on Tikhonov regularization *Comput. Phys. Commun.* **69** 99–111
- [20] Lang S B 1991 Laser intensity modulation method (LIMM): experimental techniques, theory and solution of the integral equation *Ferroelectrics* **118** 343–61
- [21] Bloß P, Steffen M, Schäfer H, Yang G M and Sessler G M 1997 A comparison of space-charge distributions in electron-beam irradiated FEP obtained by using heat-wave and pressure-wave techniques *J. Phys. D: Appl. Phys.* **30** 1668–75
- [22] Lang S B 2001 Polynomial solution of the fredholm integral equation in the laser intensity modulation method (LIMM) *Integr. Ferroelectr.* **38** 111–8
- [23] Biemond J, Lagendijk R L and Mersereau R M 1990 Iterative methods for image deblurring *Proc. IEEE* **78** 856–83
- [24] Starck J L, Pantin E and Murtagh F 2002 Deconvolution in astronomy: a review *Publ. Astron. Soc. Pac.* **114** 1051–69
- [25] van Cittert P H 1931 Zum Einfluß der Spaltbreite auf die Intensitätsverteilung in Spektrallinien II *Z. Phys.* **69** 298–308
- [26] Landweber L 1951 An iteration formula for Fredholm integral equations of the first kind *Am. J. Math.* **73** 615–24
- [27] Späth H 1995 *One-Dimensional Spline Interpolation Algorithms* (Wellesley, MA: A K Peters)
- [28] Bauer-Gogonea S, Bauer S and Gerhard-Multhaupt R 1999 Monomorphs, bimorphs and multimorphs from polar polymer electrets *Braz. J. Phys.* **29** 306–17
- [29] Bauer-Gogonea S, Bauer S, Wirges W and Gerhard-Multhaupt R 1994 Pyroelectrical investigation of the dipole orientation in nonlinear optical polymers during and after photoinduced poling *J. Appl. Phys.* **76** 2627–35
- [30] Gerhard-Multhaupt R, Künstler W, Eberle G, Eisenmenger W and Yang G 1998 High space-charge densities in the bulk of fluoropolymer electrets detected with piezoelectrically generated pressure steps *Space Charge in Solid Dielectrics* ed J C Fothergill and L A Dissado (Leicester: Dielectrics Society) pp 123–32
- [31] Eaton J W 2003 *Octave: A High-Level Interactive Language for Numerical Computations* (University of Wisconsin, www.octave.org)
- [32] Hansen P C 1998 *Rank-Deficient and Discrete Ill-Posed Problems* (Philadelphia: SIAM)
- [33] Perry K M and Reeves S J 1994 A practical stopping rule for iterative signal restoration *IEEE Trans. Signal Process.* **42** 1829–33

Errata

to: A. Mellinger, “Unbiased iterative reconstruction of polarization and space-charge profiles from thermal-wave experiments”, *Meas. Sci. Technology* **15**, 1347-1353 (2004).

On p. 1348, Eq. (3) should read

$$G_d T = \kappa \left. \frac{\partial T}{\partial z} \right|_{z=d}$$

On p. 1348, Eq. (4) should read

$$\begin{aligned} T(z, t) &= T_{\sim}(k, z) e^{i\omega t} \\ &= \frac{\eta j_{\sim}}{\kappa k} \frac{\cosh[k(d-z)] + \frac{G_d}{\kappa k} \sinh[k(d-z)]}{\left(1 + \frac{G_0 G_d}{\kappa^2 k^2}\right) \sinh(kd) + \frac{G_0 + G_d}{\kappa k} \cosh(kd)} e^{i\omega t} \end{aligned}$$

Fast thermal-pulse measurements of space-charge distributions in electret polymers

Axel Mellinger,* Rajeev Singh,† and Reimund Gerhard-Multhaupt

Department of Physics, University of Potsdam, Am Neuen Palais 10, D-14469 Potsdam, Germany

(Dated: November 23, 2004)

Space-charge depth profiles in various electret polymers have been measured in both the time and the frequency domain using thermal pulses and waves, respectively. A comparison of the two techniques on corona-charged polytetrafluoroethylene showed that the thermal-pulse method yielded similar results as the thermal-wave technique, but approximately 20-50 times faster. The article discusses sensitivity limitations as well as possible applications, including the real-time monitoring of space-charge decay under UV irradiation.

PACS numbers: 44.10.+i, 66.30.Xj, 66.70.+f, 77.84.Jd

Keywords: thermal-pulse method, LIMM, electrets, space-charge, thermal diffusivity, polytetrafluoroethylene

I. INTRODUCTION

Since their invention in the mid-1970s, thermal techniques probing the depth profiles of space-charge and polarization in dielectric materials have reached a level of maturity and contributed significantly to the understanding of space-charge dynamics. In principle, these techniques are implemented either in the time or in the frequency domain, and can therefore be divided into thermal-pulse (or step) and thermal-wave techniques. Both methods are based upon the diffusion of heat in the sample material. In the thermal-pulse method, the thermal excitation is achieved through the absorption of a short intense light pulse by an opaque electrode layer on one side of the sample [1, 2], whereas in the thermal-wave method a periodic heating of the sample is employed by means of an intensity-modulated laser beam. The latter is commonly referred to as LIMM, an acronym for Laser Intensity Modulation Method [3, 4]. Both techniques can extract a similar amount of information on the space-charge profile. However, we shall demonstrate in this work that the thermal-pulse technique offers substantial advantages in terms of acquisition speed over its frequency-domain counterpart.

A drawback of thermal techniques is a rather tedious deconvolution process, which also necessitates a careful interpretation of the results. The data analysis therefore becomes a very important and integral part to comprehend the complete space-charge and polarization profile. To process thermal-pulse data, approaches were proposed by VON SEGGERN [5] and by DEREGGI *et al.* [6, 7], based upon the determination of Fourier coefficients. The method is, however, limited by the fact that only the first few Fourier coefficients in the series can be determined with reasonable accuracy. A mathematical technique based on differential operators, suitable in particular for the field distribution near the surface of a film was

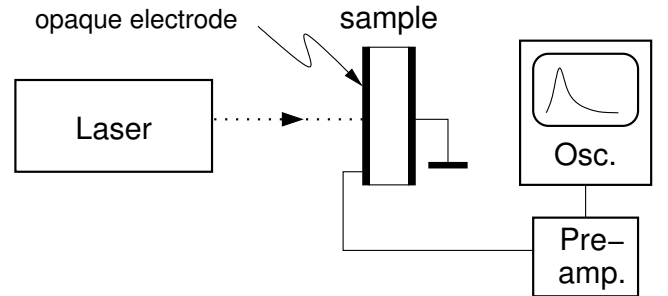


FIG. 1: Setup for thermal-pulse measurements.

reported by BAUER [8]. An alternative approach, demonstrated in the present work, is to analyze thermal-pulse data in the frequency domain.

II. EXPERIMENTAL DETAILS

Polytetrafluoroethylene (PTFE) films (Plastpolymer, St. Petersburg, Russia) with a thickness of 17 μm were rinsed in isopropanol and charged in a point-to-plane corona with a needle voltage of +12 kV (with the metallized side in contact with the grounded plate). While the electric field was applied, the temperature was kept at 200 $^{\circ}\text{C}$ for 1 min and then ramped down to room temperature during 5 min. This process results in a nearly homogeneous positive space-charge distribution in the bulk of the polymer [9]. Electrical contacts were provided by evaporating aluminum layers (50 nm) on each surface. To enhance light absorption, an extra 20 nm layer of graphite was deposited onto the front side. The experimental setup is shown in Fig. 1. Thermal pulse measurements were performed with the second harmonic output (wavelength 532 nm, pulse duration $\tau_L \approx 5$ ns) of a Nd:YAG laser (Polaris III, New Wave Research). The short-circuit pyroelectric or displacement current was amplified by a Stanford Research SR 570 current amplifier and recorded with a digital storage oscilloscope (Agilent 54833A) at a rate of $(\Delta t)^{-1} = 10$ MSamples/s. According to Nyquist's theorem, this allows frequencies

*Electronic address: axm@rz.uni-potsdam.de

†Permanent address: Department of Electronics & Communication, University of Allahabad, Allahabad, (U.P.)-211002, India

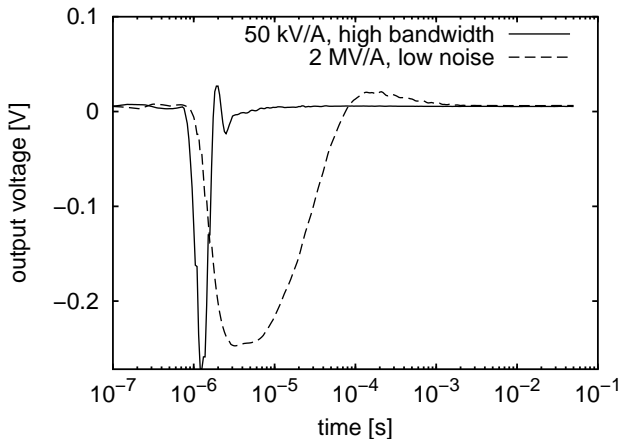


FIG. 2: Thermal pulse response of a volume-charged PTFE film, recorded at two different amplifier gain/bandwidth settings and averaged over 256 pulses.

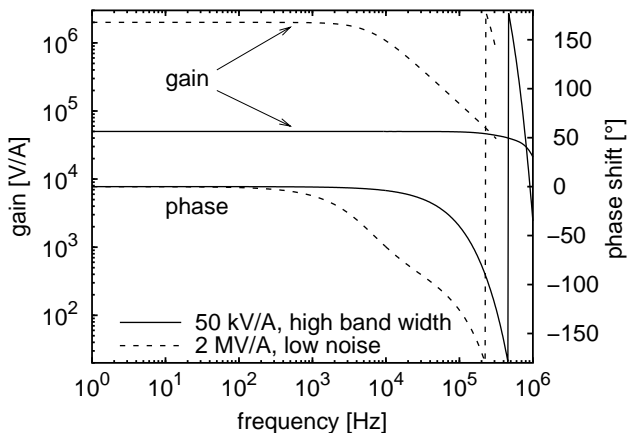


FIG. 3: Frequency dependence for the gain and phase shift of a Stanford Research SR 570 current preamplifier.

up to 5 MHz to be recorded, so that the bandwidth (and hence the spatial resolution) is limited by the high-frequency cut-off of the current amplifier, rather than the rate of digitization. After averaging between 30 and 256 laser pulses, a total of $N = 512\,000$ data points were stored for further processing.

For LIMM measurements, the sample was periodically heated with the modulated beam of a laser diode (LISA Laser Products, 50 mW optical output @ 785 nm). The preamplified current was recorded with a Stanford Research SR 850 lock-in amplifier.

III. RESULTS

Test of the method on volume-charged PTFE

Fig. 2 shows the thermal pulse response of a volume-charged PTFE film. Evidently, the signal is strongly de-

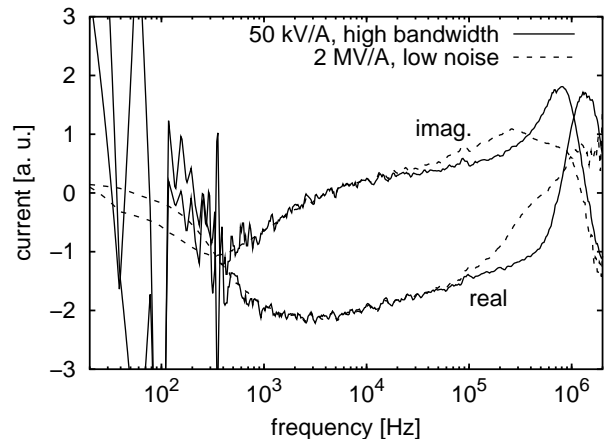


FIG. 4: Fourier-transformed displacement current of a charged PTFE film, measured with two different gain/bandwidth settings of the preamplifier.

pendent on the gain and bandwidth setting of the SR 570 current preamplifier. To compensate the amplifier-induced signal distortion, the time-domain signal $I(t_k)$ was converted to the frequency domain via a discrete Fast Fourier transform and divided by the measured gain spectrum $\tilde{\alpha}(f_n)$ of the SR 570 (Fig. 3):

$$\tilde{J}_{\text{comp}}(f_n) = \frac{\Delta t}{\tilde{\alpha}(f_n)} \sum_{k=0}^{N-1} I(t_k) e^{-2\pi i k n / N}, \quad (1)$$

where the tilde $\tilde{\cdot}$ denotes complex quantities. The frequency points are given by

$$f_n = \frac{n}{N\Delta t}, \quad n = 1 \dots \frac{N}{2}. \quad (2)$$

The resulting spectra in Fig. 4 show excellent agreement between 500 Hz and 20 kHz. Above 20 kHz, the decreasing gain and phase shift in the low-noise mode leads to a substantial signal distortion, while in the high-bandwidth mode noise starts to dominate below 500 Hz. Combining the two data sets with a smooth transition function

$$w(f_n) = \frac{1}{2} \left\{ \tanh \left[\frac{1}{w_0} \log_{10} \left(\frac{f_n}{f_0} \right) \right] + 1 \right\} \quad (3)$$

via

$$\tilde{J}_{\text{comb}}(f_n) = \tilde{J}_{\text{hbw}}(f_n)w(f_n) + \tilde{J}_{\text{ln}}(f_n)(1 - w(f_n)) \quad (4)$$

(with $f_0 = 3.0$ kHz and $w_0 = 0.2$) extends the usable frequency range to an interval from 20 Hz to 2 MHz. Here, $\tilde{J}_{\text{hbw}}(f_n)$ and $\tilde{J}_{\text{ln}}(f_n)$ are the Fourier-transformed signals recorded in high-bandwidth and low-noise mode, respectively. As shown in Fig. 5, the agreement with the LIMM signal recorded in the frequency domain is excellent.

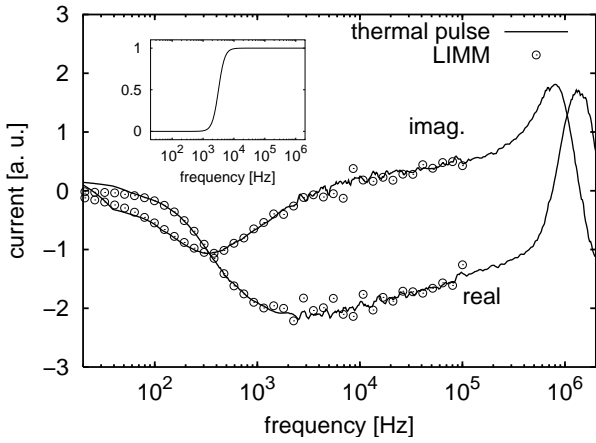


FIG. 5: Comparison of the thermal-pulse (solid line) and LIMM spectrum (open squares) of a charged PTFE film. The TP spectrum was obtained by combining two spectra recorded with different gain/bandwidth settings (cf. Fig. 4), using the transition function defined in Eq. (3) and shown in the inset.

IV. DISCUSSION

A. Signal Processing

For laser beam spot sizes that are large compared to the sample thickness d , the propagation of the thermal pulse or wave in the polymer film is described by the one-dimensional heat conduction equation

$$D \frac{\partial^2 T(z, t)}{\partial z^2} = \frac{\partial T(z, t)}{\partial t}, \quad (5)$$

where $T(z, t)$ and D are the transient temperature and thermal diffusivity, of the polymer, respectively. After the absorption of a short light pulse, the transient temperature in a free-standing polymer film is given by [6, 10]

$$T(z, t) = T_0 \exp\left(\frac{-t}{\tau_{\text{th}}}\right) + 2T_0 \sum_{n=1}^{\infty} \cos\left(\frac{n\pi z}{d}\right) \exp\left(\frac{-n^2 t}{\tau}\right). \quad (6)$$

Here, $\tau = d^2/(\pi^2 D)$ is the thermal transit time (during which the sample reaches internal thermal equilibrium), and τ_{th} is the time constant for reaching thermal equilibrium with the environment, with $\tau_{\text{th}} \gg \tau$. After a time t with $\tau \ll t \ll \tau_{\text{th}}$, the sample has reached the internal thermal equilibrium temperature T_0 . Similar solutions exist for samples attached to a heat sink [11].

In the presence of a polarization or space-charge, the thermal pulse or wave gives rise to a pyroelectric or displacement current [12]

$$I(t) = \frac{A}{d} \int_0^d g(z) \frac{\partial T(z, t)}{\partial t} dz \quad (7)$$

with the distribution function

$$g(z) = (\alpha_\epsilon - \alpha_z) \epsilon_0 \epsilon E(z) + p(z), \quad (8)$$

where α_ϵ is the temperature coefficient of the permittivity, α_z is the thermal expansion coefficient, $p(z)$ is the pyroelectric coefficient, ϵ_0 is the permittivity of free space, ϵ is the dielectric constant, $E(z)$ is the internal electric field, and A is the heated sample area. A Fourier transform of the transient current yields

$$\begin{aligned} \tilde{J}(\omega) &= \int_0^\infty I(t) e^{-i\omega t} dt \\ &= \frac{A}{d} \int_0^\infty \int_0^d g(z) \frac{\partial T(z, t)}{\partial t} dz e^{-i\omega t} dt \\ &= \frac{A}{d} \int_0^d g(z) \left\{ [T(z, t) e^{-i\omega t}]_0^\infty + \right. \\ &\quad \left. + i\omega \int_0^\infty T(z, t) e^{-i\omega t} dt \right\} dz \quad (9) \end{aligned}$$

after integration by parts. Inserting Eq. (6) into (9), we obtain

$$\tilde{J}(\omega) = T_0 A \left\{ g_0 - 2g(0) + i\omega \sum_{n=1}^{\infty} g_n \frac{\tau}{n^2 + i\omega\tau} \right\} \quad (10a)$$

$$\approx T_0 A \left\{ g_0 + i\omega \sum_{n=1}^{\infty} g_n \frac{\tau}{n^2 + i\omega\tau} \right\}, \quad (10b)$$

where the Fourier coefficients of $g(z)$ are defined by

$$g_n = \begin{cases} \frac{1}{d} \int_0^d g(z) dz & ; \quad n = 0 \\ \frac{2}{d} \int_0^d g(z) \cos\left(\frac{n\pi z}{d}\right) dz & ; \quad n > 0 \end{cases} \quad (11)$$

In Eq. (10a), the term proportional to $g(0)$ can be neglected under all practical circumstances, as it is present only when the spatial temperature distribution becomes a δ function at $t = 0$.

On the other hand, the frequency spectrum of the short-circuit current in a LIMM experiment has been shown [13] to follow

$$\begin{aligned} I_{\text{LIMM}}(\omega) &= i\omega \frac{\eta j A}{c \rho d} \sum_{n=0}^{\infty} g_n \frac{\tau}{n^2 + i\omega\tau} \\ &= \frac{\eta j A}{c \rho d} \left\{ g_0 + i\omega \sum_{n=1}^{\infty} g_n \frac{\tau}{n^2 + i\omega\tau} \right\} \quad (12) \end{aligned}$$

(where η , j , c , ρ are the absorption coefficient, laser intensity, heat capacity and density, respectively), which is the same functional form as in Eq. (10b). Therefore, analyzing the Fourier-transformed thermal pulse data in the frequency domain is equivalent to analyzing the data of a LIMM experiment.

Solving Eq. (7) for $g(z)$ is an ill-conditioned problem [14], and numerous deconvolution techniques have been developed both in the time domain [6–8] and in the frequency domain [15–18]. Here, we chose to perform the analysis in the frequency domain for two reasons:

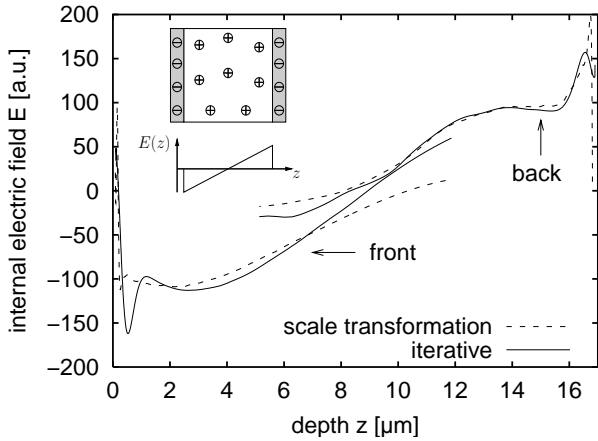


FIG. 6: Distribution of the internal electric field calculated from the front-side thermal-pulse data of Fig. 5 (and similar back-side data) using the scale-transformation [16] method and an iterative approach [17]. The inset shows the schematic space-charge distribution and the corresponding electric field $E(z)$.

- (a) Frequency-domain analysis of LIMM data has reached a mature state. In particular, the near-surface distribution can be obtained via a simple scale-transformation method [16], where $g(z)$ is proportional to the difference between the real and imaginary current $\Re\tilde{J}(f) - \Im\tilde{J}(f)$ with z given by

$$z = \left(\frac{D}{\pi f}\right)^{1/2} \quad (13)$$

- (b) Correction for the frequency-dependent gain and phase shift of the preamplifier already requires transforming the signal to the frequency domain, as described by Eq. (1).

Analyzing thermal-pulse data via a fast Fourier transform was suggested by PLOSS in 1994 [19]. Although the required linear sampling over time scales covering several orders of magnitude was considered impractical at that time due to the large number of data points, modern computer hardware can process this amount of data in less than 1 sec.

The distribution of the internal electric field $E(z)$ was calculated from the frequency spectrum using a simple scale transformation technique [16] as well as an iterative approach [17]. The former gives an accurate representation of the near-surface profile (cf. Fig. 6), whereas the latter gives a clearer picture of the overall distribution, at the expense of introducing some artifacts at small depths. In order to take advantage of the high near-surface depth resolution of the thermal-pulse technique, measurements were taken on both sides and joined at $z = d/2$. From the curves, the space-charge distribution $\rho_c(z) = \epsilon_0 \epsilon dE(z)/dz$ can be obtained via a simple differentiation.

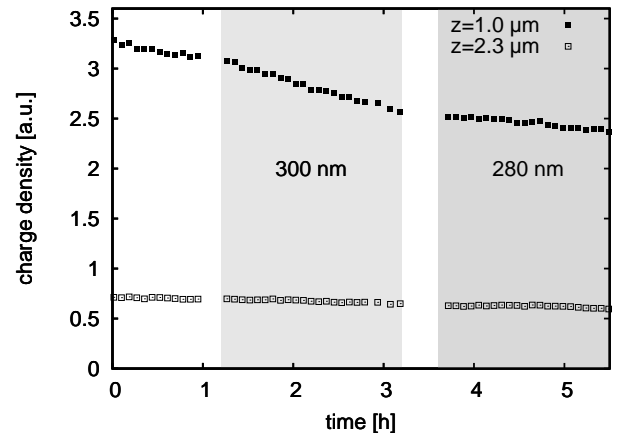


FIG. 7: Time-dependent evolution of the charge density at depths of $z = 1.0$ and $2.3 \mu\text{m}$ in a corona-charged cyclic olefin copolymer film during UV irradiation through a semitransparent back electrode. The shaded areas indicate the duration of the irradiation at the respective wavelength. Only irradiation at 300 nm accelerates the charge decay at shallow depths.

B. Applications

The greatest advantage of the thermal-pulse method over LIMM is its speed. The 256-shot average of the transient current shown in Fig. 2 was recorded in 45 s, whereas the acquisition of the LIMM spectrum of Fig. 5 took approximately 30 min. Despite the significantly shorter acquisition time, the signal-to-noise ratio level in the thermal-pulse spectrum is visibly superior. Even when taking into account the time to record two thermal transients at different gain/bandwidth settings, thermal-pulse measurements with the given setup are 20-50 times faster than LIMM measurements of similar bandwidth and quality. The short data acquisition time is highly useful in the study of time-dependent processes, such as the photoinduced depletion of space-charge [20, 21]. Under laboratory conditions, these processes typically occur on a time scale of several minutes, so that changes in the space-charge profile can be monitored in real time. As an example, Fig. 7 shows the depletion of space-charge in a chromophore-doped cyclic olefin copolymer which was irradiated with ultraviolet light through a semitransparent back electrode [22]. The initial, natural decay of the space-charge at a depth of $1 \mu\text{m}$ is significantly accelerated by irradiation at a wavelength of 300 nm, thus indicating that charges are released from deep traps with energies around 4.1 eV. No accelerated decay is observed at larger depths.

Another type of measurement that will profit from the short acquisition time is the high-resolution three-dimensional mapping of polarization or space-charge distribution. Scanning pyroelectric microscopy using LIMM has been described several times [23–25], but the long measurement times either did not permit a full three-dimensional mapping or allowed only a limited number

TABLE I: Material parameters for PTFE and two commonly used electrode materials [26]. The thermal diffusivity was calculated from $D = \kappa/(c\rho)$.

	PTFE	Al	Cu
thermal conductivity κ [$\text{W m}^{-1} \text{K}^{-1}$]	0.25	237	401
specific heat c [$\text{J kg}^{-1} \text{K}^{-1}$]	1000	897	385
density ρ [kg m^{-3}]	2200	2700	8960
diffusivity D [$\text{m}^2 \text{s}^{-1}$] $\times 10^{-7}$	1.1	979	1162
enthalpy of vaporization [MJ kg^{-1}]		10.9	4.79

of individual beam pointings. A focused beam version of the thermal-pulse technique, on the other hand, could deliver images with several hundred pixels in a comparable time.

For small space-charge densities, both the thermal-pulse and the LImm signal will eventually reach the experimental noise level. To increase the detection sensitivity, one can enhance the absorption coefficient of the front electrode and the laser power. However, this puts an additional thermal stress on the polymer film. Irradiation with cw lasers heats the entire sample to temperatures above ambient, which may eventually lead to damage or even destruction of the polymer. In a one-dimensional approximation, the rise in temperature ΔT at the front electrode is given by

$$\Delta T = \frac{\eta \langle j \rangle d}{\kappa} \quad (14)$$

if the rear surface of the sample is in thermal contact with a heat sink. Here, $\langle j \rangle$ is the average laser intensity and κ is the thermal conductivity, listed in Tab. I for PTFE and some frequently used electrode materials. Diode lasers commonly used in LImm experiments provide output powers of 10-50 mW and beam diameters of 1-5 mm, in which case ΔT remains below 1 K. However, for free-standing films, more powerful laser sources or focused beams, the bulk temperature may rise by tens of Kelvins, leading to physical or chemical modifications of the polymer.

With pulsed lasers, on the other hand, the limiting factor is ablation of the front electrode and possibly a thin surface layer of the polymer, rather than heating of bulk material. Strong ablation occurs at laser fluences higher than [27]

$$\phi_{\text{th}} = \rho \Omega \sqrt{D \tau_L} \quad (15)$$

where Ω is the specific enthalpy (per unit mass) of evaporation. For electrode materials such as aluminum or copper (cf. Tab. I), the heat diffusion length $l = \sqrt{D \tau_L}$ (where D is the thermal diffusivity and $\tau_L \approx 5$ ns is the pulse duration) in the electrode material is several hundred nm, and thus larger than the thickness of typical electrodes. The resulting ablation fluences for aluminum

and copper are 0.9 and 3.4 J cm^{-2} , although partial ablation may already occur at lower values. Additionally, the peak fluence on the beam axis may significantly exceed the average value for, e. g., Gaussian or irregularly shaped laser beam profiles. Finally, damage to the surface layers of the underlying polymer material may occur well below the ablation threshold.

Acknowledgments

The work was funded in part by the European Regional Development Fund. R.S. acknowledges financial support from the German Academic Exchange Service (DAAD). The authors wish to thank Sidney B. Lang (Beer Sheva, Israel) and Siegfried Bauer (Linz, Austria) for stimulating discussions and a critical reading of the manuscript.

-
- [1] R. E. Collins, *J. Appl. Phys.* **47**, 4804 (1976).
- [2] R. E. Collins, *J. Appl. Phys.* **51**, 2973 (1980).
- [3] S. B. Lang and D. K. Das-Gupta, *Ferroelectrics* **39**, 1249 (1981).
- [4] S. B. Lang and D. K. Das-Gupta, *Ferroelectrics* **60**, 23 (1984).
- [5] H. von Seggern, *Appl. Phys. Lett.* **33**, 134 (1978).
- [6] A. S. DeReggi, C. M. Guttman, F. I. Mopsik, G. T. Davis, and M. G. Broadhurst, *Phys. Rev. Lett.* **40**, 413 (1978).
- [7] F. I. Mopsik and A. S. DeReggi, *J. Appl. Phys.* **53**, 4333 (1982).
- [8] S. Bauer, *Phys. Rev. B* **47**, 11049 (1993).
- [9] R. Gerhard-Multhaupt, W. Künstler, G. Eberle, W. Eisenmenger, and G. Yang, in *Space Charge in Solid Dielectrics*, edited by J. C. Fothergill and L. A. Dissado (Dielectrics Society, Leicester, England, 1998), pp. 123–132.
- [10] S. Bauer and B. Ploss, *Ferroelectrics* **118**, 363 (1991).
- [11] S. Bauer and A. S. De Reggi, *J. Appl. Phys.* **80**, 6124 (1996).
- [12] G. M. Sessler, in *Electrets*, edited by R. Gerhard-Multhaupt (Laplacian Press, Morgan Hill, CA, 1999), vol. 2, chap. 10, pp. 41–80, 3rd ed.
- [13] S. B. Lang and D. K. Das-Gupta, *J. Appl. Phys.* **59**, 2151 (1986).
- [14] S. Bauer and S. Bauer-Gogonea, *IEEE Trans. Diel. Electr. Insul.* **10**, 883 (2003).
- [15] S. B. Lang, *IEEE Trans. Diel. Electr. Insul.* **11**, 3 (2004).
- [16] B. Ploss, R. Emmerich, and S. Bauer, *J. Appl. Phys.* **72**, 5363 (1992).
- [17] A. Mellinger, *Meas. Sci. Technol.* **15**, 1347 (2004).
- [18] E. Tuncer and S. B. Lang (2004), [arXiv:cond-mat/0409183](https://arxiv.org/abs/cond-mat/0409183).
- [19] B. Ploss, *Ferroelectrics* **156**, 345 (1994).
- [20] A. Mellinger, F. Camacho González, and R. Gerhard-Multhaupt, *Appl. Phys. Lett.* **82**, 254 (2003).
- [21] A. Mellinger, F. Camacho González, and R. Gerhard-Multhaupt, *IEEE Trans. Diel. Electr. Insul.* **11**, 218 (2004).
- [22] A. Mellinger, R. Singh, F. Camacho González, Z. Szamel, and I. Glowacki, in *2004 Annual Report, Conference on Electrical Insulation and Dielectric Phenomena* (IEEE Service Center, Piscataway, NJ, 2004).
- [23] Ş. Yilmaz, S. Bauer, W. Wirges, and R. Gerhard-Multhaupt, *Appl. Phys. Lett.* **63**, 1724 (1993).
- [24] A. Quintel, J. Hulliger, and M. Wübbenhorst, *J. Phys. Chem. B* **102**, 4277 (1998).
- [25] D. Marty-Dessus, L. Berquez, A. Petre, and J. L. Franceschi, *J. Phys. D: Appl. Phys.* **35**, 3249 (2002).
- [26] D. R. Lide and H. P. R. Frederikse, eds., *CRC Handbook of Chemistry and Physics* (CRC Press, 1995), 75th ed.
- [27] B. N. Chichkov, C. Momma, S. Nolte, F. von Alvensleben, and A. Tünnermann, *Appl. Phys. A* **63**, 109 (1996).

Three-dimensional mapping of polarization profiles with thermal pulses

Axel Mellinger,* Rajeev Singh,† Michael Wegener, Werner Wirges, Reimund Gerhard-Multhaupt, and Sidney B. Lang‡
Department of Physics, University of Potsdam, Am Neuen Palais 10, D-14469 Potsdam, Germany

(Dated: December 15, 2004)

High-resolution, large-area three-dimensional mapping of polarization profiles in electret polymers was carried out by means of a fast thermal pulse technique with a focused laser beam. A lateral resolution of 38 μm and a near-surface depth resolution of less than 0.5 μm was achieved. At larger depths, fast thermal diffusion in the metal electrode rather than the laser spot size becomes the limiting factor for the lateral resolution.

PACS numbers: 66.30.Xj, 44.10.+i, 66.70.+f, 77.70.+a, 77.84.Jd

Keywords: thermal pulse method, LIMM, pyroelectricity, electrets, thermal diffusivity, polyvinylidene fluoride

During the past three decades, numerous techniques for obtaining space-charge and polarization depth profiles in insulating materials have been developed [1] and applied to a wide range of topics, such as the accumulation of space-charge in high-voltage cable insulations [2], the development and optimization of pyroelectric and piezoelectric sensors [3, 4], and basic research on the mechanisms of charge storage [5] in electret polymers. Acoustic techniques rely on a pressure step, generated via the absorption of an ultrashort laser pulse [6] or by a fast piezoelectric transducer [7, 8]. Alternatively, a short electrical pulse applied to a piezoelectric material or space-charge electret generates a traveling pressure front which can be picked up with a microphone (Pulsed Electro-Acoustic technique, PEA) [9]. For thermal techniques, on the other hand, the absorption of a short light pulse (thermal pulse method [10]) or a periodically modulated laser beam (Laser Intensity Modulation Method (LIMM) [11]) by an opaque surface layer causes a time-dependent, spatially varying temperature distribution. In samples that are either pyroelectric or contain an electric space-charge, this gives rise to a short-circuit current, which again carries information on the polarization or space-charge depth profile. All-optical techniques are the method of choice for investigating soft, piezoelectric polymer foams [12], which are easily deformed upon applying a mechanical stress. In addition, they can be used *in situ* under vacuum conditions [13].

While most applications of acoustic and thermal profiling techniques yielded one-dimensional distributions, several attempts have been made to obtain two-dimensional surface maps [14] and three-dimensional (tomographic) images, using, e. g., PEA with spatially confined electrodes [15] or acoustic lenses [16], focused pressure waves [17] and focused LIMM [3, 18]. As laser beams can be brought to a tight focus, the latter technique generally achieves a higher lateral resolution than acoustic methods. However, due to the long measurement times (typically several minutes for a complete frequency spectrum), there is generally a trade-off be-

tween full spatial resolution with a limited number of beam pointings [19], or larger, high-resolution area maps at selected modulation frequencies [20]. On the other hand, thermal pulses have recently been shown to yield results similar to LIMM in 1/50th of the time [21]. In this article, we present a fast three-dimensional mapping technique using thermal pulses generated with a focused laser beam.

The samples were prepared by stretching commercial PVDF films in a hot-zone drawing process at 110 °C with a stretch ratio of 1:4. The resulting films of around 11 μm thickness consist mostly of the polar β phase. For electric poling, both surfaces were metallized with aluminum electrodes of 50 nm thickness, with a ‘T’-structure at the top and full-area metallization at the bottom. Electric poling was performed in direct contact. In order to control the polarization build-up, the hysteresis of the polarization as a function of the electric field was measured with a setup described in Ref. [22]. The coercive field was determined as 50 MV/m. A maximum poling field of 100 MV/m was applied in order to saturate the polarization build-up and to obtain a nearly homogeneous polarization profile across the sample thickness in the metallized area. This poling procedure led to a polarization of approx. 51 mC/m². After poling, the top surface was coated with a full-area copper electrode of 200 nm thickness, which served as laser-absorbing medium. The original ‘T’-electrode does not significantly alter the thermal properties of the sample and was therefore not removed.

The experimental setup is shown in Fig. 1. The second-harmonic beam (wavelength 532 nm) of a Q-switched Nd:YAG laser (Polaris III, New Wave Research) operating at a repetition rate of 6 Hz was focused onto the polymer film mounted on a computer-controlled *xy* translation stage. By adjusting the *z* position of the sample holder, the laser beam spot size could be varied from 1 mm down to 30 μm , as determined with a knife-edge profiler. The fluence was kept below 0.1 J cm⁻² to avoid ablation damage [21]. At these low pulse energies, the time-averaged temperature rise in the bulk was well below 1 K. The sample may be either free-standing or attached to a substrate, although the latter is preferred in order to avoid thermo-elastic resonances [23]. The short-circuit pyroelectric or displacement current was amplified by a Stanford Research SR 570 current-to-voltage converter and recorded by a digital storage oscilloscope (Agilent 54833A) at a rate of $(\Delta t)^{-1} = 10$ MSamples/s. For each beam pointing, 30 to 50 pulses were averaged and stored on the internal hard disk of

*Electronic address: axm@rz.uni-potsdam.de

†Permanent address: Department of Electronics & Communication, University of Allahabad, Allahabad, (U.P.)-211002, India

‡Permanent address: Department of Chemical Engineering, Ben-Gurion University of the Negev, P.O.B. 653, 84105 Beer Sheva, Israel

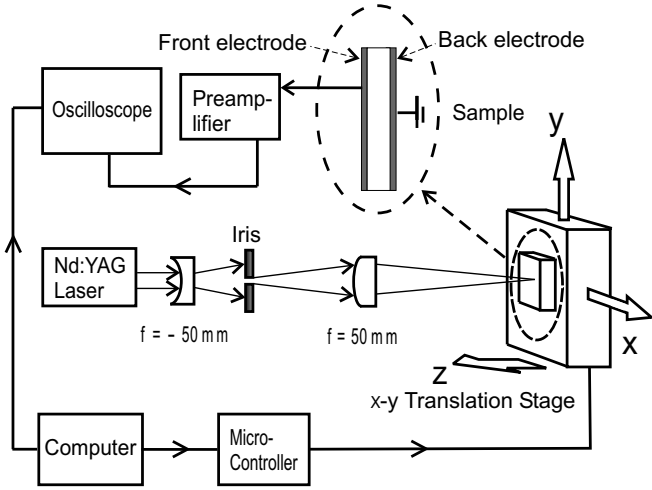


FIG. 1: Experimental setup.

the oscilloscope for further processing. The recorded current $I(t_k)$ was Fourier-transformed and divided by the measured (complex) gain spectrum $\tilde{\alpha}(f_n)$ of the SR 570 in order to compensate the amplifier-induced signal distortion:

$$\tilde{J}_{\text{exp}}(f_n) = \frac{\Delta t}{\tilde{\alpha}(f_n)} \sum_{k=0}^{N-1} I(t_k) e^{-2\pi i k n / N}. \quad (1)$$

Here, the frequency points are given by

$$f_n = \frac{n}{N\Delta t}, \quad n = 1 \dots \frac{N}{2}, \quad (2)$$

where $N = 512000$ is the number of recorded data points.

The computed complex values $\tilde{J}_{\text{exp}}(f_n)$ were analyzed in the same way as conventional LIMM data [24]. The frequency-dependent current \tilde{J}_{calc} is calculated via the LIMM equation

$$\tilde{J}_{\text{calc}}(f_n) = \frac{A}{d} \alpha_P \int_0^d P(z) \frac{\partial \tilde{T}(z, f_n)}{\partial t} dz, \quad (3)$$

where A , z , d and α_P are the irradiated area, depth coordinate, sample thickness, and the relative temperature dependence of the polarization, respectively. The time derivative of the complex temperature $\tilde{T}(z, f_n)$ was computed by solving the one-dimensional heat conduction equation. $P(z)$ is the unknown polarization distribution. This equation is a Fredholm integral equation of the 1st kind and is ‘‘ill-conditioned’’ with multiple solutions. The correct solution is found by imposing the physical requirement of smoothness on the calculated polarization profile. This is accomplished using the Polynomial Regularization Method (PRM) [24]. The polarization distribution was assumed to be an 8th degree polynomial in a normalized logarithmic spatial coordinate $\gamma = (\ln(z) - \ln(z_1)) / (\ln(z_2) - \ln(z_1))$:

$$P(\gamma) = a_0\gamma^0 + a_1\gamma^1 + a_2\gamma^2 + a_3\gamma^3 + \dots \quad (4)$$

Here, z_1 and z_2 are the spatial coordinates of the top electrode-polymer interface and the bottom of the sample, respectively.

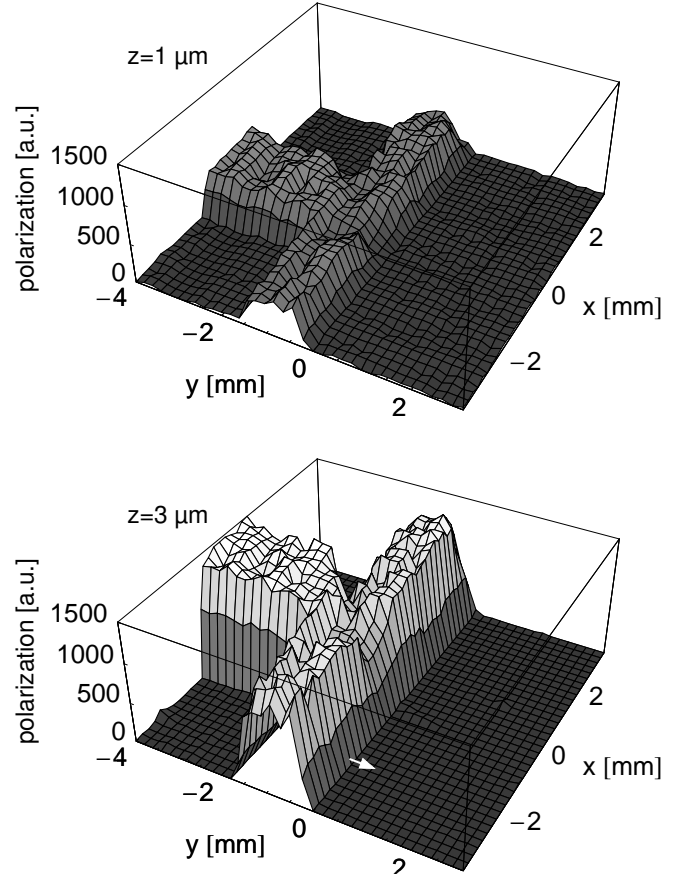


FIG. 2: Polarization map of a 11 μm thick PVDF film poled with a T-shaped electrode. At $z = 1 \mu\text{m}$ (top graph), the polarization is significantly lower than in the bulk. The arrow indicates the direction of the high-resolution scan shown in Fig. 3.

The coefficients a_i were found by minimizing the function

$$\sum_n \|\tilde{J}_{\text{exp}}(f_n) - \tilde{J}_{\text{calc}}(f_n)\|^2 + \alpha^2 \int_{z_1}^{z_2} \left(\frac{d^2 P(z)}{dz^2} \right) dz \quad (5)$$

with respect to each of the coefficients. The parameter α is the regularization parameter which controls the smoothness of the solution. It was selected using the L-curve method [25, 26]. This analysis was applied to each of the thermal pulse data sets. A near-surface depth resolution of better than $0.5 \mu\text{m}$ was achieved.

A polarization map of the PVDF test sample is shown in Fig. 2. The scan covers an area of $7 \times 7 \text{ mm}^2$ with a lateral resolution of $200 \mu\text{m}$. Acquisition of the 1296 thermal pulse measurements took approx. 3.5 hours and produced 2 GB of data. The structure of the original ‘T’ electrode is extremely well revealed. Comparing the polarization maps at depths of 1 and 3 μm reveals a substantial edge depolarization, which could be result of impurities. To test the lateral resolution of this method, one-dimensional scans in the y direction across the edge of the ‘T’ electrode were performed at the tightest

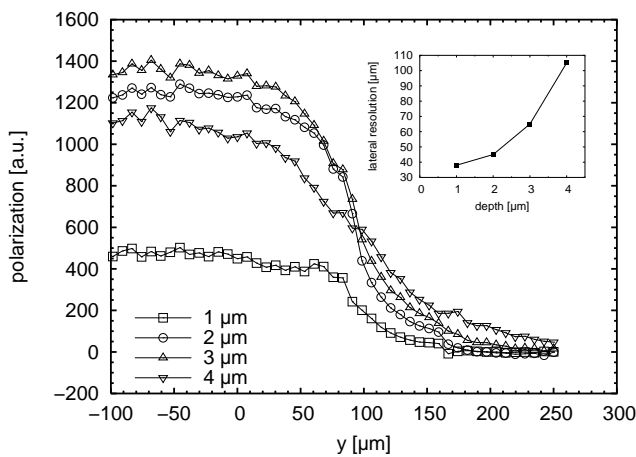


FIG. 3: One-dimensional scan of the polarization distribution in the PVDF sample shown in Fig. 2 at $x = -2.0$ mm and different depths. The lower signal at a depth of $1 \mu\text{m}$ results from edge depolarization. Fast thermal diffusion in the Cu electrode reduces the lateral resolution at larger depths. The inset shows the width of the transition region measured between 20% and 80% of the plateau height.

spot size ($30 \mu\text{m}$). The resulting pyroelectric profile is plotted in Fig. 3 for different depths. At shallow depths ($z = 1 \mu\text{m}$), the width of the transition from the poled to the unpoled area is only slightly larger than the spot size, whereas significant broadening to $105 \mu\text{m}$ is observed at a depth of $4 \mu\text{m}$. This

reduced lateral resolution can be attributed to the fact that the thermal diffusivity of the metal electrode is approximately three orders of magnitude larger than that of the polymer. As the diffusion length at a time t is given by $s = \sqrt{Dt}$ (where D is the diffusivity), the heated zone will spread out in the electrode some $\sqrt{1000} \approx 30$ times faster than in the polymer. Consequently, the resolution at larger depths is limited by thermal diffusion in the electrode, rather than the laser spot size. Nevertheless, it compares favorably with that achieved using acoustic techniques [16].

In conclusion, we have demonstrated that fast three-dimensional polarization mapping with a near-surface lateral resolution of $38 \mu\text{m}$ can be achieved using the thermal pulse technique. Work is in progress to optimize the thermal properties of the electrode and to model the three-dimensional propagation of the thermal pulse.

Acknowledgments

The work was funded in part by the European Regional Development Fund. R.S. acknowledges financial support from the German Academic Exchange Service (DAAD). S.B.L. acknowledges financial support during his sabbatical from Ben-Gurion University of the Negev. The authors wish to thank F. Camacho González, R. Flores Suárez and J.P. Dietrich for their assistance.

-
- [1] S. Bauer and S. Bauer-Gogonea, *IEEE Trans. Diel. Electr. Insul.* **10**, 883 (2003).
- [2] K. R. Bambery and R. J. Fleming, *IEEE Trans. Diel. Electr. Insul.* **5**, 103 (1998).
- [3] S. Bauer, *J. Appl. Phys.* **80**, 5531 (1996).
- [4] M. Wegener and R. Gerhard-Multhaupt, *IEEE Trans. Ultrason. Ferr.* **50**, 921 (2004).
- [5] A. Mellinger, F. Camacho González, and R. Gerhard-Multhaupt, *IEEE Trans. Diel. Electr. Insul.* **11**, 218 (2004).
- [6] G. M. Sessler, J. E. West, R. Gerhard-Multhaupt, and H. von Seggern, *IEEE Trans. Nucl. Sci.* **29**, 1644 (1982).
- [7] W. Eisenmenger and M. Haardt, *Solid State Communications* **41**, 917 (1982).
- [8] C. Alquié, C. Laburthe Tolra, J. Lewiner, and S. B. Lang, *IEEE Trans. Electr. Insul.* **27**, 751 (1992).
- [9] T. Takada, T. Maeno, and H. Kushibe, in *Proceedings, 5th International Symposium on Electrets* (IEEE Service Center, Piscataway, NJ, 1985), pp. 450–455.
- [10] R. Collins, *Appl. Phys. Lett.* **26**, 675 (1975).
- [11] S. B. Lang and D. K. Das-Gupta, *Ferroelectrics* **39**, 1249 (1981).
- [12] J. van Turnhout, R. E. Staal, M. Wübbenhorst, and P. H. de Haan, in *Proceedings, 10th International Symposium on Electrets* (IEEE Service Center, Piscataway, NJ, 1999), pp. 785–788.
- [13] A. Mellinger, R. Singh, F. Camacho González, Z. Szamel, and I. Glowacki, in *Proceedings, Conference on Electrical Insulation and Dielectric Phenomena* (IEEE Service Center, Piscataway, NJ, 2004).
- [14] C. Alquié, G. Charpak, and J. Lewiner, *J. Physique Lett.* **43**, L687 (1982).
- [15] Y. Imaizumi, K. Suzuki, Y. Tanakoa, and T. Takada, in *Proceedings, International Symposium on Electrical Insulating Materials, Tokyo* (1995), pp. 315–318.
- [16] T. Maeno, *IEEE Trans. Diel. Electr. Insul.* **8**, 845 (2001).
- [17] X. Qin, K. Suzuki, Y. Tanaka, and T. Takada, *J. Phys. D: Appl. Phys.* **32**, 157 (1999).
- [18] Ş. Yılmaz, S. Bauer, W. Wirges, and R. Gerhard-Multhaupt, *Appl. Phys. Lett.* **63**, 1724 (1993).
- [19] D. Marty-Dessus, L. Berquez, A. Petre, and J. L. Franceschi, *J. Phys. D: Appl. Phys.* **35**, 3249 (2002).
- [20] A. Quintel, J. Hulliger, and M. Wübbenhorst, *J. Phys. Chem. B* **102**, 4277 (1998).
- [21] A. Mellinger, R. Singh, and R. Gerhard-Multhaupt, *Rev. Sci. Instr.* **76** (2005, *in press*).
- [22] M. Wegener, W. Künstler, K. Richter, and R. Gerhard-Multhaupt, *J. Appl. Phys.* **92**, 7442 (2002).
- [23] P. Bloß, M. Steffen, H. Schäfer, G. M. Yang, and G. M. Sessler, *J. Phys. D* **30**, 1668 (1997).
- [24] S. B. Lang, *IEEE Trans. Diel. Electr. Insul.* **11**, 3 (2004).
- [25] S. B. Lang, R. Fleming, and T. Pawlowski, in *Proceedings, Conference on Electrical Insulation and Dielectric Phenomena* (IEEE Service Center, Piscataway, NJ, 2004).
- [26] P. C. Hanson and D. P. O’Leary, *SIAM J. Sci. Comput.* **14**, 1487 (1993).

B ITG Award Certificate

Lebenslauf

Dr. rer. nat. Axel Mellinger

Axel Mellinger wurde 1967 in München geboren. Nach seinem Physikstudium an der Technischen Universität München, das er 1992 mit dem Diplom abschloss, arbeitete er als Doktorand am Max-Planck-Institut für extraterrestrische Physik in Garching. Thema seiner 1995 fertig gestellten Dissertation war die Untersuchung hochangeregter Triplettzustände des Kohlenmonoxid-Moleküls mittels Vakuum-UV-Laserspektroskopie. Unterstützt durch ein DFG-Forschungsstipendium folgte ab Januar 1996 ein zweijähriger Aufenthalt am Department of Chemistry der University of California in Berkeley, wo er die Reaktionsdynamik des Keten-Moleküls erforschte. Seit Ende 1997 ist er wissenschaftlicher Mitarbeiter am Institut für Physik der Universität Potsdam. Seine gegenwärtigen Forschungsschwerpunkte sind optisch und thermisch stimulierte Entladungsprozesse in ladungsspeichernden Elektret-Polymeren, sowie die Untersuchung piezoelektrischer Resonanzen in elektrisch geladenen Polymerschäumen.

Laudatio zur Arbeit von Axel Mellinger

"Dielectric resonance spectroscopy: a versatile tool in the quest for better piezoelectric polymers",
IEEE Transactions on Dielectrics and Electrical Insulation, Vol. 10, No. 5, pp 842-861
(2003)

Die Arbeit stellt einen umfassenden Überblick über die Methode der dielektrischen Resonanzspektroskopie dar, einer Technik, die grundlegende Bedeutung bei der Untersuchung piezoelektrischer Materialien erlangt hat. Sie bezieht sich auf rein elektrische Messungen elektromechanischer Resonanzen in piezoelektrischen Materialien, mit denen umfassende Kenntnis über die Elemente des piezoelektrischen Tensors von Piezoelektrika gewonnen werden kann. Die Bedeutung der Technik wird ausgeleuchtet an Hand klug ausgewählter praktischer Beispiele, die von ungewöhnlichen Geometrien zu neuartigen, zellulären Polymeren mit interner Aufladung reichen. Die Arbeit stellt damit einen grundlegenden Beitrag zur derzeit aktuellen Suche nach besseren piezoelektrischen Polymeren dar.



VERBAND DER ELEKTROTECHNIK ELEKTRONIK INFORMATIONSTECHNIK e.V.

Die Informationstechnische Gesellschaft
im VDE (ITG) verleiht

Herrn Dr. rer.nat. Axel Mellinger

in Würdigung der Veröffentlichung

„Dielectric Resonance Spectroscopy: A
Versatile Tool in the Quest for Better
Piezoelectric Polymers“

den Preis der ITG 2004

Frankfurt,
den 10. November 2004

A handwritten signature in dark ink, consisting of a series of loops and a long horizontal stroke, positioned above the text of the signatory.

Der Vorsitzende der ITG

C Curriculum Vitae

Name	<u>Axel</u> Peter Lutz Mellinger
Geburtsdatum/-ort	25. August 1967 in München
Familienstand	ledig
Schulbesuch	1973 – 1975 Grundschule Leutershausen/Bergstr. 1975 – 1977 Grundschule Vaterstetten 1977 – 1986 Gymnasium Vaterstetten Abitur 27.06.1986, Prädikat: sehr gut
Studium	1986 – 1992 Physikstudium an der Technischen Universität München Juni 1991 – Juni 1992 Diplomarbeit am Max-Planck-Institut für extraterrestrische Physik in Garching. Studienabschluß 15.07.1992, Prädikat: sehr gut
Promotion	01.07.1992 – 31.12.1995 Doktorand am Max-Planck-Institut für extraterrestrische Physik in Garching Dissertation: Untersuchung hochangeregter Tripletzustände des CO-Moleküls Doktorprüfung: 15.11.1995, Prädikat: mit Auszeichnung bestanden
Post-doc	02.01.1996 – 13.12.1997 am Department of Chemistry, University of California, Berkeley, USA (mit DFG-Forschungsstipendium) Experimentelle Untersuchung der Dynamik unimolekularer Reaktionen am Beispiel des Keten-Moleküls (CH ₂ CO). Aufbau einer gepulsten Laser-Quelle, die durch Vierwellenmischung in einem Heatpipe-Ofen kohärente, abstimmbare Vakuum-UV-Strahlung erzeugt
Wissenschaftl. Mitarbeiter	seit 15.12.1997 am Institut für Physik der Universität Potsdam Untersuchung mikroskopischer Mechanismen der Ladungsspeicherung in Elektret-Polymeren Entwicklung piezoelektrischer Polymerschäume mit hoher Temperaturstabilität
Stipendien	1987 – 1992: Stipendiat der Studienstiftung des Deutschen Volkes 1996 – 1997: DFG-Forschungsstipendium
Preise	2000: Alfred Eisenstaedt Award (2. Preis) für ein Milchstraßen-Panoramabild 2004: Preis der Informationstechnischen Gesellschaft im VDE

Acknowledgments

This thesis would not have been possible without the support of the “Applied Condensed Matter Physics” group at the Department of Physics, University of Potsdam. First and foremost, my thanks go to Prof. REIMUND GERHARD-MULTHAUPT, whose stimulating comments and suggestions were a constant source of encouragement. My Ph.D. students FRANCISCO CAMACHO GONZÁLEZ and RAJEEV SINGH spent countless hours of acquiring and analyzing the data that went into our joint publications. Dr. PETER FRÜBING guided me through dielectric spectroscopy, while Dr. MICHAEL WEGENER, Dr. ENIS TUNCER and Dr. WOLFGANG KÜNSTLER were very helpful discussion partners for everything concerning ferroelectric and ferroelectret materials, theoretical aspects, poling techniques, and space-charge measurements. Dr. DENIS ROLLIK introduced me to thermal-wave probing of polarization profiles. Our engineers ANDREAS PUCHER and WERNER WIRGES provided invaluable help when new equipment had to be designed and built, or broken equipment needed fast repair. Our secretary SANDRA ZERETZKE helped me turning administrative chaos into order. And, of course, I would like to thank all other (past and present) group members – it was a great pleasure to work with you!

Many other people at our department (too numerous to be listed individually) were helpful whenever I needed their support. I would like to mention, though, that much of our experimental setup would not exist in its present form without the dedicated work of STEFAN KLEINSCHMIDT and his machine shop staff. Any modern experiment relies on computer control, which was made possible in part through the tireless effort of MIRKO KRUMPE, ALEXANDER KREMMER, SEBASTIAN BANGE and LAKSHMI MEENA GANESAN.

I am grateful to MARITA DÖRRWAND, who often helped me navigate around the pitfalls of administrative bureaucracy.

I would also like to thank our national and international cooperation partners. Special thanks go to Prof. SIEGFRIED BAUER (University of Linz, Austria) for his inspiring thoughts and critical reading of my publications. Prof. SIDNEY B. LANG gave me many new insights into pyroelectricity and thermal space-charge measurement techniques during his visits to the University of Potsdam. It is my pleasure to acknowledge the hospitality of Prof. ROBERTO M. FARIA, Dr. LUCAS FUGIKAWA SANTOS (Instituto de Física de São Carlos, Brazil) and Dr. DANTE LUIS CHINAGLIA (Universidade Estadual Paulista, Brazil), as well as their help in introducing me to electron-beam charging. I am also grateful to Prof. JACEK ULAŃSKI (Technical University of Łódź, Poland) and his group members Dr. IRENEUSZ GŁOWACKI, BEATA ŁUSZCZYŃSKA and ZBIGNIEW SZAMEL for performing thermally stimulated current and thermoluminescence experiments, Prof. POLYCARPOS PISSIS (National Technical University of Athens, Greece) for his cooperation in the investigation of humidity effects on polypropylene foams, and Prof. XIA

ZHONGFU for his hospitality during my visit to his laboratory at Tongji University in Shanghai, China.

Finally, my special thanks go to my parents for their love and support.

Potsdam, 06 December 2004

Axel Mellinger

